Copyright Warning & Restrictions

The copyright law of the United States (Title 17, United States Code) governs the making of photocopies or other reproductions of copyrighted material.

Under certain conditions specified in the law, libraries and archives are authorized to furnish a photocopy or other reproduction. One of these specified conditions is that the photocopy or reproduction is not to be "used for any purpose other than private study, scholarship, or research." If a, user makes a request for, or later uses, a photocopy or reproduction for purposes in excess of "fair use" that user may be liable for copyright infringement,

This institution reserves the right to refuse to accept a copying order if, in its judgment, fulfillment of the order would involve violation of copyright law.

Please Note: The author retains the copyright while the New Jersey Institute of Technology reserves the right to distribute this thesis or dissertation

Printing note: If you do not wish to print this page, then select "Pages from: first page # to: last page #" on the print dialog screen

NJIT
New Jersey's Science & Technology University

The Van Houten library has removed some of the personal information and all signatures from the approval page and biographical sketches of theses and dissertations in order to protect the identity of NJIT graduates and faculty.

ABSTRACT

SYNTHESIS AND CHARACTERIZATION OF LOW PRESSURE CHEMICALLY VAPOR DEPOSITED BORON NITRIDE AND TITANIUM NITRIDE FILMS

by
Narahari Ramanuja

This study has investigated the interrelationships governing the growth kinetics, resulting compositions, and properties of boron nitride (B-C-N-H) and titanium nitride (Ti-N-Cl) films synthesized by low pressure chemical vapor deposition (LPCVD) using ammonia (NH_3)/triethylamine-borane and NH_3/titanium tetrachloride as reactants, respectively. Several analytical methods such as the FTIR, UV/Visible spectroscopy, XPS, AES, RBS, SEM, and XRD were used to study the stoichiometry and structure of the deposited films.

The B-N-C-H films were synthesized over a temperature range of 300 to 850°C at various flow rate ratios of the reactants and total pressure range of 50 to 150 mTorr. The deposits were amorphous in all cases having an index of refraction ranging between 1.76 and 2.47 depending on the composition of the films. The stress of the deposited films varied from +240 to –200 MPa, depending on the deposition parameters. The hardness and Young's modulus were found to be between 5 to 12 GPa and 50 to 120 GPa, respectively. Electrical properties of the BN films were measured using metal-insulator-metal (MIM) and metal-insulator-semiconductor (MIS) structures. The films did not react with water vapor and exhibited dielectric constant between 3.12 and 5.5. Free standing X-ray windows with thickness varying from 2000Å to 12,000Å, were fabricated using the mildly tensile and compressive films and X-ray transmission studies through these windows

indicate significantly lower absorption when compared to the commercially available polymeric X-ray windows.

The Ti-N-Cl deposits exhibited an Arrhenius dependence in the deposition temperature regime of 450 to 600 °C from which an activation energy of ~42 kJ/mol was calculated. The growth rate dependencies on the partial pressures of NH_3 (50 to 100 mTorr) and $TiCl_4$ (1 to 12 mTorr) yielded reaction rate orders of 1.37 and –0.42 respectively. Films with compositions trending towards stoichiometry were produced as the deposition temperature was decreased and the NH_3 partial pressure was increased. The chlorine concentration in the films was observed to decrease from ~8 % (a/o) at the deposition temperature of 450 °C down to ~0.2 % (a/o) at 850 °C. The film density values increased from 3.53 to 5.02 g/cm^3 as the deposition temperature was increased from 550 to 850 °C. The resistivity of the films was dependent on changes in deposition temperature and flow rate ratios. The lowest resistivity value of 86 μΩcm was measured for a deposition temperature of 600°C and an $NH_3/TiCl_4$ flow ratio of 10/1.The film stress was found to be tensile for all deposits and to decrease with higher deposition temperatures. Nano-indentation measurements yielded values for the hardness and Young's modulus of the films to be around 15 and 250 GPa, respectively. X-ray diffraction measurements revealed in all cases the presence of cubic TiN phase with a preferred (200) orientation. For the investigated aspect ratios of up to 4:1, the deposits were observed to exhibit conformal step coverage over the investigated range of processing conditions.

SYNTHESIS AND CHARACTERIZATION OF LOW PRESSURE CHEMICALLY VAPOR DEPOSITED BORON NITRIDE AND TITANIUM NITRIDE FILMS

by
Narahari Ramanuja

A Dissertation
Submitted to the Faculty of
New Jersey Institute of Technology
in Partial Fulfillment of the Requirements for the Degree of
Doctor of Philosophy in Materials Science and Engineering

Materials Science and Engineering Committee

May 2000

Copyright © 2000 by Narahari Ramanuja

ALL RIGHTS RESERVED

APPROVAL PAGE

SYNTHESIS AND CHARACTERIZATION OF LOW PRESSURE CHEMICALLY VAPOR DEPOSITED BORON NITRIDE AND TITANIUM NITRIDE FILMS

Narahari Ramanuja

Dr. Roland Levy — Date
Distinguished Professor of Physics, NJIT

Dr. N. M. Ravindra — Date
Professor of Physics, NJIT

Dr. James Grow — Date
Professor of Chemistry, NJIT

Dr. Martin Green — Date
Member of Technical Staff, Lucent Technologies

Dr. Dentcho Ivanov — Date
Director of Technical Operations, MRC, NJIT

BIOGRAPHICAL SKETCH

Author: Narahari Ramanuja

Degree: Doctor of Philosophy in Materials Science and Engineering

Date: May 2000

Undergraduate and Graduate Education:

- Doctor of Philosophy in Materials Science & Engineering,
  New Jersey Institute of Technology, Newark, NJ, 2000

- Master of Science in Materials Science and Engineering,
  New Jersey Institute of Technology, Newark, NJ, 1998

- Bachelor of Engineering in Chemical Engineering,
  Rashtreeya Vidyalaya College of Engineering,
  Bangalore University, Bangalore, India, 1996

Publications and Presentations:

N. Ramanuja, R. A. Levy, and S. N. Dharmadhikari, "Synthesis and Characterization of LPCVD Titanium Nitride Films Using $TiCl_4$ and NH_3", Pending Publication in the Journal of Applied Physics.

N. Ramanuja, M. Narayan, and R. A. Levy, "Characterization B-N-C-H Films Synthesized by LPCVD using NH_3 and TEAB", Pending Publication in the Journal of Electrochemical Society.

N. Ramanuja, S. N. Dharmadhikari, R. A. Levy, and E. Ramos, *Proc. International Symposium on Interconects and Contact Metallization for ULSI*, Electrochemical Society, October 1999.

N. Ramanuja, W. Lolertpiphop, E. Ramos and R. A. Levy, *Proc. Second International Symposium on Environmental Issues with Materials and Processes for the Electronic and Semiconductor Industries*, Electrochemical Society, Vol. 99-8, May 1999.

This thesis is dedicated to my parents and sister
Mr. Narayanaswamy Ramanuja,
Mrs. Pushpa Ramanuja, and
Ms. Deepa Ramanuja

ACKNOWLEDGMENT

The author wishes to express his sincere gratitude to his supervisor, Professor Roland Levy, for his guidance, friendship, and moral support throughout this research. The following ancient hindu saying correctly represents his contribution;

> A hundred suns may blaze,
> A thousand moons may shine,
> In this intense brilliance,
> Without my teacher,
> There is pitch darkness.

Special thanks are due towards Prof. J. Grow, Prof. N. M. Ravindra, Dr. D. Ivanov, and Dr. M. Green for serving as committee members and taking time to review my work. I appreciate their efforts in helping me to refine my thesis. Thanks are also due towards Mr. Vitaly Sigal, for taking time to fix the problems that I had with the CVD reactor and to Dr. Roumiana Petrova and Dr. E. Ramos for their encouragement and help from time to time.

Last but not the least, I would like to thank my friends who have supported me all the way. Without their encouragement and competitive spirit I would not have been able to complete my degree in this time frame. Some of them such as Krit Aryusook, Kiran Kumar, Dianhong Luo, Sameer Dharmadhikari, Lim Heechuan, Yew Fong, M. Tungare, M. Sonnenberg, R. Dhavalikar deserve special mention for their good wishes, time, many interesting conversations, and good friendship.

TABLE OF CONTENTS

Chapter **Page**

1 INTRODUCTION.. 1

1.1 Thin Film Deposition Methods.. 13

1.1.1 Physical Vapor Deposition.. 13

1.1.2 Chemical Vapor Deposition.. 16

1.1.2.1 Overview of Chemical Vapor Deposition Process............ 17

1.1.2.2 CVD Reactor Systems.. 18

1.1.2.3 Nucleation and Growth.. 20

1.1.2.4 Chemical Reactions and Kinetics.............................. 20

1.1.2.5 Reaction Mechanism in CVD.................................. 21

1.1.2.6 Transport Phenomena.. 23

1.1.2.7 Factors Affecting Film Uniformity............................ 25

1.2 Types of CVD Process.. 26

1.2.1 Plasma Enhanced CVD (PECVD).. 26

1.2.2 Photo Induced CVD.. 27

1.2.3 Thermally Activated CVD.. 27

1.3 Low Pressure Chemical Vapor Deposition (LPCVD) Process.................. 28

1.3.1 Advantages of CVD.. 29

1.3.2 Limitations of CVD.. 30

1.4 Dielectric Materials.. 31

1.4.1 Requirements of Dielectric Materials for VLSI Technology............ 31

1.4.2 Requirements for Low Dielectric Constant ILD Materials............... 33

1.4.3 Applications of Dielectric Materials in VLSI Technology............... 34

1.4.4 BN as a Dielectric Materials.. 34

TABLE OF CONTENTS
(Continued)

1.4.5 Boron Triethylamine Complex as a Precursor.......................... 35

1.5 Refractory Materials.. 36

1.5.1 Application of Refractory Materials in ULSI........................... 36

1.5.2 TiN as a Refractory Interconnect Material.............................. 38

1.5.3 Titanium tetrachloride and Ammonia as Precursors..................... 41

1.6 Objectives of this Study... 41

2 LITERATURE REVIEW OF BN AND TIN FILMS.. 43

2.1 Introduction.. 43

2.2 Deposition Techniques of Boron Nitride Thin Films.............................. 45

2.2.1 Synthesis by CVD Techniques.. 45

2.2.2 Synthesis by LPCVD Technique... 49

2.3 Deposition Techniques of Titanium Nitride Thin Films........................ 50

2.3.1 Synthesis by CVD and LPCVD Techniques....................................... 52

2.4 Properties of Boron Nitride and Titanium Nitride Films........................ 54

2.5 Applications of CVD Boron Nitride.. 60

2.5.1 Dielectric Thin Films.. 64

2.5.1.1 Organic Fluorinated Dielectric Films.. 65

2.5.1.2 Fluorinated SiO_2 Dielectric Films.. 67

2.5.1.3 BN and SiBN Thin Films.. 68

2.5.2 Transparent Boron Carbon Nitrogen Thin Films................................. 69

2.5.2.1 X-ray Windows.. 71

2.5.2.2 Next Generation Lithography (NGL).. 73

TABLE OF CONTENTS
(Continued)

2.6 Applications of CVD Titanium Nitride........ 78

2.6.1 Refractory Metal Interconnects for VLSI........ 78

2.6.2 Diffusion Barriers........ 79

2.7 Aim and Scope of the Present Work........ 82

3 EXPERIMENTAL PROCEDURE........ 83

3.1 Introduction........ 83

3.2 LPCVD Reactor........ 83

3.2.1 Vapor Phase Flow Mechanism........ 86

3.3 Experimental Setup........ 88

3.3.1 Leakage Test........ 88

3.3.2 Calibration of Gas Flow System........ 88

3.3.3 Calibration of Vapor Phase Flow Controller........ 90

3.4 Deposition Procedure........ 91

3.5 Characterization of Boron Nitride and Titanium Nitride Films........ 93

3.5.1 Thickness........ 93

3.5.2 Growth Rate........ 94

3.5.3 Density........ 94

3.5.4 Refractive Index........ 95

3.5.5 Fourier Transform Infrared Spectroscopy........ 95

3.5.6 Film Stress........ 96

3.5.7 X-Ray Diffraction (XRD)........ 98

3.5.8 UV/Visible Spectroscopy........ 99

3.5.9 Hardness and Young's Modulus Measurements........ 100

TABLE OF CONTENTS
(Continued)

3.5.10 X-Ray Photoelectron Spectroscopy (XPS)........ 101

3.5.11 Auger Electron Spectroscopy (AES)........ 102

3.5.12 Scanning Electron Spectroscopy (SEM)........ 102

3.5.13 Rutherford Backscattering Spectrometry (RBS)........ 103

3.5.14 Resistivity........ 103

3.5.15 Emissivity........ 105

3.6 Electrical Characterization of BN Thin Films........ 105

3.6.1 Metallization of BN Films........ 105

3.6.2 Device Fabrication........ 107

3.6.3 Capacitance-Voltage and Current-Voltage Measurements........ 109

3.7 Free Standing B-N-C-H Membrane........ 110

3.7.1 Fabrication of Free Standing B-N-C-H Membranes........ 110

3.7.2 Characterization of B-N-C-H Free Standing Membranes........ 112

4 RESULTS AND DISCUSSION........ 113

4.1 Introduction........ 113

4.2 Kinetic Study of Boron Nitride Deposition by LPCVD........ 114

4.2.1 Influence of Temperature on the Deposition Rate and Film Composition........ 114

4.2.2 Influence of Reactant Flow ratio on the Deposition Rate and Film Composition........ 117

4.3 FTIR Spectroscopy and Auger Analysis of BN Thin Films........ 120

4.4 Properties of LPCVD BN Thin Films........ 122

4.4.1 Film Density........ 122

4.4.2 Refractive Index........ 123

TABLE OF CONTENTS
(Continued)

Chapter **Page**

4.4.3 Film Stress.. 125

4.4.4 Optical Properties.. 126

4.4.5 Structure Study.. 130

4.4.6 Electrical Characterization of BN Films.................................. 133

4.4.6.1 Dielectric Constant Measurements............................... 133

4.4.6.2 Investigation of LPCVD BN-Si interfaces using MIS Structures.. 135

4.4.6.3 Current-Voltage (I-V) Characteristics of the Films............ 140

4.4.7 Boron Nitride X-Ray Masks and Windows............................. 141

4.4.7.1 B-N-C-H X-Ray Window Fabrication.......................... 141

4.4.7.2 Characterization of B-N-C-H X-Ray Windows............... 144

4.5 Kinetic Study of LPCVD Titanium Nitride.................................... 145

4.5.1 Influence of Temperature on Deposition Rate.......................... 145

4.5.2 Influence of Reactant Partial Pressures on Deposition Rate.......... 148

4.5.3 Rate Equation.. 152

4.5.4 Reaction Mechanism.. 154

4.6 Characterization Study.. 157

4.6.1 X-Ray Photoelectron Spectroscopy (XPS)............................... 157

4.6.2 Rutherford Backscattering Spectrometry (RBS)........................ 159

4.7 Properties of LPCVD TiN Films... 160

4.7.1 Color... 160

4.7.2 Density... 161

4.7.3 Film Stress... 162

TABLE OF CONTENTS
(Continued)

Chapter **Page**

4.7.4 Resistivity.. 163

4.7.5 Hardness and Young's Modulus.. 164

4.7.6 Optical Properties.. 165

4.7.7 Step Coverage and Film Morphology.................................. 166

4.7.8 X-Ray Diffraction Study... 171

4.8 Etching Study.. 172

4.9 Effect of Aluminum on LPCVD TiN.. 173

5 CONCLUSIONS.. 175

REFERENCES... 178

LIST OF TABLES

Table **Page**

1.1 Evaporation Vs. Sputtering........ 15

1.2 Desired Dielectric Constant (k) for Future Technologies........ 32

1.3 Properties of ILD........ 32

1.4 Properties of CVD Boron Nitride Dielectric........ 34

1.5 Properties of TEAB........ 35

1.6 Properties of Silicides and Refractory Metals........ 37

1.7 Physical Properties of Titanium Nitride........ 40

1.8 Properties of Titanium Tetrachloride........ 40

2.1 Mechanical and Thermal Properties of Hard Materials........ 44

2.2 Synthesizing Techniques of Boron Nitride Thin Films........ 46

2.3 Summary of Different Deposition Techniques and Reactants Used for TiN Thin Film Deposition........ 51

2.4 Properties of BN Thin Films........ 54

2.5 Summary of Properties of TiN Films deposited by different Processes........ 59

2.6 Aluminum-Diffusion Barrier-Silicon Reactions........ 80

3.1 Specifications of the Si Wafer........ 92

3.2 Parameters for Metallization of BN Thin Films........ 106

4.1 Comparison of experimental XRD data with standard data........ 172

LIST OF FIGURES

Figure **Page**

1.1 Scheme to show the transport and reaction processes underlying CVD........... 18

1.2 Deposition rate as a function of substrate temperature exemplifying diffusion controlled and surface-reaction controlled regimes................................. 24

2.1 Trends in ULSI miniaturization, exposure wavelength and limits of resolution enhancement techniques (RET) as a function of time..................... 73

2.2 Trends in ULSI miniaturization, exposure wavelength and limits of resolution enhancement techniques (RET) as a function of time............................. 74

2.3 Basic SCALPEL principle of operation showing contrast generation by differentiating more or less-scattered electrons..................................... 76

2.4 Schematic cross-section of a SCALPEL mask showing patterned membrane area and supporting grillage... 76

3.1 Schematic representation of the LPCVD reactor.................................... 84

3.2 Schematic diagram of the modified experimental setup........................... 86

3.3 Schematic representation showing the experimental setup to measure the radius of curvature of the bending of silicon substrate due to film stress.... 96

3.4 Schematic representation of a four point probe.................................... 105

3.5 Process flow diagram for the fabrication of the MOS device...................... 108

3.6 Process flow diagram for the fabrication of the MIM device (Si Type-2)....... 108

3.7 Process flow diagram for the fabrication of the MIM device with metal film... 109

3.8 Process flow diagram for the fabrication of the free standing B-N-C-H membranes.. 110

3.9 Cross sectional view of the X-ray window... 111

4.1 Variation of average growth rate as a function of temperature.................. 115

LIST OF FIGURES
(Continued)

4.2 Film composition as a function of deposition temperature........................ 116

4.3 Carbon concentration in the films as a function of deposition temperature..... 117

4.4 Variation of growth rate with the flow ratio of the reactants...................... 118

4.5 Variation of Film composition as a function of NH3/TEAB flow ratio.......... 119

4.6(a) Typical FTIR spectrum of BN films at 400°C.. 120

4.6(b) Typical FTIR spectrum of BN films at 550°C.. 121

4.7 Variation in the spectra with the flow ratio at 550 C............................... 121

4.8 Variation of film density with increasing flow ratio of NH_3/TEAB.................. 123

4.9 Variation of refractive index with increasing flow ratio of NH_3/TEAB............ 124

4.10 Variation of film stress with increasing flow ratio of NH_3/TEAB.................. 126

4.11 Optical transmission of BN thin films.. 127

4.12 Optical absorption coefficient α as a function of the incident photon wavelength for varying NH3/TEAB flow ratios.................................. 128

4.13 Determination of the optical band gap from the plot of $(\alpha h\nu)^{1/2}$ vs $h\nu$.......... 129

4.14 X-ray diffraction pattern for a boron nitride film on silicon deposited at a temperature of 575 °C, pressure of 0.05 Torr, TEAB flow rate of 1 sccm, and NH_3 flow rate of 50 sccm.. 131

4.15 Typical MIS capacitance-voltage curves for LPCVD boron nitride............. 133

4.16 Capacitance-frequency plot for BN MIS structures................................ 135

4.17 C-V curve shift along the voltage axis due to (+) or (-) fixed oxide charge...... 136

4.18 Capacitance-Voltage measurements on MIM structures.......................... 138

4.19 Variation of dielectric constant with flow ratio of NH_3/TEAB.................. 139

4.20 I- V characteristics of BN films on (a) type-1 Si and (b) type-2 Si.............. 140

LIST OF FIGURES
(Continued)

4.21 Variation of etch rate of the B-N-C-H films with power........................ 142

4.22 Variation of etch rate of the B-N-C-H films with CH_4 flow.................... 143

4.23 X-ray transmission through the B-N-C-H films of varying thickness........... 143

4.24 Plot of growth rate vs. 1000/T for TiN films..................................... 147

4.25 Variation of Film Composition with Deposition Temperature................. 148

4.26 Plot of growth rate as a function of partial pressure of $TiCl_4$..................... 149

4.27 Plot of growth rate as a function of partial pressure of NH_3.................... 150

4.28 Variation of Film Composition as a Function of TiCl4 Partial Pressure........ 151

4.29 Variation of Film Composition as a function of NH3 Partial Pressure.......... 151

4.30 Elemental compositional analysis by X-ray photoelectron spectroscopy....... 157

4.31 Depth analysis of the TiN films by XPS.. 158

4.32 Depth analysis of the TiN deposits by XPS...................................... 159

4.33 Rutherford backscattering spectrometry of the TiN films....................... 160

4.34 Variation in film density with deposition temperature.......................... 161

4.35 Variation in film density with $NH_3/TiCl_4$ flow ratio............................ 162

4.36 Variation in film stress with deposition temperature............................ 163

4.37 Variation in film resistivity with deposition temperature....................... 164

4.38 Variation in film hardness with deposition temperature........................ 165

4.39 Optical Properties of TiN.. 166

4.40 SEM micrograph of TiN deposited at 475°C and NH_3/TEAB of 10/1.......... 167

4.41 SEM micrograph of TiN deposited at 475°C and NH_3/TEAB of 10/1.......... 168

4.42 SEM micrograph of TiN deposited at 525°C and NH_3/TEAB of 10/1.......... 169

LIST OF FIGURES
(Continued)

4.43 SEM micrograph of TiN deposited at 600°C and NH_3/TEAB of 10/1 170

4.44 X-ray diffraction spectra for TiN 171

4.45 Etching characteristics in $NH_4OH/H_2O_2/H_2O$ solution 173

CHAPTER 1

INTRODUCTION

Legend tells of a very rich and powerful Maharaja in Kashi, called Purushotama (1400 AD), who ruled most of India during its golden period. Known for his generous charities and confidence in his ability at the game of chess, he put forth an open challenge to everyone and promised to grant any wish to the victor. Finally, a wise Brahmin defeated him and on being asked to name his reward, the Brahmin asked only to be given one grain of rice for the first square of the chess board, two for the second, four for the third and so on. Foolishly the king agreed to this seemingly trivial request. Anyone who has never tried to calculate the numbers corresponding to the other squares will appreciate how the repeated doubling rapidly produces huge numbers: the number of grains of rice for the sixty-four square is a nineteen digit number, far in excess of the total number of grains of rice in the world.

The phenomenal rise of the integrated circuit, better known as silicon chip, is due to a similar exponential increase[1]. The origin of the integrated circuit can be traced back to the developments in 1959 by Jack Kilby at Texas Instruments and Robert Noyce at Fairchild Semiconductor Corporation, laying the foundations for what was to follow. Two years later a circuit comprising of four transistors was successfully fabricated on a single piece of silicon, and over the next few years increasingly complex circuits were produced. In 1964 Gordon Moore, also at Fairchild, examined this trend and predicted that the number

of transistors on a chip would continue to double every year. This now famous prediction has come to be known as Moore's law.

Just like the Brahmin's request, it is hard to grasp the implications of Moore's law, and yet Moore's law continues to hold true after thirty-five years. Granted, the rate of increase has slowed down somewhat so that the current rate of increase is closer to a factor of two every two years. Nevertheless, it is now possible to accommodate around 64 million transistors on a single chip. In terms of the chessboard analogy we are at about the twenty-sixth square, with little sign of the progress slowing.

It may be helpful to put the evolution of the computer into a larger historical context. Many computer analysts divide the history of the computer into three or more distinct phases[2]. The first phase was dominated by the clunky but powerful mainframe computer, pioneered by IBM, Burroughs, Honeywell, and others. These systems were so expensive that entire division of scientists and engineers were forced to share one machine.

The second phase of computing began in the early 1970s, when the engineers at Xerox PARC realized that the computer power was exploding even as the size of the chips was imploding. They envisioned a ratio of computers to people that would eventually reach one-to-one. To test their ideas, in 1972 they created ALTO, the first PC ever built.

The third phase of computing is now known as ubiquitous computing, which refers to a time when computers will be connected to each other and the ratio of computers to people

flips the other way, with as many as one hundred computers for every person. It is estimated that by 2020, the era of ubiquitous computing should be in full flower. Beyond 2020, it is likely that the reign of silicon will end and entirely new computer architectures will have to be created. Computer analysts believe that this will lead to a fourth phase, the introduction of artificial intelligence into computing systems. From 2020 to 2050, the world of computers may well be dominated by invisible, networked computers having the power of artificial intelligence, reason, speech recognition, even common sense. “Long-term, the PC and workstation will wither because computing access will be everywhere: in the walls, on wrists, and in ‘scrap computers’ (like scrap paper) lying about to be grabbed as needed.” – Mark Weiser, Xerox PARC. The drive towards invisibility of the PC may be a universal law of human behavior. As Weiser says: “Disappearance is a fundamental consequence not of technology but of human psychology. Whenever people learn something sufficiently well, they cease to be aware of it.”

Today transistors are made by using beams of light to make microscopic grooves and lines on silicon wafers (a process called “photolithography”). Computer experts today debate as to how many transistors can be crammed into a microprocessor by means of this etching process. The Motorola Power PC 620, for example has almost seven million transistors squeezed into silicon chips smaller than a postage stamp. This miniaturization process however cannot continue indefinitely. There is a limit to how many wires can be etched on a wafer. This limit is the result, in part, of the wavelength of the light beam.

Typically, light beams do the etching of silicon wafers from a mercury lamp, which have wavelengths measured in microns. Over the last few decades, Moore's law has been driven by using increasingly smaller and smaller wavelengths of mercury light to manufacture microprocessors. Mercury lamps emit light of wavelength 0.43 micron and 0.365 micron (ultraviolet). These distances are about 300 times thinner than a human hair. The technology that may dominate the first few years of this century, perhaps untill 2005, is based on the pulsed excimer laser, which can push the wavelength down to 0.193 micron (deep UV). But beyond 2020, this process will end and entirely new technologies will be required.

In the past the increase in the number of devices on a chip has been almost totally due to constant improvements in the fabrication methods, enabling ever-smaller devices and more complex circuits to be constructed. Quite amazingly, amidst such a rapidly changing environment, the transistor itself has changed very little. Progress has been made simply be scaling down the dimensions of the individual devices and adjusting certain related properties accordingly. However several factors suggest that this approach may not be viable for much longer. If this trend is to continue into the twenty-first century, a replacement for the conventional semiconductor transistor must be found.

There are several advantages of integration. The prime intention for this dramatic miniaturization has been an economic one. It costs little more to manufacture a chip containing one million components than it does to produce a single discrete device. In addition, the chip already contains the necessary interconnections between the

components, whereas discrete devices have to be individually connected to form a circuit, a process that is both expensive and unreliable. This means that an integrated circuit manufacturer who wants to remain competitive has been forced to follow, if not lead the way, in producing ever more complex circuits on a single chip. The other key factor is performance. Small transistors operate faster than larger ones and at the same time are more reliable since the electrical contacts within an integrated circuit are far less likely to fail than the conventional soldered joints used to attach discrete components on to a circuit board.

At the same time as the circuit size has been increasing, the size of the individual components has decreased substantially. This has been achieved primarily by progressively refining the photolithographic techniques, allowing finer structures to be resolved. The benefits of this reduction in size are easy to appreciate. If we reduce all of the dimensions by a factor of two, then four times as many devices can be squeezed on to the same area as before. Since the cost of a circuit is effectively governed by the surface area that it occupies, this reduces the cost per function by a factor of four. There is also a second major incentive to reduce the size of the individual components, and that is the effect it has on the speed of the operation of the devices. The speed of a MOSFET is governed by the time it takes an electron to cross the gate region. By reducing this distance by a factor of two we therefore also obtain a similar increase in the performance of the devices. These advantages of reduced cost, smaller size and increased performance have fuelled the rapid increase in the number of electronic devices that can be placed on a single chip.

Having the technology to transfer the image to the wafer is not the only problem associated with manufacturing smaller devices. As the size of the individual devices is reduced, the chance of a microscopic dust particle causing a catastrophic failure of one of the elements increases. Also, since several lithographic stages are required, it is vital that each mask should be precisely aligned on the wafer. Current technology is more than able to cope with these requirements, and therefore on the manufacturing side there seems little reason why the progress towards ever-smaller devices should not continue at least into the next century.

A second point concerns the devices themselves. How far can the dimensions of a transistor be reduced before it ceases to function in the desired way? The rules governing the behavior of these structures as the dimensions are reduced, or scaled, are in principle quite straightforward – all the dimensions, both lateral (along the surface of the chip) and vertical (perpendicular to the surface), are reduced by a common scaling factor. Let us consider the implications of applying a scaling factor of two. As we have already seen, this leads to a fourfold increase in the number of devices that can be accommodated within a given area.

Let us suppose for a moment that the current and voltages are maintained at the same levels as before. The electrical power consumed by each device is given by the product of the current and switching voltage. Consequently, the power required by each device remains constant. However, since there are now four times as many devices within a given area, the power requirements per unit area are increased by a factor of four. This poses a

serious problem since the power is converted into heat. Consequently, the amount of heat produced also increases by a factor of four. This excess heat must be dissipated somehow or the temperature of the chip will increase until something catastrophic occurs. As it is, a standard chip produces about the same amount of power as a dim light bulb. This may not sound like terrific amount, but it is actually several times more than the amount of heat produced by the same area of an element on an electric cooker.

The usual way to combat this problem is to apply a technique known as constant field scaling. Since the distance between the source and drain has been reduced by the scaling factor of two, we need to reduce the voltage difference by a similar factor in order to obtain the same gradient as before. The switched voltage is reduced by the scaling factor, as is the current flowing through the device. Consequently, the power produced by each device decreases by a factor of four.

The greatest problems facing further miniaturization of integrated circuits concern the humble interconnect, the tiny connecting lines that form the electrical links between the devices on the chip. Various materials are used to form these conducting elements, ranging from heavily doped silicon, to silicides and metals, principally aluminum and copper. One of the key problems with interconnects is their resistance to the flow of an electric current. The time required for propagation of electrical signals depends on two factors. These are the resistance of the wire to the flow of current, and the capacitance, or amount of charge stored in the system. The time taken for a signal to propagate along a wire is therefore dependent on what is called the RC factor, the product of resistance and

capacitance of the wire. It may seem surprising that the time depends not explicitly on the length of the wire, but there is a strong implicit dependence since both resistance and capacitance vary with the length of the wire.

The most obvious approach when reducing the size of components in integrated circuits is to scale the interconnects in the same manner, so that the width and thickness of the connecting wires are decreased accordingly. We can predict the effects of these measures by considering how the resistance and capacitance change under such scaling. Let us examine capacitance first. The interconnect runs across the top surface of the semiconductor below. The amount of charge stored in the interconnect depends inversely on the thickness of the oxide layer separating the interconnect from the semiconductor wafer. We have proposed that the width of the interconnect is reduced by the scaling factor of two, but how does the length of the interconnect change? For the time being let us suppose that it is also subject to the same factor. From these considerations we estimate that the area of the interconnect in contact with the surface of the oxide is a factor of four times smaller in the scaled circuit. However, this partially offset by the fact that the oxide layer is reduced in thickness, and so overall the capacitance decreases by a factor of two.

This result seems quite promising, but the effects of scaling on resistance are not so good. As the cross-sectional area of the wires is reduced it becomes increasingly difficult for the current to flow through the wires, and so the resistance increases. If both the thickness and width of the interconnects are scaled, then the cross-sectional area is reduced by a factor of four and the resistance increases accordingly. However, since the resistance is

also proportional to the length of the wire, we find that overall the resistance is also proportional to the length of the wire, we find that overall the resistance increases by a factor of two. Since the resistance increases by the same factor as the capacitance decreases, the time delay stays the same as in the unscaled system. This is bad news. Although the switching times of the individual devices are reduced by scaling, the delays in propagating signals between them are not. This suggests that the speed of an integrated circuit will ultimately be limited by the need for devices to communicate with one another.

We have seen that the current flowing between the devices is reduced by a factor of two, but the cross sectional area of the wires is reduced by a factor of four. As a result the current per unit area is twice as large as it was before scaling. Since the decrease in the cross-sectional area also leads to an increase in resistance, this in turn means that more heat is generated as the current flows through the wire. The heat causes the ions to vibrate rapidly, and since they are under constant bombardment from the concentrated flow of electrons, they may literally be wrenched out of their lattice sites. This movement of the ions, known as electromigration, may be so severe that all the atoms in a small region are removed, physically destroying the connection.

This assessment of the effects of scaling the interconnects may seem pessimistic, but in reality the situation can be much worse. We assumed in our argument that the length of the interconnect scales down in proportion to the other dimensions, but this is not necessarily the case. In particular, although great efforts are taken in the layout of the circuits, there is always a requirement for some long interconnects which pass from one

side of the chip to the other. Obviously, these are not reduced in length as the size of the device is reduced. If anything the trend to increase the size of the individual circuits has tended to make these interconnects progressively longer. This poses serious problem. If we repeat the above analysis but consider the interconnect length to remain the same with scaling, then we find that reducing the dimension by a factor of two means that capacitance remains the same, while the resistance increases by a factor of four. In consequence, the time taken for a signal to propagate along these long interconnects will actually increase quite dramatically with scaling.

We arrive at the following conclusion that putting too many devices on a chip may seriously slow down the operating speed of the system. What can be done about this? The answer to any question lies in the 3 pillars of science, which are Matter, Life, and Mind. Matter forms the building block of anything that exists and determines the behavior of the macroscopic properties. In this case there are 4 materials to be dealt with, Semiconductor, Insulator, and Conductor. Gallium Arsenide has already been studied as an alternative for the semiconductor and devices with higher efficiency and speed have been fabricated and used in wireless communication chips. Copper has found its way into the chip by replacing aluminum as the metallic conductor because of its lower resistivity. As for the insulator and conducting materials, the need is for lower dielectric constant, lower resistivity, and higher thermal stability. This has been our motivation for extensively investigating Boron Nitride and Titanium Nitride as promising materials for the above mentioned and several other applications.

Nitride ceramics combine the superior hardness of ceramics with high thermal and mechanical stability, making them suitable for applications as cutting tools, wear-resistant parts and structural components at high temperatures[3]. Boron nitride is a very promising inorganic dielectric material because of its low atomic number, chemical inertness and thermal stability[4]. Titanium nitride on the other hand is attractive as a metallic conducting film with superior mechanical, thermal, optical and electrical properties[5].

The boron nitride films have properties such as multiband electro-, photo-, and cathode-ray luminescence[6], electrically insulating, chemically inert, thermally stable, resistant to corrosion, and having desirable mechanical properties. Potential applications of boron nitride films include using the boron nitride film as high temperature dielectric[7], heat-dissipation coatings[8], passivation layers[6], diffusion sources of boron[9], and sodium barrier[6]. Since boron nitride is highly transparent to x-rays, it can be used in the fabrication of masks for x-ray lithography[10]. Also, the lubricative characteristics of its laminar structure make it a uniquely qualified material for fiber coatings in ceramic matrix composites (CMC)[4].

Titanium nitride is an extensively investigated material because of its many potential applications. It is already widely used as a wear resistant coating on tools[11], as a gold substitute for decorative coatings, and for thin film resistors. The integrated circuit (IC) industry has also shown an increasing interest in TiN because of its thermal stability, good diffusion barrier properties, and low electrical resistivity[12-13]. Recently TiN films have been investigated as a contact layer for silicon and as a gate electrode in

metal/oxide/semiconductor integrated circuits[14]. Potential applications also include solar energy absorber and transparent heat mirror because of its optical properties in the visible and IR regions[15-16]. These different applications of TiN result from its properties, which depend on the composition (Ti:N ratio), impurity (O_2,Cl,etc.) content and the structure, which in turn depend on the growth technique used and the deposition parameters employed.

The RC time delay can be reduced by using a low dielectric constant material between the interlevel metals, or by using a refractory low resistivity barrier material between the poly and the metal film. This results in a reduction of the wiring capacitance between interlevel metals and a decrease in the resistance of the metallic film, which enhances switching performance. A desirable interlevel dielectric (ILD) material should exhibit, in addition to a low dielectric constant, low mechanical stress, high thermal stability, and low moisture absorption. Several ILD candidates have been explored over the last few years including fluorinated SiO_2[17-27], fluorinated polymers[28,29], aerogels, and boron nitride[30,31]. Boron nitride films produced by LPCVD offer an attractive combination of properties that include high mechanical strength, good optical and x-ray transparency, chemical inertness, low coefficient of thermal expansion, high thermal conductivity and thermal stability. A desirable conducting metallic film should exhibit good thermal stability and chemical passiveness, in addition to low resistivity. In recent years, Titanium nitride films are conventionally deposited by reactive sputtering[32], however these films suffer from poor step coverage due to the shadowing effect, resulting in inadequate heat resistance. LPCVD can realize such desirable properties if the surface reaction deposition mechanism

is dominant. Presence of chlorine in the TiN films is a reliability threat and is likely to shorten the lifetime of an integrated circuit, because the metal alloy on the TiN film could be easily corroded by chlorine. All the current and potential applications of the B-N-C-H and Ti-N-Cl films depend on the film properties which further depends on the growth parameters. Hence, a study was initiated to investigate the influence of the process parameters on growth rate and film properties of LPCVD TiN.

1.1 Thin-Film Deposition Methods

Thin-film deposition techniques have traditionally been used in the microelectronics industry for microchip coating, wear and corrosion resistance, and thermal protection. Deposition methods can be classified under two groups: Physical Vapor Deposition (PVD) and Chemical Vapor Deposition (CVD).

1.1.1 Physical Vapor Deposition

Physical vapor deposition (PVD) is mainly focused into two categories, evaporation and sputtering. The objective of these deposition techniques is to controllably transfer atoms from a source to a substrate where film formation and growth proceed atomistically, without the need of a chemical reaction.

In evaporation, atoms are removed from the source by thermal means, whereas in sputtering the atoms are dislodged from a solid target by the impact of gaseous ions. Advances in vacuum-pumping equipment and Joule heating sources spurred the emergence of PVD as a suitable industrial film deposition process. In general, the

properties of the film obtained by PVD are governed by the following: evaporation rate of the atoms, vapor pressure of the target materials, deposition geometry, temperature, pressure, and thermal history of the substrate[28].

Traditionally, evaporation was the preferred PVD technique over sputtering. Higher deposition rates, better vacuum (thus cleaner environments for film formation and growth), and versatility in the fact that all classes of materials can apply were some of the reasons for the dominance of evaporation. The microelectronics revolution required the use of alloys with strict stoichiometric limits, which had to conformally cover and adhere well to substrate surfaces. This facilitated the need for the sputtering technique and so, as developments were made in radio frequency, bias, and magnetron variants, so were advances made in sputtering. The decision to use either technique depends solely on the desired application and has even spurred the development of hybrid techniques[28]. A comparison of the two is given in Table 1.1.

Table 1.1 Evaporation vs. Sputtering

Evaporation	Sputtering
A. Production of Vapor Species	
1. Thermal evaporation mechanism	Ion bombardment and collisional momentum transfer
2. Low kinetic energy of evaporant atoms (@ 1200 K , E = 0.1 eV)	2. High kinetic energy of sputtered atoms (E = 2-30 eV)
3. Evaporation rate ~ 1.3 x 10^{17} atoms/cm^2-sec	3. Sputter rate ~ 3 x 10^{16} atoms/cm^2-sec
4. Directional evaporation according to cosine law	4. Directional sputtering according to cosine law at high sputter rates
5. Fractionation of multicomponent alloys, decomposition, and dissociation of compounds	5. Generally good maintenance of target stoichiometry, but some dissociation of compounds
6. Availability of high evaporation source purities	6. Sputter target of all materials are available; purity varies with material
B. The Gas Phase	
1. Evaporant atoms travel in high or ultrahigh vacuum (~ 10^{-6} - 10^{-10} torr) ambient	1. Sputtered atoms encounter high pressure discharge region (~ 100 mtorr)
2. Thermal velocity of evaporant 10^5 cm/sec	2. Neutral atom velocity ~ 5 x 10^4 cm/sec
3. Mean-free path is larger than evaporant-substrate spacing; evaporant atoms undergo no collisions in vacuum	3. Mean-free path is less than target-substrate spacing; Sputtered atoms undergo many collisions in the discharge
C. The Condensed Film	
1. Condensing atoms have relatively low energy	1. Condensing atoms have high energy
2. Low gas incorporation	2. Some gas incorporation
3. Grain size generally larger than for sputtered film	3. Good adhesion to substrate
4. Few grain orientations (textured films)	4. Many grain orientations

Chemical vapor deposition is discussed next. Some factors that distinguish PVD from CVD are:

1. Reliance on solid or molten sources
2. Physical mechanisms (evaporation or collisional impact) by which source atoms enter the gas phase
3. Reduced pressure environment through which the gaseous species are transported.
4. General absence of chemical reactions in the gas phase and at the substrate surface (reactive PVD processes are exceptions).

1.1.2 Chemical Vapor Deposition

Chemical Vapor Deposition (CVD) is one of the most important methods of film formation used in the fabrication of very large scale integrated (VLSI) silicon circuits, as well as of microelectronic solid state devices in general. It may be defined as the formation of a non-volatile solid film on a substrate by the reaction of vapor phase chemicals (reactants) that contain the required constituents. In this process, chemicals in the gas or vapor phase are reacted at the surface of the substrate where they form a solid product. A large variety of materials, practically all those needed in microelectronic device technology, can be created by CVD. These materials comprise insulators and dielectrics, elemental and compound semiconductors, electrical conductors, superconductors and magnetics. In addition to its unique versatility, this materials synthesis and vapor phase growth method can operate efficiently at relatively low temperatures. For example, refractory oxide glasses and metals can be deposited at temperatures of only 300° to 500°C. This feature is very important in advanced VLSI devices with short channel lengths

and shallow junctions, where lateral and vertical diffusion of the dopants must be minimized. This also helps in minimizing process-induced crystallographic damage, wafer warpage and contamination by diffusion of impurities.

1.1.2.1 Overview of Chemical Vapor Deposition Process: The individual process steps in the CVD technique are outlined as follows[33]:

1. Mass transport in the bulk gas flow region from the reactor inlet to the deposition zone.
2. Gas phase reactions leading to the formation of film precursors and byproducts.
3. Mass transport of film precursors to the growth surface.
4. Adsorption of film precursors on the growth surface.
5. Surface diffusion of film precursors to growth sites.
6. Incorporation of film constituents into the growing film.
7. Desorption of byproducts of the surface reactions.
8. Mass transport of byproducts in the bulk gas flow region away from the deposition zone towards the reactor exit.

Schematically, this is seen in Figure 1.1.

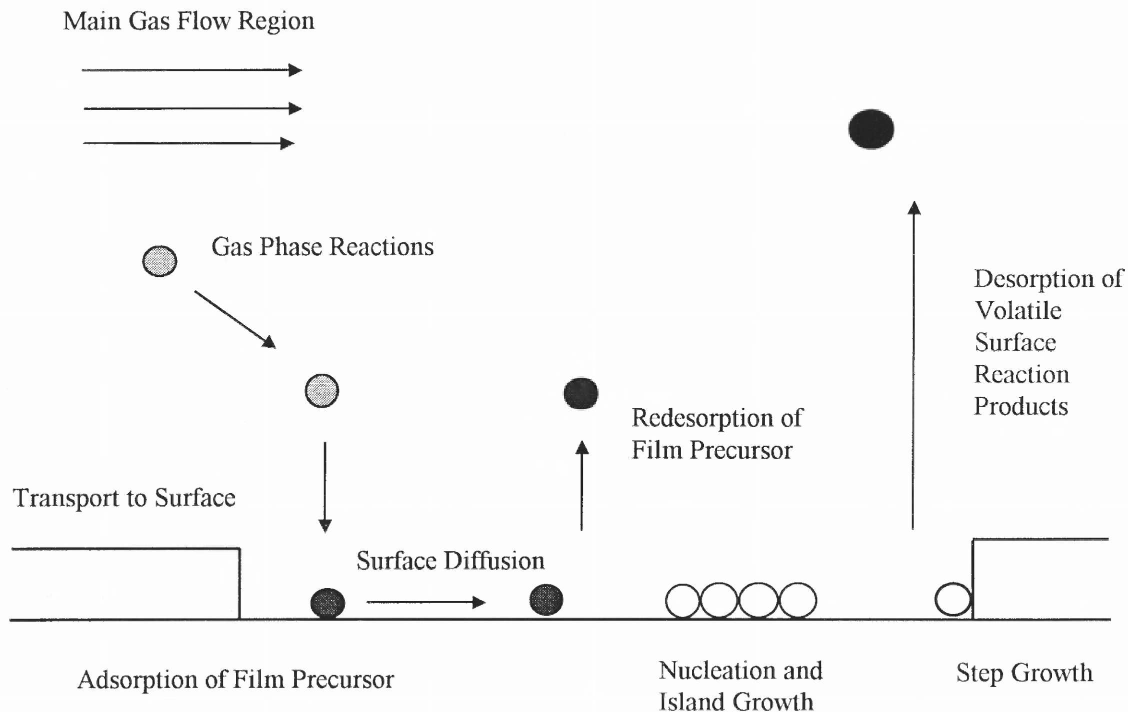

Figure 1.1 Scheme to show the transport and reaction processes underlying CVD.

1.1.2.2 CVD Reactor Systems: CVD reactors are designed to obtain optimal film thickness, crystal structure, surface morphology, and interface composition. A CVD reactor system typically consists of a reagent handling arrangement for delivering the source compounds, a reactor unit, and an exhaust system. The reagent handling system mixes and meters the gas mixture to be used in the reactor. The design depends on the source compounds. Gaseous sources are fed from a high pressure gas cylinder through a mass flow controller, in this case nitrous oxide. Liquid and solid sources are typically used by contacting them with a carrier gas in a bubbler. The source temperature, carrier gas

flow rate, and the total pressure of the source determine the amount of reagent transported from the bubbler. In this study, a carrier gas is not needed because of the high vapor pressure of DES and the low pressure nature of the deposition. The need for films with reproducible and controllable optical, electrical, and mechanical properties means that CVD reagents must be pure, must not produce byproducts that incorporate into the growing film or interact with gas handling and reactor construction materials.

There are a wide variety of CVD reactor geometries used to accommodate the many CVD applications. These include horizontal reactor, vertical reactor, barrel reactor, pancake reactor, and multiple-wafer-in-tube LPCVD reactor. Essentially, this study involves a multiple-wafer-in-tube LPCVD (low pressure chemical vapor deposition) reactor. LPCVD is the main production tool for polycrystalline silicon films, especially for the films used in the microelectronics industry[19-21]. A typical configuration for this reactor is shown in Figure 2.2. This reactor operates around 0.5 Torr and wall temperatures are approximately equal to those of the deposition surfaces. The main advantage of LPCVD is that is allows a large number of substrates to be coated simultaneously while maintaining film uniformity. This is a result of the large diffusion coefficient at low pressures, which makes the growth rate limited by the rate of surface reactions rather than the rate of mass transfer to the substrate.

Finally, the exhaust system treats the effluents so that hazardous byproducts are disposed of in a safe and environmentally sound manner. Mechanical pumps are typically added for

the low-pressure operation. Dry and wet chemical scrubbers, as well as pyrolysis units, are used to clean up the reactor effluent.

1.1.2.3 Nucleation and Growth: The growth of a thin film by CVD is initiated by exposing a substrate to the film precursors in the reactor. The resulting growth and microstructure of the film is determined by surface diffusion and nucleation processes on the growth interface, which are influenced by the substrate temperature, reactor pressure, and gas-phase composition. An amorphous film is formed at low temperatures and high growth rates when the surface diffusion is slow relative to the arrival of film precursors. At high temperatures and low growth rates, the surface diffusion is fast relative to the incoming flux, allowing the adsorbed species to diffuse to step growth and to form epitaxial layers replicating the substrate lattice. Nucleation occurs at many different points on the surface at intermediate temperatures and growth rates. Adsorbed species then diffuse to the islands which grow and coalesce to form a polycrystalline film. The presence of impurities increases the nucleation density. CVD film growth modes may be characterized in terms of three main growth models for thin films: Volmer-Weber growth (three-dimensional island growth), Franck-van der Merwe growth (two-dimensional layer by layer), and Stranski-Krastanov growth (layer plus island)[33].

1.1.2.4 Chemical Reactions and Kinetics: The versatility of the CVD technique is demonstrated through the multitude of films synthesized by various reaction schemes, including pyrolysis, reduction, oxidation, and disproportionation of the reactants. The underlying chemistry is typically a complex mixture of gas-phase and surface reactions.

The fundamental reaction pathways and kinetics have been investigated for only a few well characterized, industrially important systems. These include silane chemistry (pertinent to this study and discussed in detail in the experimental procedure) and thus silicon deposition, free-radical reactions, and intramolecular reactions of organometallic compounds.

1.1.2.5 Reaction Mechanism in CVD: Adsorption, surface reaction and desorption are important steps in the CVD process, which need to be understood properly in order to be able to explain the reaction mechanism.

- ***Adsorption and Desorption:*** CVD reactions being surface catalyzed, reactants adsorb on the surface. The simplest expression for the amount of a gas adsorbed on a surface, is given by the Langmuir Adsorption Isotherm[34] as:

$$\theta = KP/(1+KP)$$

where: θ = fraction of the total sites adsorbed by the gas,

P = pressure of the gas,

K = equilibrium adsorption constant for the gas.

In CVD reactions, many times, both the reacting species adsorb onto the surface, thereby resulting in what is known as competitive adsorption. The adsorption isotherm in this case is given by:

$$\theta_A = K_A P_A / (1 + K_A P_A + K_B P_B) \quad (1.1)$$

$$\theta_B = K_B P_B / (1 + K_A P_A + K_B P_B) \quad (1.2)$$

where: θ_A, θ_B = fraction of total sites covered by species A and B,

K_A, K_B = equilibrium adsorption constant for species A and B,

P_A, P_B = partial pressure of species A and B.

- ***Reaction:*** The surface catalyzed reaction in a CVD process is usually a bimolecular reaction between the two adsorbed species. In that case, the rate of the reaction is dependent on the concentration or the fraction of the sites occupied by each of the species. If this reaction is the rate determining step, which it usually is, the rate of film deposition can be given as:

$$\text{rate} = k\theta_A\theta_B$$

$$\therefore \text{rate} = kK_AK_BP_AP_B/(1+K_AP_A+K_BP_B)^2 \qquad (1.3)$$

This method of treating a surface catalyzed reaction is known as the Langmuir-Hinshelwood kinetics[34]. If one of the pressures is maintained constant and the other is varied, the rate first increases, passes through a maximum and then decreases. The falling off of the rate at high pressures can be explained to be due to the fact that one reactant displaces the other reactant, as its pressure is increased. Two special cases of equation 1.3 are[34]:

1) Sparsely covered surfaces, where both P_A and P_B are sufficiently low (due to dilution or very high vacuum), for the pressure terms in the denominator to be neglected, so that the rate equation (1.3) becomes,

$$\text{rate} = kK_AK_BP_AP_B \qquad (1.4)$$

2) When reactant A is weakly adsorbed (i.e. $K_A << 1$), the term K_AP_A in the denominator in equation 1.3 might be neglected to give,

$$\text{rate} = kK_AK_BP_AP_B/(1+K_BP_B)^2 \qquad (1.5)$$

Further if the reactant B is very strongly adsorbed so that $K_BP_B >> 1$, we have,

$$\text{rate} = kK_AP_A/K_BP_B \qquad (1.6)$$

1.1.2.6 Transport Phenomena: Fluid flow, heat transfer, and mass transfer are all characterized under transport phenomena. Transport phenomena govern the access of film precursors to the substrate and influence the degree of desirable and unwanted gas-phase reactions taking place before deposition. The complex reactor geometries and large thermal gradients of CVD reactors lead to a wide variety of flow structures impacting film thickness and composition uniformity, as well as impurity levels. Direct observation of flow is difficult because of a lack of a suitable visualization technique for many systems and because of practical constraints such as no optical access and possible contamination of a production reactor. Therefore, experimental observations and approximately chosen computer models are employed on individual systems[35].

The sequential steps of deposition process can be grouped into (i) mass transport-limited regime and (ii) surface-reaction-limited regime. If the mass transfer limits the deposition process, the transport process occurred by the gas-phase diffusion is proportional to the diffusivity of the gas and the concentration gradient. The mass transport process that limits the growth rate is only weakly dependent on temperature. On the other hand, it is very important that the same concentration of reactants be present in the bulk gas regions adjacent to all locations of a wafer, as the arrival rate is directly proportional to the concentration in the bulk gas. Thus, to ensure films of uniform thickness, reactors that are operated in the mass-transport-limited regime must be designed so that all locations of wafer surfaces and all wafers in a run are supplied with an equal flux of reactant species.

If the deposition process is limited by the surface reaction, the growth rate, R, of the film deposited can be expressed as $R = R_o * \exp(-E_a/RT)$, where R_o is the frequency factor, E_a is the activation energy, usually 25-100 kcal/mole for surface process, R is the gas constant, and T, the absolute temperature. In the operating regime, the deposition rate is a strong function of the temperature and an excellent temperature control is required to achieve the film thickness uniformity that is necessary for controllable integrated circuit fabrication.

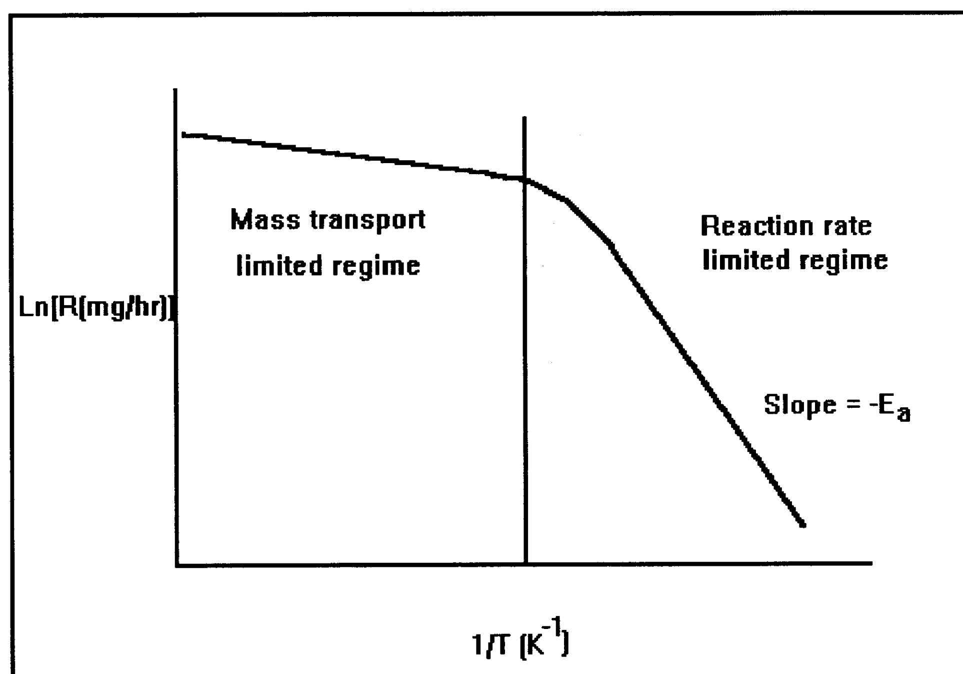

Figure 1.2 Deposition rate as a function of substrate temperature exemplifying diffusion controlled and surface-reaction controlled regimes

On the other hand, under such conditions the rate at which reactant species arrive at the surface is not as important. Thus, it is not as critical that the reactor be designed to supply an equal flux of reactants to all locations of the wafer surface. It will be seen that in horizontal low-pressure CVD reactors, wafers can be stacked vertically and at very close

spacing because such systems operate in a surface-reaction-rate limited regime. In deposition processes that are mass-transport limited, however, the temperature control is not nearly as critical. As shown in Figure 1.2, a relatively steep temperature range, and a milder dependence in the upper range, indicating that the nature of the rate-controlling step changes with temperature.

1.1.2.7 Factors Affecting Film Uniformity: Some of the main factors affecting the film thickness uniformity in LPCVD are the temperature profile in the reactor, the pressure level in the reactor and the reactant gas flow rates. To obtain a flat thickness profile across each substrate wafer throughout the reactor requires a judicious adjustment of these parameters. In tubular reactors, increase in temperature or pressure, increases the deposition rate upstream, thereby using up more reactant gases and leaving less to react at the downstream end; the opposite effect takes place on lowering the temperature and pressure. Similar effects occur with variations of the reactant gas flow rates at constant gas partial pressure, or with changes in the size and number of the wafers processed per deposition run. The uniformity of thickness and step coverage of these films are very good. These films have fewer defects, such as particulate contaminants and pinholes, because of their inherently cleaner hot wall operations and the vertical wafer positioning that minimize the formation and codeposition of homogeneously gas phase nucleated particulates.

1.2 Types of CVD Process

As mentioned in the previous section, chemical reactions are very intrinsic to any CVD process and hence energy in some form or the other must be provided for the desired chemical reaction to take place. This energy could be supplied by heat (thermal), by an electric glow discharge (plasma) or by some kind of electromagnetic radiation (e.g. laser). Depending on the type of energy supplied to initiate and sustain the reaction, CVD processes have been classified as[35] : (i) Plasma enhanced CVD, (ii) Photo induced CVD, or (iii) Thermally activated CVD.

1.2.1 Plasma Enhanced CVD (PECVD)

In this method, gaseous reactants are introduced in a region of glow discharge (plasma) created by applying an electric field, using A/C, D/C or microwave sources, between two electrodes. This results in the formation of highly reactive species, which react and form a solid thin film product on the substrate and electrode surfaces. The molecules can be near to the ambient temperature but the breakdown electrons will be at higher temperatures, causing the reaction. Thus this method can be employed at relatively low temperature and is useful for temperature sensitive materials. Film deposition rates are substantially higher in this method than in thermally activated CVD. Also, conformal step coverage can be achieved. However, the disadvantage of this method is the complex process that occurs in the plasma state making the synthesis of stoichiometric films difficult.

1.2.2 Photo Induced CVD

Short wavelength UV radiation is used to activate the reactants in the gaseous phase forming the product material. A selective absorption of photon energy by the reactant molecules or atoms initiates the process. The advantage of this method is low deposition temperature (needed for films like SiO_2) and absence of radiation damage. The limitation of this method is unavailability of effective production equipment. In another type, laser beams are used for activating the reactants. In yet another type, the reactant atoms or molecules absorb a specific wavelength of the laser energy applied resulting in chemical gas phase reaction that are very specific, leading to highly pure film deposits. But, these methods are still in developing stages[35].

1.2.3 Thermally Activated CVD

This process uses direct thermal energy for the chemical reaction. The simplest type of this CVD is the conventional atmospheric pressure CVD (APCVD) where the reactant gases are allowed into the chamber at normal atmospheric pressure. Energy is supplied by heating the substrate directly. The temperature and the reactant flow rates determine the film growth rate. The advantage of the APCVD is its simplicity in that no vacuum pumps are needed. The disadvantage is the tendency for homogeneous gas phase nucleation, which leads to particle contamination, unless special optimized gas injection techniques are used. The deposition rate and uniformity of the films deposited using CVD process can be determined by the rate of mass transfer of reactant gases to the substrate, or the rate of surface reaction of the reactant gases. In atmospheric pressure CVD, these two rates are of the same magnitude.

Lowering the gas pressure by about 3-4 orders of magnitude enhances the mass transfer rate relative to the surface reaction rate. This makes it possible to deposit films uniformly with a highly economical close spaced positioning of the substrate wafers kept vertically inside the chamber. Thus low pressure CVD (LPCVD) is a widely used method in cost competitive semiconductor industry. Another advantage of this method is that the gas phase nucleation is reduced.

Depending on the method of supply of thermal energy, CVD reactors can be classified as either hot wall or cold wall reactors. In a hot wall reactor system, the reactor is heated to a high temperature and the gas molecules hitting the wall receive the thermal energy. Here, the substrate is indirectly heated. The advantage of this system is a temperature gradient that can be provided to the chamber, which results in uniform thickness. In the cold wall system, the substrate is heated to high temperature directly. The reactants that are adsorbed on the surface undergo chemical change due to the temperature of the substrate. But in this case, controlling the wafer's temperature is difficult and hence uniform deposition is difficult to achieve.

1.3 Low Pressure Chemical Vapor Deposition (LPCVD) Process

Most LPCVD processes use resistance heating to attain isothermal conditions so that the substrate and the reactor walls are of similar temperature. However, infrared radiation heating techniques are also sometimes used.

The mass transfer of the gases involves their diffusion across a slowly moving boundary layer adjacent to the substrate surface. The thinner this boundary layer and the higher the gas diffusion rate, the greater is the mass transport that results. Surface reaction rates, on the other hand, depend mainly upon reactant concentration and deposition temperature. In LPCVD, the rate of mass transfer is enhanced with respect to the heterogeneous surface reaction rate by lowering the gas pressure. This improved rate of mass transfer makes it possible to deposit films uniformly even on closely placed wafers. Moreover, high deposition rates are attainable with LPCVD because of the large mole fraction of reactive gases in the reactor, since no or little diluent gas is required[36].

Some of the main factors affecting the film thickness and uniformity in LPCVD are the temperature profile in the reactor, the pressure level of the reactor and the reactant gas flow rates. To obtain a uniform thickness profile across each substrate wafer throughout the reactor, a judicious adjustment of these parameters is required[37]. In general, the uniformity of thickness and step coverage of the films obtained by LPCVD is very good. These films have fewer defects, such as particulate contaminants and pinholes, due to their inherently cleaner hot wall operations and the vertical wafer positioning that minimize the formation and codeposition of gas phase particulate[37].

1.3.1 Advantages of CVD

Thin films are used in a host of applications in VLSI fabrication, and can be synthesized by a variety of techniques. Regardless of the method by which they are formed, however, the process must be economical, and the resultant films must exhibit uniform thickness, high

purity and density, controllable composition and stoichiometries, high degree of structural perfection, excellent adhesion and good step coverage. CVD processes are often selected over competing deposition techniques because they offer the following advantages:

1. A variety of stoichiometric and non-stoichiometric compositions can be deposited by accurate control of process parameters.
2. High purity films can be deposited that are free from radiation damage without further processing.
3. Results are reproducible.
4. Uniform thickness can be achieved by low pressures.
5. Conformal step coverage can be obtained.
6. Selective deposition can be obtained with proper design of the reactor.
7. The process is very economical because of its high throughput and low maintenance costs.

1.3.2 Limitations of CVD

Fundamental limitations of CVD are the chemical reaction feasibility and the reaction kinetics that govern the CVD processes. Technological limitations of CVD include the unwanted and possibly deleterious but necessary by-products of reaction that must be eliminated, and the ever present particle generation induced by homogeneous gas phase nucleation that must be minimized.

1.4 Dielectric Materials

A dielectric is a material of low dc electrical conductivity and hence a good insulator or storage medium of electric energy as in a capacitor. Dielectrics play an important role in the fabrication and development of semiconductor microcircuits. Their major functions have been for the isolating circuit elements, impurities, masking against oxygen and dopant diffusion, passivating and protecting device surfaces, insulating double-level conductor lines, and tapering or planarizing the device topography.

The requirements of these dielectric materials in the form of thin films for VLSI circuits for high density devices featuring linewidths in the low micron to submicron range, should have minimal structural defects and good step coverage. The particle density must be as low as possible, and the size of the particulate contaminants should not exceed 25% of the smallest feature size in the integrated circuit to avoid electrical failures of device reliability problems.

1.4.1 Requirements of Dielectric Materials for VLSI Technology

Dielectric films for insulating applications of multiple level VLSI devices must sustain relatively high dielectric breakdown fields, should have a low dielectric constant (to minimize the parasitic capacitance between conductors) and a high electrical resistivity, must have a low loss factor for high frequency applications, must be free of pinholes and microcracks and should have a low compressive stress and excellent adhesion properties. In addition, depending on the layer structure, some of the films must allow hydrogen to diffuse through to allow removal of interface states by annealing in hydrogen, and be able

to block alkali ions. All films must be readily depositable at temperatures compatible with the device structural materials and device performance requirements, with excellent compositional control and good step coverage. There materials must be patternable by precision lithography and selective etching.

Table 1.2 Desired dielectric constant (K) for future technologies[9]

Technology (MFS* in μm)	Maximum number of wiring levels**	Dielectric	K	Year
0.35	4 – 5	SiO_2 or SiO_2 (F)	3.9	1995
0.25	5	Polymer	3 – 3.7	1998
0.18	5 – 6	Polymer	< 3	2001
0.13	6	Polymer	≤ 2 – 5	2004
0.1	6 – 7	Polymer / aerogels / air	1 – 2	2007
0.07	7 – 8	Polymer / aerogels / air	1 – 2	2010

* MFS = minimum feature size; ** microprocessor

1.4.2 Requirements for Low Dielectric Constant ILD Materials

The electrical, chemical, mechanical and thermal requirements for the interlayer dielectric materials may be summarized in a table as follows:

Table 1.3 Properties of ILD[9]

Electrical	Mechanical	Chemical	Thermal
K, anisotropy	Film thickness/ unif	High chemical resist	High th stability
Low dissipation	Adhesion	High etch sel	T_g
Low leakage	Low stress	Low moist abs	Low TCE
Low charge trap	High tensl modulus	Low sol in H2O	Low th shrink
High E strength	High hardness	Low gas perm	High th cond
High reliability	Low shrinkage	High purity	

1.4.3 Applications of Dielectric Materials in VLSI Technology

A. In device structures for

- isolation of circuit elements
- vertical insulation of high-temperature conductor levels in multilevel structures (polysilicon, silicides, refractory metals)
- vertical insulation of low-temperature conductor levels in multilevel structures (aluminum and its alloys)
- alkali ion and moisture barrier
- impurity gettering
- contour leveling or planarization
- over-metal top passivation

B. For temporary layers and processing aids as

- masking structures against oxidation
- gettering layers for impurities
- sacrificial material in lift-off patterning

1.4.4 BN as a Dielectric Material

CVD BN has unique properties because it is usually highly oriented, which emphasizes the effect of the layered structure. The boron and nitrogen atoms are 1.46 Å apart in the ab plane and the layers are separated by 3.34 Å. Thus properties such as thermal expansion and electrical resistivity differ in directions parallel and perpendicular to the substrate surface. The large c direction spacing makes it easy for the planes to slip over one another giving BN good lubricating properties.

Some of the attractive properties of BN are its low deposition temperature, high insulation, high passivation effects against moisture and the alkali metal ions, conformal step coverage, high crack resistance and chemical inertness. It starts dissociating at 2700°C in vacuum and is oxidized in air only at temperatures as high as 1200°C. It has a reported dielectric constant close to that of silicon dioxide and electrical resistivity in the order of 10^{14}ohm-cm with a dielectric strength in the order of 10^6 V/cm and an optical band gap of 4-6 eV. This makes a good material to study the electrical properties.

Table 1.4 Properties of CVD boron nitride dielectric[4]

Tensile strength (ksi)	6
Modulus (Msi)	3.6
Flex strength (ksi)	15
Poisson's ratio	-0.025
Thermal conductivity (W/M.K)	a-62.7 c-1.45
Coeff. T.E. (10^{-6})	a-3.24 c-81
Electr. Resist. (ohm-cm, 437 /°C)	a-3 x 10^7 c-3 x 10^9
Dielectric strength (V/mil)	c-4000
Dielectric constant (5 x 10^9 Hz)	a-5.1 c-3.4
Loss tangent	3 x 10^{-4}
Density (g/cm^3)	2.22
Melting point	3000 °C

1.4.5 Borane Triethylamine Complex as a Precursor

Extensive work has been done on the chemical vapor deposition of BN thin films on various substrates including silicon, quartz, and glass. A wide range of precursors have been used to obtain these thin films which include diborane, borontrichloride, triethyl boron, dicarborane and borane triethylamine (TEAB). TEAB has several advantages over many of the other precursors. Table 1.1 gives some of the properties of TEAB.

Table 1.5 Properties of TEAB (Aldrich Chemicals)

Chemical name	Borane triethylamine complex (TEAB)
Chemical formula	$(C_2H_5)_3N.BH_3$
Molecular weight (g/mol)	115.03
Specific gravity (g/cc)	0.777
Freezing Point	-3°C
Boiling point	97°C
Appearance	Colorless liquid
Vapor pressure	20 Torr at 97°C
CAS Registry number	1722-26-5

TEAB is a relatively non-toxic and non-pyrophoric substance and this obviates the need for expensive cabinets and a cross-purging gas supply for safety reasons. However, TEAB has a low vapor pressure and hence has to be forced into the reactor under high pressure.

1.5 Refractory Materials

Ceramic materials are inorganic, nonmetallic materials which consist of metallic and nonmetallic elements bonded together primarily by ionic and/or covalent bonds. In general most ceramic materials have low thermal conductivities due to their strong ionic-covalent bonding and are good thermal insulators. Because of their ability to resist the action of hot environments, both liquid and gaseous, such materials are termed as refractory materials. Low resistivity interconnection paths are critical in order to fabricate dense, high performance devices. These materials are characterized by extremely high hardness, very high melting points, and resistance to chemical attacks. Hence these materials find applications as hard coating materials, diffusional, protective, and thermal coatings.

1.5.1 Application of Refractory Materials in ULSI

In contrast to the dielectric materials discussed in the previous sections, these materials have only become of interest recently for ULSI. Up to the present, the integrated circuit gate electrodes have been fabricated from LPCVD polysilicon, which is heavily doped with phosphorus. Such heavily doped polysilicon can have resistivities as low as 500 $\mu\Omega$-cm, so it behaves as a conductor, although not a very good one. Its compatibility with standard processing steps, however, makes it a very attractive gate material. The final metallization of the standard single-layer metal conductor circuits have been provided by sputtered aluminum. As required, the sputtered Al can be doped with Si to minimize spiking of Al into the Si that it must contact. It can also be doped with copper to minimize electromigration effects.

In recent years, ULSI requirements have led to closely spaced long interconnection lines with smaller cross sections. The ensuing RC time delay can limit the speed with which circuits can be operated. Also, the power consumption due to high resistance can be appreciable and heat the circuits more than permitted. Therefore, the doped poly available is becoming inadequate for the new generation of circuits. This has led to the development of refractory metal silicide films because of their high-temperature processing capability and low resistivities. These are WSi_2, $MoSi_2$, $TaSi_2$, and $TiSi_2$. The properties of silicides and refractory metals is shown in Table 1.6.

Table 1.6 Properties of silicides and refractory metals

Material	Melting Point (°C)	Resistivity (μΩ-cm)	Thermal Coeff. of Expansion (10^{-6}/°C)
Si	1420	500 (heavily doped)	3.0
TiSi2	1540	13 – 17	10.5
MoSi2	1870	22 - 100	8.2
TaSi2	2400	8 – 45	8.8
WSi2	2050	14 - 17	6.2
Ti	1690	43 - 47	8.5
Mo	2620	5	5.0
Ta	2996	13 - 16	6.5
W	3382	5.3	4.5

The first problem occurs with the gate electrode. The solution that has been developed has been to create a "polycide" structure. Here, a thin layer of phosphorus-doped poly is

deposited and then a conducting layer of silicide is deposited on top of the first layer. The combination is a much better conductor than the doped poly. The common choices for polycide applications are the refractory-metal silicides, which include WSi2, MoSi2, TiSi2 and TaSi2, among which titanium disilicide is the most promising candidate owing to its low resistivity and schottky barrier height of 0.55 eV to n-type silicon; this is advantageous in the formation of ohmic contacts. As ULSI requirements become more demanding, multilevel conductor circuits are being developed. The final metallization layer can be aluminum, since there are no additional processing steps that require temperatures above 350 C. However, if we wish to use a second conductor level between the gate electrode and the final metallization, then aluminum is no longer acceptable. It melts at about 660 C, should not be heated above 500 C, and there would be additional processing steps well above these temperatures. Some IC developers have tried to develop low-temperature processing techniques for dielectrics, and others have tried to use multiple layers of polysilicon in this application. Both approaches have severe short comings, so CVD of refractory metals has some attraction. The resistivity of the refractory metals or silicides are not as good as aluminum, but for tungsten or molybdenum, it can be within a factor of two, a large improvement over poly. The low resistivity refractory materials find application as low resistance gate interconnections, ohmic contacts, planarized low resistance vias, and contact barrier materials.

1.5.2 TiN as a Refractory Interconnect Material

From a device point of view, the use of heavily-doped n-type poly-Si films as gate materials even in a polycide structure has a major disadvantage in the CMOS technology.

Using n+ poly-Si as the gate electrode for each type of device, the work-function difference, ϕ_{ms}, will be different for the n- and p-channel transistors thereby causing an asymmetry in threshold voltages[38]. The performance of p-channel devices can be improved by using, as the gate electrode, a conductive material having a work function very close to the mid-gap of silicon; thereby the step for threshold voltage adjustment is considerably simplified. Refractory metal nitrides seem to be convenient for this purpose and TiN is the most promising candidate for its relatively low resistivity and the work function value near Si midgap, which enables both types of transistors to operate in surface channel mode[38]. Further, upon high temperature processing of polycide, the metal component of the silicide diffuses into the gate oxide causing the failure of the device. This creates the need for low resistivity diffusion barrier materials like TiN, TiW, and WSi_2. TiN barrier seems to be the most preferred due to its inertness and processing ease. The high conductivity and fine-line patternability of refractory metals makes them attractive gate materials in ULSI applications. However, W and Mo are not used as stand-alone conductor materials due to poor adhesion to SiO_2 surfaces. Instead, a layer such as Ti, TiW, or TiN is required under W or Mo films to promote adhesion to SiO_2. The physical properties of TiN have been listed in Table 1.6.

Table 1.7 Physical properties of titanium nitride[39]

Melting Point	3200 °C
Thermal Expansion	8×10^{-6} °C^{-1}
Thermal Conductivity	24 W/m-K
Hardness	1770 kg/mm^2
Resistivity	30×10^{-6} Ω-cm
Density	5.4 g/cm^3
Young's Modulus	36 Msi

Table 1.8 Properties of titanium tetrachloride (Alfa Aesar, Inc)

Chemical name	Titanium Tetrachloride
Chemical formula	$TiCl_4$
Molecular weight (g/mol)	189.88
Specific gravity (g/cc)	1.726
Freezing Point	-25 °C
Boiling point	136.4 °C
Appearance	Colorless to light yellow liquid
Vapor pressure	10mm Hg @ 20 °C
CAS Registry number	7550-45-0

1.5.3 Titanium Tetrachloride and Ammonia as Precursors

In this study, titanium tetrachloride ($TiCl_4$) and ammonia (NH_3) are used as precursors to deposit a titanium nitride film on silicon substrates by low pressure chemical vapor deposition (LPCVD). Some properties of $TiCl_4$ used for the study are listed in Table 1.7.

1.6 Objectives of this Study

This thesis seeks to: (a) study the growth kinetics of the reaction and establish a rate equation, (b) characterize the mechanical, optical, chemical, electrical, and structural properties of the deposited films, (c) study the effect of variation in the process parameters on these film properties, and (d) study the feasibility of using these materials for a wide range of applications. The primary goals of the present work are listed is to:

- Fabricate BN and TiN thin films by low-pressure chemical vapor deposition.
- Study the growth kinetics and reaction mechanism of the deposited films.
- Determine the mechanical, optical, chemical and electrical properties of these films.
- Correlate the properties of the deposited films to the film stoichiometry and deposition parameters.
- Optimize deposition parameters to obtain low stress and low dielectric constant BN films and to obtain low resistivity and chlorine content in the TiN films.
- Fabricate freestanding x-ray window from BN films.
- Investigate the use LPCVD BN as an inorganic low dielectric constant material.
- Obtain highly reflective stoichiometric TiN films at temperatures below 600 °C.
- Investigate the use of LPCVD TiN as a wear resistant coating for tooling applications.

In Chapter 2, a review of literature of boron nitride and titanium nitride thin films, the preparation techniques and the influence of microstructure of these thin films on the properties are discussed. In addition, an overview of low dielectric constant materials in general, X-ray windows, and Diffusion barriers are discussed.

In Chapter 3, the experimental procedure to fabricate boron nitride and titanium nitride films and the characterization techniques used are described.

The important results of this work are described in Chapter 4 and this is followed by the concluding remarks and suggestions for future work are given in Chapter 5.

CHAPTER 2

LITERATURE REVIEW OF BN AND TiN FILMS

2.1 Introduction

Hard coating materials can be divided into three categories, depending on the nature of the bonding. The first includes the ionic hard oxides of Al, Zr, Ti, etc. Next are the covalent hard materials exemplified by borides, carbides, and nitrides of Al, Si, and B, as well as diamond. Finally, there are the metallic hard compounds consisting of the transition metal borides, carbides, and nitrides. Typical mechanical and thermal property values for important representatives of these groups of hard materials are listed in Table 2.1[40]. From the table, we can see that BN and TiN films offer a very well balanced set of desirable properties with BN being second only to diamond with respect to hardness. BN happens to be a covalent nitride, where as TiN is a metallic nitride. Hence, BN is a dielectric and TiN is a conductor with a high coefficient of thermal expansion.

In this chapter a review of the deposition techniques of boron nitride (B-C-N-H) and titanium nitride (Ti-N-Cl) thin films, their properties, and their applications will be discussed. A brief review of dielectric and interconnect materials along with their mechanical, optical, chemical, structural, and electrical characteristics, including hardness, stress, optical transmission, and electrical resistivity and the dielectric constant of thin films in general and BN and TiN films in particular will be discussed. This is followed by a review of the applications of these films, such as X-ray windows, diffusion

Table 2.1 Mechanical and Thermal Properties of Hard Materials.

Material	Melting Temperature (°C)	Hardness (kg-mm^{-2})	Density (g-cm^{3})	Young's Modulus (kN-mm^{-2})	Thermal Exp. Coeff. (10^{-6} K^{-1})	Thermal Conductivity (Wm^{-1}K^{-1})	Fracture Toughness (MPa-m$^{1/2}$)
Ionic							
Al2O3	2047	2100	3.98	400	6.5	25	3.5
TiO2	1867	1100	4.25	200	9.0	9	
ZrO2	2710	1200	5.76	200	8.0	1.5	4 - 12
SiO2	1700	1100	2.27	151	0.55	2	<1
Covalent							
C(Diamond)	3800	8000	3.52	1050	1	1100	
B4N	2450	4000	2.52	660	5		
BN	**2730**	**5000**	**3.48**	**440**			
SiC	2760	2600	3.22	480	5.3	84	3
Si3N4	1900	1700	3.19	310	2.5	17	4
AlN	2250	1200	3.26	350	2.7		
Metallic							
TiB2	3225	3000	4.5	560	7.8	30	
TiC	3067	2800	4.9	460	8.3	34	0.46
TiN	**2950**	**2100**	**5.4**	**590**	**9.3**	**30**	
TaC	3985	1600	14.5	560	7.1	23	
WC	2776	2300	15.7	720	4.0	35	
HfN					6.9	13	
HfC	3928	2700	12.3	460	6.6		
Substrates							
High-Speed Steel	1400	900	7.8	250	14	30	50 – 170
Ni Superalloys	1280		7.9	214	12	62	>100
Ti	1667	250	4.5	120	11	13	80

barriers, and next generation lithography (NGL). Finally, the aim and scope of this work will be discussed.

2.2 Deposition Techniques of Boron Nitride Thin Films

Thin films of boron nitride have been grown on various substrates including copper, steels, silicon, quartz, sapphire and fibers. The techniques used (Table 2.1) have included chemical vapor deposition (CVD)[6-10,41-47], low pressure chemical vapor deposition (LPCVD)[48,49], plasma assisted CVD[43,50-54], reactive sputtering[55,56], electron beam irradiation[57], ion beam deposition[58-60], ion plating and pulse plasma method[61-63]. Boron sources have included diborane[6-9,43,48] (B_2H_6), boron trichloride[41,45,52], borazene[49], triethyl amine borane complex[53,54], decaborane[46], hexachloroborazene[47], Organoamine boranes[47], B-vinylborazenes[47], 2–vinyl-pentaborane[47] 2,4,6-B-triamino-1,3,5-N-triphenylborazene[47], etc. In this section a review of the synthesis of boron nitride by chemical vapor deposition and low-pressure chemical vapor deposition techniques is done, as it is relevant to the present work.

2.2.1 Synthesis by CVD Techniques

CVD BN can be prepared from BCl_3 and NH_3, BF_3 and NH_3, B_2H_6 and NH_3, borazine, trichloroborazine, borontriethylamine and NH_3. Four reactions for forming CVD BN are most common. They are:

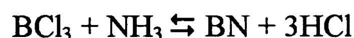

$$BCl_3 + NH_3 \leftrightarrows BN + 3HCl$$

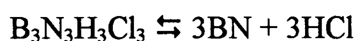

$$B_3N_3H_3Cl_3 \leftrightarrows 3BN + 3HCl$$

$$B_3N_3H_6 \leftrightarrows 3BN + 3HCl$$

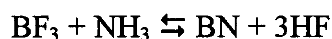

$$BF_3 + NH_3 \leftrightarrows BN + 3HF$$

The reaction involving BCl_3 forms an amorphous material at temperatures of 1100°C and below[4] and dense hexagonal BN in the temperature range of 1600 to 1900°C with pressures below 2 Torr[4]. The orientation improved with increasing deposition temperatures, but crystallinity can also be attained at lower temperatures by the use of plasmas[4]. Better crystallinity can also be obtained by using low pressures.

Table 2.2 Synthesizing techniques of boron nitride thin films

Technique	Reactants	Remarks	References
CVD	B_2H_6, NH_3, H_2, N_2	Deposition temp. 400-1250°C, max. Deposition rate at 800°C, clear, vitreous films	6 - 8
CVD	BCl_3, NH_3, H_2 (Ar)	Deposition temp. 250°-1250°C, films deposited below 450°C are unstable in moist atmosphere, transparent and smooth films are produced between 1000° and 1200°C	41-45
MFCVD	$B_{10}H_{14}$, NH_3	Stoichiometric films are deposited at temp. Of about 850°C	46
LPCVD	B_2H_6, NH_3	Physical and optical properties of the films formed at temp. 300°-400°C are stable and inert towards water and aqueous solutions	48, 50
LPCVD	Borazine	Films formed at temp. 300°-400°C react with atmospheric moisture	49
PECVD	B_2H_6, NH_3	Deposition temp. 1000°C, polycrystalline structure appears	43
PECVD	B_2H_6, NH_3	Deposition temp. 550°-620°C, amorphous structure	52
PECVD	$BH_3N(C_2H_5)_3$, NH_3	Deposition temp. 200°-350°C, amorphous structure, good electrical properties	53-55
Sputtering	B, BN, N_2 (Ar)	Films can be deposited without heating the substrate	55, 56
Electron beam evaporation	BN	Stable amorphous structure, deposition temp. 1050°C	57
Ion beam deposition	B, N_2, NH_3 (Ar)	Ion beam plating of e-beam evaporated boron	58-60
Ion beam deposition	$B_3N_3H_6$ (Ar)	Plasma decomposition	58- 60
Pulse plasma	B_2H_6, B, N_2, H_2	Plasma decomposition, cubic phase	61 - 63

When hydrogen was included with BCl_3 and NH_3, it resulted in less crystallinity, decreased moisture resistance, and free boron and chlorine incorporation in the deposits. Oxygen and carbon inclusions tend to break up the hexagonal deposits. Baronian[41] used this BCl_3-NH_3 system to form CVD BN films at deposition temperatures from 600 to 900°C on a quartz substrate heated by inductive coupling to a graphite susceptor. The gas flows were 230 cc/min of NH_3 and 25 cc/min of BCl_3, and the gas pressure was held between 200 and 600 μm to obtain a deposition rate of 50 Å/min. the refractive index of these films ranged from 1.9 to 2.0.

The BCl_3-NH_4 system was also studied by Matsuda et al.[4] but with H_2 addition, over a temperature range of 1200 to 2000°C and a pressure of 5 to 60 Torr. The BCl_3 and H_2 were introduced in an outer tube and NH_3 in the inner tube at a rate of 90, 670, and 140 cm^3/min, respectively, and passed over a hot graphite substrate. The flow rates used were 0.1 ml/s of BCl_3, 0.5 ml/s of NH_3, 0.4 ml/s of H_2 and 0.7 ml/s of argon at 1200°C to produce a hexagonal material. The crystalline phase was stable in air from 20 to 900°C.

Kuntz[4] formed CVD BN using BF3 and NH3 using temperatures from 1600 – 1700 °C and pressures below 2 Torr. The material produced was highly crystalline. The BF3 reaction tends to be much cleaner. Hexagonal deposits have been prepared at lower temperatures and BF3 is less apt to produce boron in the deposit. Pierson[4] produced these hexagonal BN deposits at only 1100°C and pressures of 30 – 40 Torr. Many investigators[6-9] have deposited BN thin films from diborane and NH_3 using an inert carrier gas according to the reaction

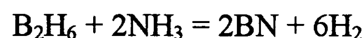

$$B_2H_6 + 2NH_3 = 2BN + 6H_2$$

Rand et al.[6] used many substrates such as Si, Ta, Mo, Ge and fused silica, at various temperatures ranging from 600°C to 1080°C. The typical deposition rates varied from 12.5 to 60 nm/min. in H_2 or He and 100 nm/min. in nitrogen. The dependence of the deposition rate on temperature and NH_3 to B_2H_6 ratio was found to be complex. The deposition rate exhibited a maximum at 800°C and it decreased as the NH_3/B_2H_6 ratio was increased from 10:1 to 20:1.

Makoto Hirayama et al[9] deposited amorphous and polycrystalline boron nitride films on n-type Si substrates using a B2H6-NH3-H2 system. When the deposition temperature was below about 1000°C, the film was amorphous. When the deposition temperature was over 1000°C, the film was polycrystalline with a hexagonal structure. During deposition of BN films, boron diffused into the silicon substrates. BN films thicker than 500 Å deposited below 1000°C acts as infinite diffusion source of boron. When these films were used as diffusion source, the maximum values of boron surface concentration correspond to the solid solubility of boron in Si at each temperature. A thin BN film (about 80Å deposited at 700°C) gave a surface concentration of boron in the range between 10^{16} and 10^{20} cm^{-3} by varying the prediffusion heat-treatment conditions.

Murarka et al.[56,58] studied the growth process on silicon substrates. The deposition rate was proportional to the flow rate of B_2H_6 and to the negative fifth power of the flow rate of NH_3. For a fixed NH_3/B_2H_6 ratio, the deposition rate increased linearly with the flow

rate. The deposition rate increased with temperature in the temperature range 400°C to 700°C, and at higher temperatures, the reaction was nearly independent of temperature.

Baronian[41], Motojima et al.[43] and Takahashi et al.[44,45] used BCl_3 and NH_3 with the following reaction

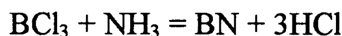

$$BCl_3 + NH_3 = BN + 3HCl$$

Baronian deposited BN thin films on quartz substrates at temperatures ranging from 600°-900°C. Motojima et al. used Cu substrates at temperatures in the range 250°-700°C. The films deposited at temperatures below 450°C were unstable in a moist atmosphere. Takahashi et al. studied in detail the effect of the substrate material on the growth process. According to their results, Fe and Ni were the favorite elements for forming BN crystalline deposits. The formation of the first layer of BN was initiated by a catalytic action of the Fe atoms.

Nakamura[46] proposed a new CVD method in the molecular flow region (MFCVD) for depositing BN films using $B_{10}H_{24}$ and NH_3 reaction gases at substrate temperatures between 300° and 1200°C. He has reported that the decomposition of the films could be closely controlled by regulating the pressure of the source gases and stoichiometric BN films could be deposited at $NH_3/B_{10}H_{24}$ ratios of 20 or more at a substrate temperature.

2.2.2 Synthesis by LPCVD Technique

A.C. Adams and C.D. Capio[50] deposited films of a boron-nitrogen compound with a composition of approximately B_6NH_x at reduced pressure by reacting diborane and

ammonia at 250° - 600°C in an LPCVD reactor. The thickness uniformity was within ± 3% for films deposited at 350°C. Infrared spectra showed that the films contain boron and nitrogen, possibly bonded in a ring structure and hydrogen bonded as BH, NH_2, and possibly NH. The film properties are nearly independent of the ratio of the reactants, but are affected by the deposition temperature. The film refractive index is about 2.2 for films deposited at 340°C. At 600nm, the absorption coefficient is about 2.5×10^4 cm^{-1} and increases with increasing temperature. The films were chemically inert, being insoluble in all the etching solutions investigated. However the films are easily etched in a CF_4-O_2 plasma. The step coverage is conformal with no pin holes and surface defects.

Levy et al[20] studied the microstructure of amorphous hydrogenated LPCVD boron nitride films with respect to hydrogen bonding and distribution. NMR, ESR and EGA techniques were used in the characterization. It was found that the hydrogen is essentially randomly distributed as monohydrides; other configurations such as dihydrides and monohydride clusters, are estimated to be less than 20% total. Radiation damage to the film was revealed by a strong ESR signal. However the radiation damage does not cause hydrogen to aggregate.

2.3 Deposition Techniques of Titanium Nitride Thin Films

Titanium nitride (TiN) thin films have been deposited over the past years using different reactants have been used as the precursors for these depositions. The choice of the deposition method as well as the precursors is dictated by the temperature requirements and the equipment availability. The properties of the deposited film are dependent to a

great extent on the deposition technique (CVD, PVD, etc) as well as on the precursors used. TiN has been commonly deposited using reactive sputtering or by rapid thermal nitridation of sputter deposited titanium[32]. However the sputter deposited films suffer from a lot of disadvantages like poor conformality, low step coverage, etc. In the recent years, as the aspect ratios of features have increased, CVD methods have been sought as a better alternative for TiN thin film deposition. Many workers have studied the deposition of TiN films by different types of CVD. Table 2.1 shows a summary of the methods and reactants different researchers have used to deposit titanium nitride.

Table 2.3 Summary of different deposition techniques and reactants used for TiN thin film deposition.

Technique	Reactants	T (°C)	P(Torr)	Remarks	Ref.
LPCVD (cold wall)	TDMAT, NH_3	327	0.1	Single wafer reactor, argon used as a diluent.	64
LPCVD (cold wall)	$TiCl_4$, NH_3	650		Single wafer reactor, nitrogen used as a diluent.	65
LPCVD	$TiCl_4$, NH_3	480	20	Single wafer rotating disk reactor, nitrogen used as a diluent.	66
LPCVD (cold wall)	TDEAT, NH_3	250-450	10-500	Single wafer MOCVD reactor.	67
LPCVD (hot wall)	$TiCl_4$, NH_3	450-750		Single wafer load-locked reaction chamber	68
LPCVD (cold wall)	$TiCl_4$, NH_3, H_2	550-750	0.15	Argon used as a diluent	69
APCVD	$TiCl_4$, NH_3	400-700	760		70
APCVD (hot wall)	$TiCl_4$, N_2, H_2	800-900	760	Deposition of film on molybdenum substrates.	71
PVD (sputtering)	Ti cathode, N_2	300		Bias at a power of 250 W was used.	72
PVD (cathodic arc dep.)	Ti cathode, N_2	280, 460		Bias of 350-600 V	73

2.3.1 Synthesis by CVD and LPCVD Techniques

As can be seen from Table 2.1, TiN CVD has been done using different combinations of reactants. Commonly NH_3 and N_2 have been used as sources of N while titanium halides (more commonly $TiCl_4$), titanium dialkylamides, tetrakisdimethyl (or ethyl) amino titanium (TDMAT/TDEAT) have been the common sources for Ti. But whatever the reactants, the reaction rate is always important since it ultimately determines the film growth rate. This study of the reaction rate and mechanism, better known as the kinetic study, has been carried out by several researchers, for different reactant combinations and reactor geometries.

Buiting et. al.[69] deposited TiN films from $TiCl_4$, NH_3, H_2 and Ar gas mixtures, in a small cold wall LPCVD system. They found out that the reaction rate and hence the deposition rate to be proportional to the 1.3 power of the partial pressure of NH_3 and inversely proportional to 0.5 power of the partial pressure of $TiCl_4$. They proposed the following rate equation with an apparent activation energy of 61 kJ/mol.

$$\text{rate} = 1.3 * 10^{-5} \exp(-7500/T) \, (P_{H2})^{0} (P_{NH3})^{1.3} (P_{TiCl4})^{-0.5}$$

A similar study was carried out by Imhoff et. al.[74] using the same reactants and a similar reactor system, with the only difference being that in this case, instead of $TiCl_4$, NH_3 was introduced closer to the substrate. In this case, the deposition rate was obtained to be:

$$\text{rate} = 2.7 * 10^{-5} \exp(-9600/T) \, (P_{H2})^{0} (P_{NH3})^{-0.63} (P_{TiCl4})^{1.27}$$

Imhoff et. al. proposed that these contradictory rate orders were a result of a difference in the gas injection configuration in the two reactor systems. The gas (say A), which was injected closer to the substrate, poisoned the sites for adsorption by the other gas (say B). As a result, increasing the partial pressure of A, gave lesser sites for adsorption of B, thereby leading to a decrease in the deposition rate, hence the negative power. The apparent activation energy was determined to be 79 kJ/mol.

Dekker et. al.[71] carried out TiN deposition in a hot wall CVD reactors at temperatures higher than 800°C, using $TiCl_4$, N_2 and H_2 as the reactants. They found the growth rate dependence on $TiCl_4$ concentration to change from a positive order to a negative order with increasing $TiCl_4$. The rate order was 0.5 with respect to N_2 concentration and changed from 1 to 1.5 for H_2 concentration. The apparent activation energy was around 100 kJ/mol.

Jiang et. al.[75] used a cold wall CVD to deposit TiN on graphite substrates using $TiCl_4$, NH_3 and H_2 at temperatures from 1100-1600 °C and for different NH_3:$TiCl_4$ flow ratios. For low flow ratios, they found the deposition rate to increase with increasing flow ratio and deposition temperature. For higher flow ratios, the deposition rate decreased with increasing flow ratio and was almost constant with increasing deposition temperature.

Bouteville et. al[76] have carried out a thermodynamic study of titanium nitride formation on a patterned silicon substrate, using $TiCl_4$, NH_3 and H_2. They performed calculations in the

temperature range of 700-1300 K and in the pressure range 27-133 Pa so as to determine the yield.

2.4 Properties of Boron Nitride and Titanium Nitride Films

In this section the mechanical, optical, chemical, thermal and radiation hardness are discussed. It is found that the structure of the BN thin films are amorphous or polycrystalline (hexagonal or cubic) depending on the method of synthesis. Table 2.2 gives a few details of the properties of BN films based on the method of synthesis. The density[41] of the BN films is 1.7-2.1 gm/cc.

Table 2.4 Properties of BN thin films

Deposition technique	Refractive index	Optical band gap (eV)	Dielectric constant	Electrical resistivity (Ω-cm)	Dielectric strength (V/cm)	Ref-erences
CVD	1.7 - 1.8	3.8	3.7	10^{14}	5×10^{6}	6
CVD	1.7 - 2.8	-	-	-	-	77
CVD	-	-	3.3 - 3.7	10^{9} - 10^{10}	10^{7}	9
CVD	1.9 - 2.0	5.83	-	-	-	41
CVD	-	5.8 - 6.2	-	-	-	42
CVD	-	-	-	-	-	43
CVD	1.65	-	-	10^{14}	-	44
MFCVD	-	5.9	-	-	-	46
PECVD	-	-	2.7 - 7.7	10^{9}	-	51
PECVD	-	-	3.5	-	7×10^{6}	53, 54
PECVD	1.746	4.7	3.8 – 5.7	-	7×10^{6}	78
Sputtering	-	4.9 - 5.6	3.8	-	-	55
Sputtering	1.6 - 1.9	3.3 - 5.6	-	-	-	56
Magnetron Sputtering	1.6 – 2..5	4.8 - 5.14	-	-	-	
Ion beam deposition	-	-	-	10^{10} - 10^{14}	-	60
Plasma pulse	1.5 - 1.6	5.0	5.6 7.0	10^{16}	10^{6}	63

The chemical composition of the films depends on several experimental parameters. Films synthesized by r.f. sputtering[56] in argon gas discharge have an excess of boron and BN. however, by controlling the experimental parameters, stoichiometric BN thin films can be grown. It was also found that boron nitride thin films prepared by ion beam deposition method[58,59] contain a considerable amount of oxygen and those obtained from pulse plasma method[63] show the presence of microinclusions of B_2O_3 and boron. Some films react with moist atmosphere. The intrinsic cause of such a reaction was reported[6,53] to be due to the presence of oxygen at the time of deposition.

Guanghu Chen et al. report that the optical absorption edge of BN films consists of a low energy region in which α increases exponentially as incident photon energy $h\nu$, and a high energy region in which α varies as $(h\nu)m$, which is the characteristics of amorphous materials. An increase in the cubic boron nitride (c-bn) content, the absorption edge shifts to the higher energy and the optical band gap increases. For a BN film with a 88% cubic phase, the optical band gap exceeds 6.0 eV, which is compared to that of c-BN single crystal.

O. Stenzel et al. have deposited both cubic and hexagonal boron nitride films by magnetron sputtering. The optical constants of the films have been determined from the near incidence reflection spectroscopy (NIR) up to the UV. h-BN films showed a steep absorption edge with an Eg located near 4.8 eV, while that for c-BN was around 3.4 eV.

The refractive index of c-BN was found to be identical to the bulk value of 2.12, while that of h-BN varied from 1.6 to 2.5.

The IR spectrum of a film deposited on silicon shows two typical absorption bands. A strong asymmetrical band at 1400 cm^{-1} is attributed to B-N bond stretching. A weaker sharper band at 800 cm^{-1} is attributed to B-N-B bond bending. The broadness and frequency shifting of the BN stretching vibration band depend on experimental conditions. The adherence of the films depends on the substrate material and deposition conditions. However, the adherence of the films has been generally satisfactory. The films deposited at reduced pressure at 340°C have a lower stress at all NH_3 to B_2H_6 ratio is less than about 0.3; at higher ratios, the film stress is compressive. For the B-H-N structure[41], the hydrogen content affects the stress. When the hydrogen content is less than about 21 atom percent, the films are under tensile stress and, for hydrogen concentrations of about 24 atom percent, the films are under compressive stress.

The thermal stability of the BN films depends on the deposition conditions. For example, the films deposited by CVD[43] at above 600°C were stable decreased in mass by 1-2 percent on heating and were stable in air at temperatures below 750°C. For films deposited at temperatures over about 1000°C, no changes were observed in the polycrystalline patterns even after a long treatment in hydrogen or nitrogen for several tens of hours at 1250°C. However, amorphous films deposited below 1000°C were decomposed during heat treatment in nitrogen[9].

The boron nitride films are chemically stable and cannot be attacked by etching solutions except for phosphoric acid[6,9,41]. The etch rate of the film[9] is about 8 nm/min. in a solution of equal volumes[6] of deionized water and phosphoric acid at 130°C and 15 nm/min. in phosphoric acid at 180°C. The films can be etched easily in a CF_4-O_2 [41] plasma, but the etch rate depend on the deposition temperature of the film.

The optical band gap and the refractive index vary according to the experimental parameters and boron-to-nitrogen ratio. The reported values of the band gap lie in the range from 3.3 to 6.2 eV (Table 2.2) and the refractive index from 1.5 to 2.8. In the visible region, the stoichiometric BN film is highly transparent and colorless but, on increase in the boron-to-nitrogen ratio in the film structure, the color becomes pale yellow, deep brown or light golden[56].

BN films are good electrical insulators. Their electrical resistivity is about 10 Ω-cm at room temperature and 10^3 at 200°C. The dielectric constant is about 4. BN films have a low dielectric losses at frequencies ranging from dc to microwave. The dielectric breakdown field strength is about 10V/cm.

The chemical composition of the films prepared by LPCVD[48-50] differs from stoichiometric BN film and these films are called borohydronitride (B-H-N) films. Johnson et al.[79] reported that B_3NH films produced using LPCVD in a manner similar top that used by Adams and Capio[50] were susceptible to radiation damage from 1-3 KeV X-ray radiation. This would lead to pattern distortion and shorten the life span of the masks. They related

the problem to hydrogen content of the film and there by the deposition temperature of the film. Levy et al.[85] showed that the heat treatment of the film resulted in the loss of the hydrogen bond to the ammonia at around 700°C and the loss of hydrogen bond to the boron at around 1100°C. The result indicated that the conduction follows the Frenkel-Poole emission mechanism. The current-voltage (I-V) characteristics of BN films are non linear. The conduction mechanism through BN films is either Schottky type (Poole-Frenkel) or space charge limited depending upon the conditions of the film deposition.

In the last few years there has been a great interest in the study of the physical properties of titanium nitride thin films. This is due to the variety of applications found for this material in several areas. It is widely used as a wear resistant coating on tools, as a gold substitute for decorative coatings and for thin film resistors[65]. Recently it has been investigated as a diffusion barrier in various semiconductor metallization schemes (as a diffusion barrier), a contact layer for silicon, a gate electrode in metal / oxide / semiconductor integrated circuits and even as a solar energy absorber and transparent heat mirror because of its optical properties in the visible and IR regions. These different applications of TiN are a result of its properties, which depend on the composition (N:Ti ratio), impurity (O_2,Cl,etc.) content and the structure, which in turn depend on the growth technique used and the deposition parameters employed. Table 2.2 gives a brief summary of the different properties of TiN film and the process by which these films were deposited.

Table 2.5 Summary of properties of TiN films deposited by different processes

Deposition Technique	Density (g/cc)	Resistivity (μΩ-cm)	Chlorine cont. (%)	Hardness (Mohs)	Step coverage	Ref.
LPCVD (450-750 °C)	4.2-4.9	200-650	2-6	-	-	68
APCVD (400-700 °C)	-	200-6000	0.5-50	8.5	-	70
PECVD	3.7	550-4500	NA	-	30-90% for an aspect ratio of 1:1	80
LPCVD (550-750 °C)	-	100-1100	0.5-10	-	100% for an aspect ratio of 1.9	69
LPCVD (rotating disk reactor)	-	80-1000	1-14	-	100% for aspect ratio > 2	81

TiN is widely used in a variety of applications due to its different properties. Many researchers have studied the properties of thin film and coatings of TiN by a variety of methods. Wu et. al.[82] demonstrated the capabilities, advantages and limitations of different techniques, namely scanning electron microscopy (SEM), transmission electron microscopy (TEM), thin film X-ray diffraction (XRD), secondary ion mass spectroscopy (SIMS), X-ray photoelectron spectroscopy (XPS) and Rutherford backscattering spectroscopy (RBS), to obtain valuable information primarily about the morphology of TiN thin films.

Several researchers[64,65,80,82] studied conformality and step coverage of TiN films deposited by different methods. Almost all of them found TiN films to be nearly 100% conformal for aspect ratios as high as 1.7. For higher aspect ratios, conformality was found to be pretty good.

Many researchers[70,69,82] have studied the variation of film resistivity. They found that the Cl content was responsible for high resistivity and that Cl content decreased with increasing temperature. Thus, high deposition temperature led to the formation of films with low resistivities of around 100 μohm-cm. Presence of oxygen in the film was also found to cause an increase in the film resistivity[72]. Roman et. al.[73] found out that presence of oxygen during deposition even resulted in weaker adhesion of the film because of the TiO_2 formed. Arena et. al.[81] used XPS and Auger electron spectroscopy (AES) to obtain qualitative information about Cl in TiN films and even studied its effect on the corrosion and step coverage of the films.

Oh et. al.[83] have studied the preferred orientation of TiN thin films using XRD technique. They observed that as the thickness of the TiN deposited increased, the preferred orientation changed from (200) to (110) to finally (111). They concluded it to be a combined effect of strain energy and surface energy of the film. Yokoyama et. al.[84] also found the preferential orientation to be (200) by carrying out XRD of TiN films deposited by cold wall LPCVD. Kurtz and Gordon[70] tested hardness of TiN film 3 μm thickness grown on stainless steel substrate and found it to be 8.5 on Moh's hardness scale, on which diamond is 10. Roman et. al.[73] used Vicker's method to determine hardness of sputter deposited TiN on high-speed steel, to be around 2000 kg/mm^2.

2.5 Applications of CVD Boron Nitride

CVD BN has been well known as a release agent and has been used in crucibles because, it is chemically inert to many reagents and metals in a temperature range of 1020 to

2020°C. It doesn't react with graphite at 2220°C and reacts only slightly with W at 2020°C. It has been immersed in boiling water for extended periods without any changes.

It can also be used as an electrical insulator or heat shield especially when it is highly oriented so the basal planes are perpendicular to the electrical current or heat flow. Because of its high dielectric strength, it can also be used in high temperature capacitors. film can be used as an insulator in a metal-insulator-semiconductor (MIS) memory diode[9]. BN films form a transparent substrate for X-ray lithography mask[41,86,87]. The BN mask is inexpensive and easy to fabricate, highly transparent to Pd L X-rays and dimensionally stable through all phases of mask processing. This mask is also optically transparent to facilitate registration.

BN films are useful as a restricted-area boron diffusion source. This method can be used to fabricate planar diodes using only one photomask. The n type Si wafers are thermally oxidized to about 300 nm, and the windows are opened in the silicon dioxide. Next a BN film is deposited. To diffuse the boron in the windows, the BN film must be decomposed. For this, the samples are heated in nitrogen atmosphere at 1100°C for about 120 minutes. Boron diffuses into the silicon through the windows, and the bare silicon surface appears on the windows. Then, to make ohmic contacts, Ni can be deposited directly by electroless plating on bare silicon surfaces of the windows and on the back face of the silicon wafer. Thus by these processes, planar diodes can be made by using only one photomask.

BN film coatings are useful to increase the hardness of materials[58-60] as protective coatings against the oxidation of base materials. BN thin films show a stable, strongly non-ohmic high field conductivity[6]. A film of about 100 nm thick (or thinner) may be used in integrated circuits as thin film varistors or voltage limiters. BN films can be used as high quality insulating films[53,54] for MIS structures based on III-V compounds such as GaAs and these structures are suitable for high frequency device applications.

Other applications of CVD BN include furnace components, boats, trays and tank liners which can be used at very high temperatures in the absence of air. Even in air, the BN is protected by B_2O_3 until the B_2O_3 begins to vaporize at about 1100°C. when it is ground up, it can also be used as a thermal insulating powder. It can also be used as a window at 5.5μm, 12 μm and above 15 μm where it can be employed as an infrared polarizer. Its low dielectric constant of 3.4 in the c direction also makes it useful in microwave applications, such as radomes.

In addition to the above applications, CVD BN has also been used as a fiber coating in composites to densify composites and as a matrix in composites. As a fiber coating, it provides a weak bond between the fiber and matrix resulting in a tough composite. In carbon-carbon composites, it increases the oxidation resistance by protecting the fibers. In view of BN good thermal conductivity, it is valuable as a heat sink and mounting material in value and transition circuits, which can replace the toxic and less readily worked beryllia. Another importance, but still with some conservations; is that it can be used as a

distortion-free radiation mask for its structurally stability and free of distortion over the range of common processing conditions.

Boron nitrogen compounds have attracted the attention of a lot of researchers to work with for two main factors. First, the BN moiety is isoelectronic with C-C. Second, the sum of the covalent single-bond radii of boron and nitrogen is very similar in magnitude to that of the two carbon atoms. Consequently, there are superficial analogies between certain boron nitrogen compounds and their organic counterparts.

Potential applications of boron nitrogen films have been proposed such as:

1- high temperature dielectrics
2- heat-dissipation coatings
3- passivation layers
4- diffusion sources of boron
5- sodium barriers
6- Next generation lithography (NGL)

All the above mentioned applications have encouraged us to synthesize a new compound which may have some unique properties. The starting point of this research work stemmed from the idea of combining the properties of both boron nitrogen and carbon films. This led us to form a hard and transparent B-C-N. Ease of formation, suitable mechanical properties, transparency, stability, optical transparency, etching resistivity and low defect density.

2.5.1 Dielectric Thin Films

Within the next three years, 0.35-μm and early 0.25-μm generation devices will become available. To accommodate these smaller design rules and higher device densities, the number of interconnect levels must increase from three levels to five or possibly six. Use of more interconnect levels complicates the manufacturing process, but means that interconnect linewidths and packing densities need not shrink in proportion to the reduction in transistor gate length. This postpones the need to adopt revolutionary copper interconnect / low-k dielectric schemes. However a time will definitely come when further increase in the number of levels will not decrease the signal propagation time because the signal propagation time would be limited by the capacitance between the interconnect layers as reflected in the delay constant[88].

$$RC = \rho_m \varepsilon_{die} L^2/d_{die}$$

Where ρ_m is the sheet resistance of the interconnect, L is the interconnect length, ε_{die} is the dielectric constant of the interlevel dielectric (ILD), d_{die} is the thickness of the ILD, R is the resistance of the interconnect metal, and C is the capacitance of the ILD. It is evident from the relationship that a low RC constant can readily be achieved through material modification by reducing the resistance of the interconnect metal and the dielectric constant of the ILD.

A desirable ILD material should exhibit in addition to a low dielectric constant, low mechanical stress, high thermal stability and low moisture absorption. Several ILD candidates have been explored over the last few years. These have included fluorinated SiO_2 [17-27], fluorinated polyamides[28,29] and BN[30,31] films. Fluorine is the most

electronegative and the least polarizable element. Therefore, incorporation of F reduces the number of polarizable geometry. These changes result in lowering polarizability of the fluorinated SiO_2 film itself, thus lowering the dielectric constant.

2.5.1.1 Organic Fluorinated Dielectric Films: As interconnect dimensions in integrated circuits shrink well below 0.5 μm, traditional dielectric insulators have inadequate performance. Organic polymers, in general, exhibit lower dielectric constants than inorganic oxides and nitrides, and thus are candidates for the intermetal dielectric at these small dimensions. Most organic polymers do not possess adequate thermal stability for backend processing, however. A few candidates, such as fluorinated poly(arylenethers), may prove useful if they possess sufficient dimensional stability to withstand multilayer interconnect processing.

Organic polymers, specifically polyimides, were used for integrated circuit IMD in production by IBM from the early 1970s through the late 1980s. In addition to organic polymers, many of which exhibit ε of 3 or below, at least two classes of materials are currently under investigation. One is SiO_2 that has been fluorinated by a variety of methods[22]. Another is the class of silicon-oxygen polymers called silesquioxanes, which can be thought of as high organic content spin-on glasses[22]. For subsequent generations, it appears that only a few unique and thermally stable polymers exhibit sufficiently low ε combined with other important properties and processing characteristics.

A family of thermally stable, low-dielectric constant polymers are under development at AlliedSignal Advanced Microelectronic Materials as an alternative to polyimides for IC intermetal applications. The polymers, fluorinated poly(arylenethers), are envisioned for use in devices fabricated with design rules of 0.25 μm and below. They are prepared by condensation of decafluorobiphenyl with aromatic bisphenols[22]. Compared to polyimdes, these polymers exhibit comparable thermal stability while providing significantly lower ε, lower moisture absorption, higher outgassing rates, and greater ease of processing.

Silsesquioxanes polymers typically result from hydrolysis and condensation of alkyl- or aryltrialkoxysilanes, Rsi(OR')3. With ε of 1.7 – 3.0, they may provide an intermediate dielectric solution for the 0.35 or 0.25 μm generation of devices. These materials, also under development, can contain upto 50% organic content by weight, but possess a silicon-oxygen backbone that contributes to their relatively high stability when exposed to oxygen plasmas. The silsesquioxanes exhibit high thermal stability, low residual stress, low moisture absorption, and excellent gap filling and local planarization properties. Since they are processed in a similar fashion to spin-on glass, they may offer a much lower dielectric constant than traditional dielectrics, without the major process integration challenges that will surely accompany purely organic polymer dielectrics.

The primary means of reducing the dielectric constant and refractive index has been fluorination of the polymer backbone. This has been achieved by incorporation of hexafluoro groups and by aromatic substitution of fluorine atoms, trifluoromethyl groups, fluorinated alkoxy side chains, and more recently, pentafluoro sulfur groups. Reduction of

dielectric constant in polyimides has also been achieved by introducing fluorine-containing additives and by blending Teflon into the bulk polyimide material. Control of the refractive index of polyimide waveguide materials has been achieved through copolymerization of fluorine containing monomers. It is believed that the dielectric constant and refractive index of fluorinated polyimides are reduced by a combination of mechanisms. First, the electronic polarizability is reduced through the addition of fluorine-carbon bonds. In addition, interchain charge transfer complexation and associated chain packing are impeded by bulky fluorinated side groups, by kinks in the polymer backbone, and by spacer groups. Low refractive indices in fluorinated polyimides can be accurately predicted by current property prediction techniques. This suggests that it is the fluorine atoms and the bonds in the polymer repeat unit that have the largest effect in reducing refractive index. As a result of the preferential alignment of the most polarizable groups in the polyimide, i.e., the main chain phenyl rings, control of refractive index in polyimides in and out of the plane of the film by introducing orientation into the polymer film, increases the refractive index in the direction of orientation and reduces normal to the direction of orientation.

2.5.1.2 Fluorinated SiO_2 Dielectric Films: Several reports[17-27] have indicated that the dielectric constant of silicon dioxide films can be reduced with increasing amounts of F in the films. Usami et al.[17] used a parallel-plate electrode CVD system to deposit SiOF films using tetraethoxysilane (TEOS)-He-O_2-C_2F_6 gas plasma generated by r.f. power at 13.56 MHz at a temperature of 360°C and a pressure of 9 Torr. They found that the deposition rate and refractive index of the film decreases with increasing C_2F_6 flow rate. This

suggested that the there is a change in the film composition and also a decrease in film density with increase in C_2F_6 addition. They suggested that the Si-O bond strength was influenced by Si-F bond formation due to the high electronegativity of fluorine was the cause of reduction of refractive index due to the structural changes in the film. The dielectric constant of the SiOF films were compared before and after annealing at 400°C in a hydrogen atmosphere for 30 minutes. Before annealing, the relative dielectric constant of the conventional PE-TEOS oxide was 4.9. this value was higher than that of thermally grown silicon dioxide (3.9). This result is due to the presence of highly polarized compounds such as Si-OH and H_2O in the film. With increasing fluorine concentration, however, the relative dielectric constant decreased. It is supposed that polarization of Si-O bonds was changed with the presence of Si-F bonds due to the high electronegativity of fluorine. After annealing the relative dielectric constant was lower (4.5) than that before annealing at all fluorine concentration indicating that the highly polarized compounds such as Si-OH and H_2O content in the films decreased even though a small amount of fluorine desorbed from the film. The least dielectric constant of 3.6 was obtained at 14 atomic % fluorine.

2.5.1.3 BN and SiBN Thin Films: Recent publications[78,89] have reported on the use of plasma enhanced chemical vapor deposition (PECVD) to synthesize BN and SiBN as potential low ε materials. Maeda et al.[85] deposited amorphous SiBN ternary films using a parallel plate electrode reactor using a SiH_4-B_2H_6-NH_3-Ar gas mixture at a frequency of 13.56 MHz to obtain low dielectric constant films. Strong and broad absorption bands were seen at wavenumbers 890 cm^{-1} and 1320 cm^{-1} in the IR absorption spectrum

corresponding to Si-N and B-N lattice vibrations respectively. The refractive index was found to decrease with increasing B atomic ratios. An observed value of 1.71 obtained from stoichiometric boron nitride was similar to hexagonal like amorphous boron nitride films. The static dielectric constant (at 1MHz) monotonically decreased from $6.8\varepsilon_o$ of silicon nitride to $3.0\varepsilon_o$ for stoichiometric boron nitride with increasing boron atomic ratio. The optical dielectric constant also decreased with increasing boron atomic ratio to obtain a value of $2.9\varepsilon_o$ for BN. Thus the difference between the static and the optical dielectric constants was extremely small for BN films while the static dielectric constant was 1.75 times larger than the optical one for Si_3N_4.

2.5.2 Transparent Boron-Nitrogen-Carbon Thin Films

Compounds containing only boron and nitrogen have some special properties, such as being electrically insulating, chemically inert, thermally stable, and resistible to corrosion. Besides, they have desirable mechanical properties and reasonable wide bandgap. The addition of an atom having different bonding radii to a matrix film is an effective method for changing the stress of the film. Mechanical stress can pose serious problems in semiconductor technology where layers of differing materials must be grown on a silicon substrate. For example, stress may cause crystal defects in the underlying substrate, cracking of deposited films, or voiding in aluminum conductor lines. Each of these examples leads to a loss of device yield. Stress is caused partly by differing thermal expansion coefficients between substrate and grown layer. For films produced by chemical vapor deposition the actual stress measured varies considerably from thermal stress which is predicted from thermal exapansion coefficients. The difference, called intrinsic stress, is

a heavily dependent on process conditions during film growth. Plasma-enhanced CVD induces intrinsic stress by ion bombardment and cross linking effects. But intrinsic stress also is found with CVD-layers deposited without plasma enhancement. BN is usually deposited by the reaction of diborane and ammonia in hydrogen or an inert carrier gas. The group at Bell Laboratories, Murarka et al.[90], found that the stress was compressive for temperatures above 700 C and that films richer in boron were tensile. In other words, stoichiometric boron nitride deposited at high temperatures and a high NH_3/B_2H_6 ratio was compressive. The LPCVD-BN developed at Bell Laboratories was deposited using B_2H_6 and NH_3 as source gases at around 400C. In order to get the tension required for x-ray mask membranes, B-rich off stoichiometric composition was inevitable for this material. In fact the atomic ratio of B/N was between 3 and 5. The bandgap for an amorphous material is characterized by the local chemical environment. Therefore, the excess metallic B-B bonds, which are a result of off-stoichiometry, narrower the bandgap. In order to widen the optical gap of LPCVD-BN while retaining tension, lowering the deposition temperature is effective. Unfortunately, this condition lowers the Young's modulus because excessive hydrogen incorporation. Hence, it is difficult to simultaneously get a high optical transparency and a high Young's modulus using this material. Addition of a small amount carbon improves the film stoichiometry and also decreases the hydrogen content. The increase in the stoichiometric structures of boron to nitrogen increased optical transparency. The low hydrogen content also increases the Young's modulus of the films. The radiation resistance of BNC was also improved over LPCVD-BN. It is well known that it is easy to change the atomic structure of materials having low average coordination number, such as a material with many bondings terminated by hydrogen

atoms having one-fold coordination. Therefore, the stress relaxes easily due to changes in the atomic structure. Since the atomic structure of BNC is mainly dominated by B-N bonding networks with a large binding energy, the radiation resistance of BNC must exceed that of LPCVD-BN. A transparent ternary boron compound film B-C-N was first reported by Montasser et al. at room temperature. However, the optical data indicates the film to be like a soft organic film. Masao Yamada et al. have deposited rigid ternary boron compound film, boron-nitro-carbide (BNC), deposited by plasma-enhanced chemical vapor deposition between 300 C and 500C.

2.5.2.1 X-ray Windows:

Modern analytical instruments are often equipped with a wide variety of signal detectors. Signals such as transmitted electrons, diffracted electrons, backscattered electrons, secondary electrons, and characteristic x-rays can all be collected using various types of signal detectors. The above discussed signals are collected by either a solid state detector or a scintillator/photomultiplier detector. Both these detectors are isolated from the microscope column by means of a x-ray window. A major consideration for windows is their ability to withstand adverse environments and special conditions necessary to make critical measurements. The window provides separation between the environment of the sample and the detector. These differences include pressure of one atmosphere (or greater) and sample environments of helium, water vapor or atmospheric gasses typical of the environment of the analytical instrument installation.[91]

Typically thin beryllium or polymeric films have been used as windows. Yet these films have limitations on their usefulness. For example, the potential for pinhole leaks increases as the beryllium foil thins, and a thin beryllium foil is more likely to fail through exposure to atmosphere. Nor can it be used in a harsh chemical environment. Also beryllium is extremely poisonous and processing of such a material endangers the workers. The polymeric film on the other hand is far more fragile and must be treated carefully. One of the most important criteria for selecting a window is its transparency to x rays. The polymer windows lose some transmission due to the silicon support grid, which is installed to provide mechanical support to the soft membrane.[91] The corrosion and temperature resistance is far less than desirable and hence there is a need for materials that are optically transparent and possess good thermal, mechanical, and chemical properties. Boron nitride due to its low atomic weight and extremely good mechanical, thermal, chemical and optical properties is believed to be an excellent candidate for the x-ray windows.

2.5.2.2 Next Generation Lithography (NGL)[92]: As figure 1 illustrates, there will soon be a need for a new lithographic technology, if we are to maintain the present rate of progress in IC development. The figure shows the trend of wavelength reduction, which has driven the resolution improvements in optical lithography over the past two decades. The line is drawn such that the minimum features (half-pitch) are roughly equal to the exposure wavelength. With resolution enhancement technology (RET), such as phase shifting and OPC, it is possible, theoretically, to print features as small as half the wavelength (half-pitch) also shown in the figure.

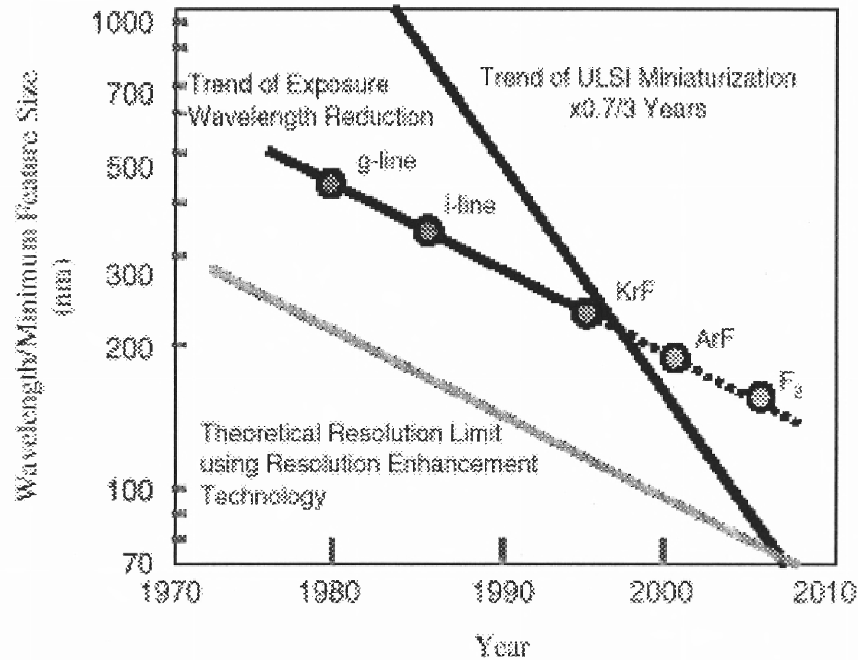

Figure 2.1 Trends in ULSI miniaturization, exposure wavelength and limits of resolution enhancement techniques (RET) as a function of time. The current trend in miniaturization will reduce feature sizes below the capability of optical lithography around 2005. The cost will probably be prohibitive before then. (Graph courtesy of Dr. S. Okazaki, Hitachi Ltd.)

The difference between printing at the wavelength (binary masks) and at half the wavelength, using RET is cost. Even with this, the trend line for chip features (Moore's law) has a much steeper slope than that for wavelength reduction. The two lines intersect at roughly the 250 nm node (DUV 248). Moore's law intersects the RET limit at about the 70 nm node, which implies is that optical lithography, although technically possible, gets very expensive beyond the 250 nm node and probably not possible below the 70 nm node. This offers the opportunity for NGL technology such as SCALPEL.

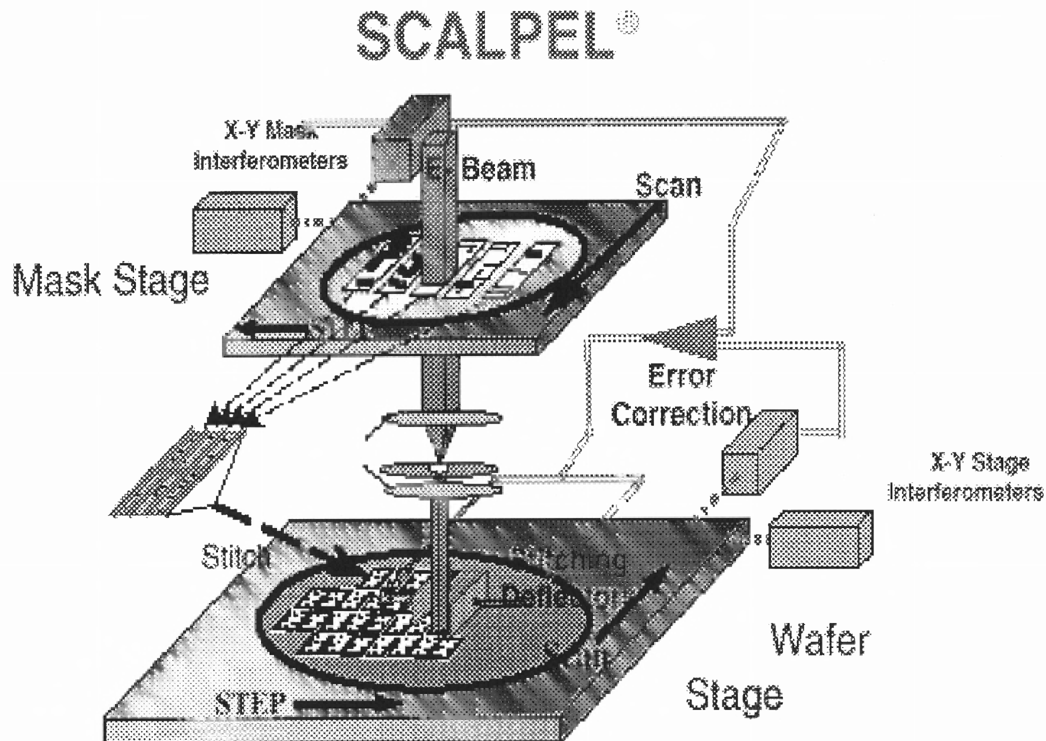

Figure 2.2 Trends in ULSI miniaturization, exposure wavelength and limits of resolution enhancement techniques (RET) as a function of time.

Over the next several years, it will be necessary for the semiconductor industry to identify a new lithographic technology that will carry it into the future, eventually enabling the printing of lines as small as 30 nanometers. Potential successors to optical projection lithography are being aggressively developed. Collectively known as Next-Generation Lithographies (NGLs), Extreme UV lithography (EUVL) is one of the leading NGL technologies; others include x-ray lithography, ion-beam projection lithography, and electron-beam projection lithography. "On the other side of that wall is the SCALPEL electron-beam technology, which will allow printing of much smaller features because there aren't the wavelength restrictions with electrons that one encounters with light," says

Dr. Harriott from Lucent Technology. Electrons have an equivalent wavelength of 0.0037 nanometers, compared to the 250 nanometers wavelength of the current technology.

SCALPEL (SCattering with Angular Limitation Projection Electron-beam Lithography) has the potential to satisfy the lithographic requirements for many IC generations, down to the minimum feature sizes contemplated in the semiconductor industry association roadmap. The aspect of SCALPEL that differentiates it from previous attempts at projection electron-beam lithography is the mask. This consists of a low atomic number membrane covered with a layer of a high atomic number material. The high atomic number material is the one on which the pattern is delineated. While the mask is completely electron transparent at the energies used (100 keV), contrast is generated by utilizing the difference in electron scattering characteristics between the membrane and the patterned materials. The membrane scatters electrons weakly and to small angles, while the pattern layer scatters them strongly and to high angles. An aperture in the back-focal plane of the projection optics blocks the strongly scattered electrons, forming a high contrast aerial image at the wafer plane. The membrane, which is only 0.1 to 0.15 micron thick, is supported on a grill of struts spaced 1 mm apart. The resulting image has to be stitched together from hundreds of narrow stripes into a seamless pattern on the wafer. The SCALPEL system is schematic represented in figure 4.

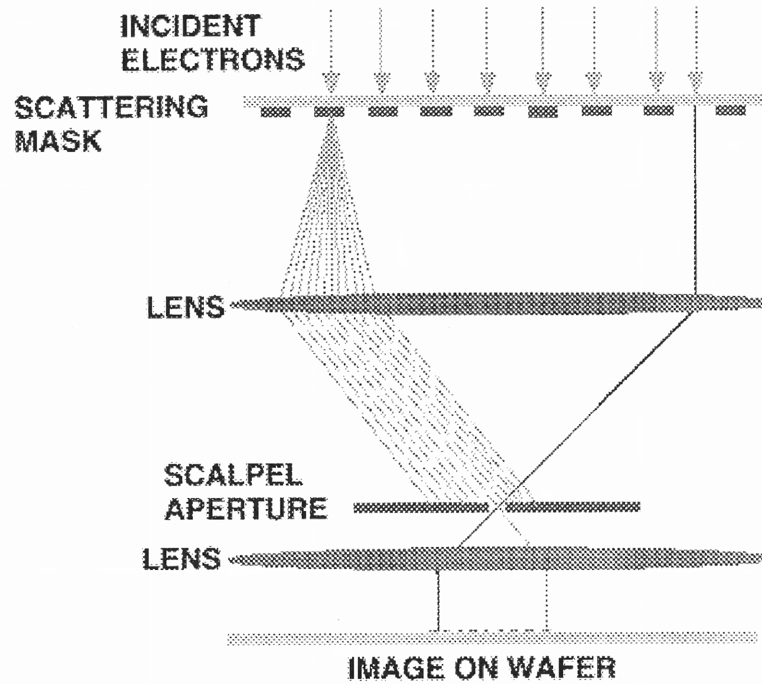

Figure 2.3 Basic SCALPEL principle of operation showing contrast generation by differentiating more or less-scattered electrons.

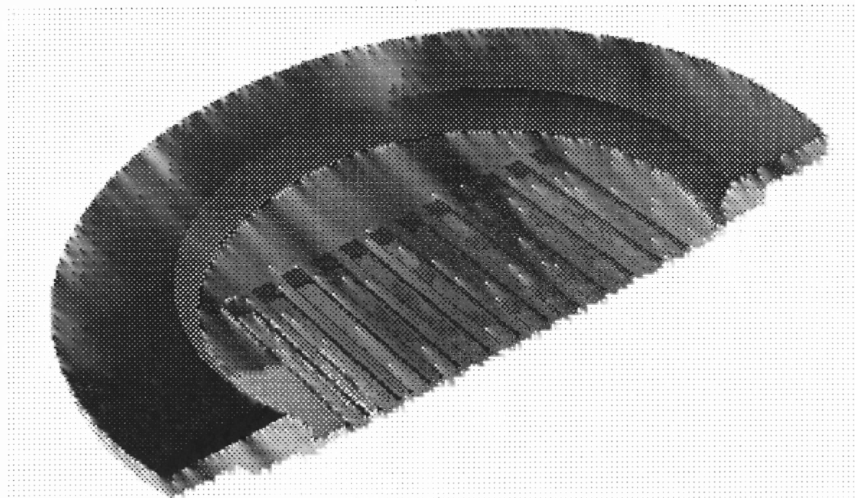

Figure 2.4 Schematic cross-section of a SCALPEL mask showing patterned membrane area and supporting grillage.

With no consensus yet on what the new-generation lithography will be, it appears increasingly unlikely that one will be ready in time for the 100 nanometers chip generation, which, according to Moore's Law (Figure 2) is expected in the year 2006. At the same time, industry giants are reluctant to shell out the $1 billion or more needed for the development of any option, which creates the risk of advances in lithographic technology possibly becoming bottlenecked. Hence there is renewed interest in pushing optical lithography yet one more notch. Optical technology possesses an enormous resource base from which to draw for addressing technical problems.

With shorter light wavelengths and resolution enhancement optics, optical lithography could be the basis for both the 100-nanometer and 70-nanometer chip generations. If that were to be the case, the need for NGL would be pushed back by only a single generation, at 50 nanometers, before the limits of microelectronic device structures would be reached and no further developments would be possible due to the quantum effects.

Whether chipmakers will want to make the large research investments needed to push silicon-microchip technology to its limits remains to be seen. Several years ago, it was assumed that an NGL would be needed by around 2005 in order to implement the 100 nanometer generation of chips. Currently, industry consensus is that 193-nanometer lithography will have to do the job, even though this will be difficult. There has recently been discussion of using light at 157 nanometers to push the current optical technology even further, which would further postpone the entry point for an NGL technology. It is therefore crucial that any potential NGL be able to address the printing of feature sizes of

50 nanometers and smaller. The race to develop the technology that will succeed 193-nanometer lithography will be interesting to watch!

2.6 Applications of CVD Titanium Nitride

2.6.1 Refractory Metal Interconnects for VLSI

The most important application area for conductive films is to provide interconnections between contacts which are made to devices in a microcircuit. Both single-metal and multimetal films are used for this purpose. In addition, the complexity of VLSI circuits has brought about the need for multi-level metallization schemes. Films used for interconnections must adhere firmly to the semiconductor contact and also to the insulating layer that is placed over the semiconductor. They should be readily deposited by a relatively low temperature process, since metallization is one of the last steps in microcircuit fabrication. They should be easily patterned with high resolution, without etching the insulating layer on which they are placed. They should be relatively soft and ductile, so that they can withstand cyclic temperature variations during processing and in service. They must be highly conductive, and capable of handling high current densities while still maintaining their electrical integrity. Finally, they should be easily connected to external terminations[40]. Most of these requirements are met by gold and aluminum films. However, aluminum is a viable choice as the metal, since it bonds well to SiO_2 as well as to Si_3N_4 insulating layers, by a relatively short heat treatment.

The unusual materials which comprise these coatings are drawn from several classes of solids and include ionic ceramic oxides (e.x., Al_2O_3, ZrO_2, TiO_2), covalent materials (e.g., SiC, BC, diamond), transition metal compounds (e.g., TiC, TiN, WC) and metal alloys (e.g., CoCrAlY, NiAl, NiCrBSi)[40]. As a whole they are characterized by extremely high hardness, very high melting points, and resistance to chemical attack, attributes that have earmarked their use in critical applications where one or more of these properties is required; correspondingly the respective categories of hard, thermal and protective coatings denote the functions to which they are put.

2.6.2 Diffusion Barriers

Diffusion barriers are thin film layers used to prevent two materials from coming into direct contact in order to avoid reactions between them. Paint and electrodeposited layers are everyday examples of practical barriers employed to protect the underlying materials from atmospheric attack. Ideally, a barrier layer X sandwiched between A and B should possess the following attributes:

1. It should constitute a kinetic barrier to the traffic of A and B across it. In other words, the diffusivity of A and B in X should be small.
2. It should be thermodynamically stable with respect to A and B at the highest temperature of use. Further, the solubility of X in A and B should be small.
3. It should adhere well to and have low contact resistance with A and B and possess high electrical and thermal conductivity. Practical considerations also require low stress, ease of deposition, and compatibility with other processing.

A large number of materials have been investigated for use as barrier layers between silicon semiconductor devices and Al interconnections. These include silicides, refractory metals, transition metal alloys, transition metal compounds, as well as dual-layer barriers such as refractory metal-silicide, transition metal-silicide and transition metal compound-silicide combinations. A compilation of these materials and reaction is given in Table 8-3.

Table 2.6 Aluminum – Diffusion Barrier – Silicon Contact Reactions[40]

Diffusion Barrier	Reaction Temperature (°C)	Reaction Products	Failure Mechanisms
Cr	300	Al_7Cr	C
V	450	Al_3V, Al-V-Si	C
Ti	400	Al_3Ti	C
Ti-W	500		D
TiN-PtSi	550	AlN, Al_3Ti	C
ZrN	550	Al-Zr-Si	C
PtSi	350	Al_2Pt, Si	C
Pd_2Si	400	Al_3Pd, Si	C
NiSi	400	Al_3Ni, Si	C
$CoSi_2$	400	Al_9Co_2, Si	C
$TiSi_2$	550	Al-Ti-Si	D
$MoSi_2$	535	$Al_{12}Mo$, Si	D
TaN-NiSi	600	AlN, Al_3Ta	C

C= Compound formation; D= Diffusion

To appreciate the choice of barrier materials, we first distinguish among three models that have been proposed for successful diffusion-barrier behavior.

1. ***Stuffed Barriers.*** Stuffed barriers rely on the segregation of impurities along otherwise rapid diffusion paths such as GBs to block further passage of two-way traffic there. The marked improvement of sputtered Mo and Ti-W alloys as diffusion barriers when they contain small quantities of intentionally added N or O impurities is apparently due to this mechanism. Impurity concentrations of ~10-1

to 10-3 at% are typically required to decorate GBs and induce stuffed barrier protection. In extending the electromigration life of Al, Cu may in effect "stuff" the conductor GBs.

2. ***Passive Compound Barriers.*** Ideal barrier behavior exhibiting chemical inertness and negligible mutual solubility and diffusivity is sometimes approximated by compounds. Although there are numerous possibilities among the carbides, nitrides, borides, and even the more conductive oxides, only the transition metal nitrides, such as TiN, have been extensively explored for device applications. Although TiN has proved effective in solar cells as a diffusion barrier between N-Si and Ti-Ag, contact resistances are higher than desired in high current density circuits.

3. ***Sacrificial Barriers.*** A sacrificial barrier maintains the separation of A and B only for a limited duration. Sacrificial barriers exploit the fact that reactions between adjacent films in turn produce uniform layered compounds AX and BX that continue to be separated by a narrowing X barrier film. So long as X remains and compounds AX and BX possess adequate conductivity, this barrier is effective.

2.7 Aim and Scope of the Present Work

The aim of the present study was

- Fabricate BN and TiN thin films by low-pressure chemical vapor deposition.
- Study the growth kinetics and reaction mechanism of the deposited films.
- Determine the mechanical, optical, chemical and electrical properties of these films.
- Correlate the properties of the deposited films to the film stoichiometry and deposition parameters.
- Optimize deposition parameters to obtain low stress and low dielectric constant BN films and to obtain low resistivity and chlorine content in the TiN films.
- Fabricate freestanding x-ray window from BN films.
- Investigate the use LPCVD BN as an inorganic low dielectric constant material.
- Obtain highly reflective stoichiometric TiN films at temperatures below 600 °C.
- Investigate the use of LPCVD TiN as a wear resistant coating for tooling applications.

In Chapter 3, the experimental procedure to fabricate boron nitride and titanium nitride films and the characterization techniques used are described. The important results of this work are described in Chapter 4 and the effect of various deposition parameters on the properties is discussed in detail. Concluding remarks and suggestions for future work are given in Chapter 5.

CHAPTER 3

EXPERIMENTAL PROCEDURE

3.1 Introduction

Boron nitride (B-N-C-H) and titanium nitride (Ti-N-Cl) thin films with varying compositions were synthesized in a LPCVD reactor with a vapor phase flow system adjusting various parameters including temperature, pressure, gas composition and time of deposition. The chemical, mechanical, optical, electrical, and structural properties of the films were determined as a function of deposition parameters. Ellipsometry and interferometry measured refractive index and thickness of the films respectively. The current-voltage (I-V), capacitance-voltage (C-V), resistivity and the dielectric constant of the BN films were measured. Hardness and Young's modulus were determined using a Nanometrics nano-indenter. The composition of these films were determined by AES, XPS, and RBS. X-ray diffraction study revealed the structural properties of these films.

3.2 LPCVD Reactor

The deposition reactor is schematically shown in Figure 3.1. This reactor was manufactured by Advanced Semiconductor Materials America Inc.(ASM America, Inc.) as a poly silicon micro-pressure CVD system. The horizontal reaction chamber consists of a 13.5 cm diameter fused quartz tube and a 144 cm long encapsulated with a three-zone, 10 kwatt, Thermco MB-80 heating furnace. The process tube door was constructed of a 300 series stainless steel, with a side hinge and sealed with an O-ring. At one end a heating

jacket maintained the temperature of the bubbler to a constant value ranging between 0°C and 70°C, depending on the flow required. The vapors of the precursor (TEAB and $TiCl_4$) were passed to a vapor phase flow controller, which was connected to the reactor by means of a pipe. The lines that carried the vapors of the precursor were heated to 70°C and the vapor phase controller was maintained at 90° to avoid the condensation of the precursor. A MKS mass flow controller controls the flow of ammonia into the reaction chamber. A spare nitrogen mass flow controller was installed to incorporate any necessary additional reactant gas into the chamber or for backfilling. This spare controller could be calibrated for the gases other than nitrogen.

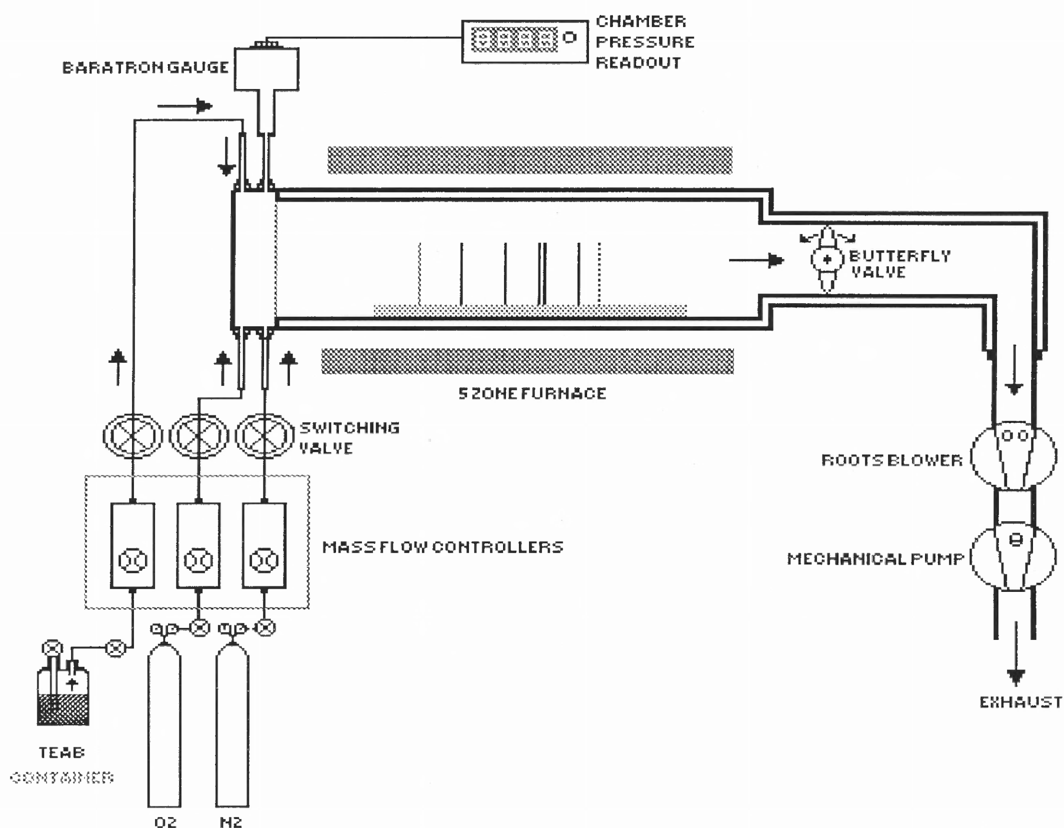

Figure 3.1 Schematic representation of the LPCVD reactor

The other end of the reaction chamber is connected to a vacuum station comprised of a Leybold-Heraeus Trivac dual stage rotary vane pump backed by a Leybold-Heraeus roots pump to create the necessary vacuum in the system. An oil filter system is used to filter unnecessary particles from oil and thereby increasing the lifetime of the pump. End caps designed for this reactor have a provision for cold water circulation to avoid overheating of the O-rings. A ceramic tube was setup between the chamber and the heater to enhance the radiation heat transfer thus reducing the temperature deviation through the reaction tube. The temperature was kept constant across all zones and confirmed using a calibrated K type thermocouple. Mass flow controller set points were programmed with a MICON 3 microprocessing controller which produces the set point voltage and automatically monitors the flow vs. the programmed flow limits. The pressure in the reactor is monitored with an automatic exhaust valve and measured at the reactor inlet using a capacitance manometer (13 Torr MKS baratron pressure gauge). For the deposition of TiN films, the reactor described above was modified to insert the precursor vapors near the wafers as shown in Figure 3.2. This was done in order to avoid the formation of a yellow solid complex on the walls of the reactor which are cooled to protect the O-rings.

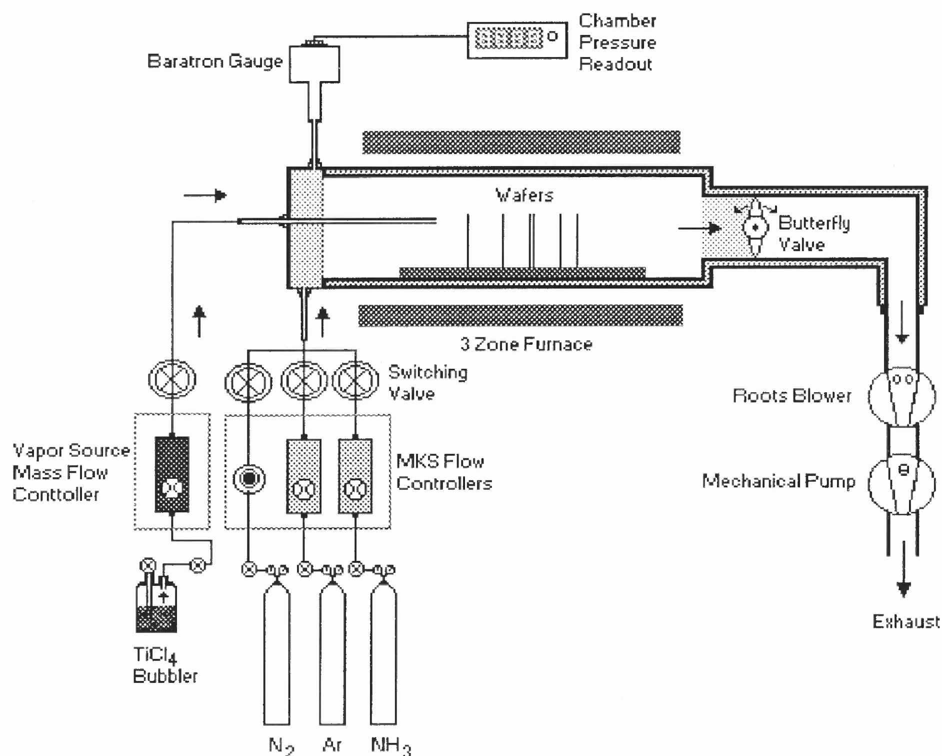

Figure 3.2 Schematic diagram of the modified experimental setup.

3.2.1 Vapor Phase Flow Mechanism

The vapor phase flow system, designed and fabricated in-house[20], consists of a stainless steel bubbler connected to a precalibrated capillary tube fastened onto the re action chamber. The vapor phase flow system was developed on the basis of thermodynamic principles, which states that when the phases are not in equilibrium, mass transfer occurs between the phases. The rate of transfer of each species depends on the departure of the system from equilibrium. Equilibrium is a static condition in which no changes occur in the macroscopic properties of the system with time. This implies a balance of all potentials

that may cause change. If vapor and liquid are to exist in equilibrium one cannot exercise independent control over these two variables for this system. The number of independent variables that must be arbitrarily fixed to establish the intensive state of a system, i.e., the degrees of freedom F of the system, is given by the celebrated phase rule of J. William Gibbs, which can be given as follows:

$$F = C - P + 2 \tag{3.1}$$

Where;

F = number of degrees of freedom

C = number of components

P = number of phases

On applying the above equation to our system, which consists of a single component i.e., TEAB or $TiCl_4$, two phases involving the liquid and the vapor phase, we get the number of degrees of freedom to be 1. This implies that on changing one of the variables, which was temperature in our case, the pressure of TEAB or $TiCl_4$ in the vapor phase automatically gets fixed.

On the basis of the above principle, a heating jacket was made to cover the precursor bubbler and by varying the temperature of the jacket, the amount of precursor in the vapor phase was controlled. The goal was to maintain at any time sufficient vapor in the bubbler so that the vapor phase flow controller that was connected in series to the bubbler would always remain the rate-determining step. The precursor used as a source of boron and titanium can slowly react with oxygen and forms an undesirable white powder

contamination and hence requires handling in an inert glove box. The flow rate of the precursors was maintained between 1 and 10 sccm for all the runs. This was achieved by maintaining the temperature of the bubbler between 40 to 65°C.

3.3 Experimental Setup

3.3.1 Leakage Test

The leak check is one of the most important steps in these experiments because the usage of a vapor phase flow system does not allow the bubbler to be maintained at a positive pressure. This results in a high probability of leakage into the bubbler. A leak would result in a change in the deposit structure (due to oxygen) and could result in haze depending on the size of the leak, therefore a leakage check in the CVD is an important step before making an experiment. After pumping the reaction system for a whole day, the rate of pressure increase in the chamber was measured at a fixed period of time in the chamber by closing the outlet valve of the chamber, to obtain the leakage rate. For this LPCVD system, the leakage rate deviated from 0.13 to 2 mTorr/min. Depending on the chamber conditions, a very low leak rate for relatively new chambers and higher leak rate for a chambers with long service time was observed. Overall, the leakage rate in the system was sufficiently low to carry out the depositions.

3.3.2 Calibration of Gas Flow System

CVD reactors and other process systems require that the rates of introduction of the process gases into the process chambers be controlled. In some applications, this is

achieved by adjusting the gas influx to maintain a constant chamber pressure. More commonly, the process gas flow is directly controlled. To do this, mass flow controllers are used. Mass flow controllers consist of a mass-flowmeter, a controller, and a valve. They are located between the gas source and the chamber, where they can monitor and dispense the gases at predetermined rates. The operation of a thermal mass flowmeter relies on the ability of a flowing gas to transfer heat. The mass flowmeter consists of a small sensor tube in parallel with the larger main gas flow tube. A heating coil is wrapped around the sensor tube midway along its length, and temperature sensors are located upstream and downstream of the heated point. When the gas is not flowing, and the heat input is constant, the temperatures at both sensors are equal. Flowing gas causes the temperature distribution in the sensor to change. It can be shown that the mass flow, m_f, is given by:

$$m_f = (\kappa\, W_h\, \Delta T)^{1.25} \tag{3.2}$$

Where W_h is the heater power, ΔT is the temperature difference between the points where the sensors are located, and κ is a constant that depends on the heat transfer coefficients, the specific heat of the gas, the density of the gas, and the thermal conductivity of the gas. Mass rate can be thus measured by the temperature difference.

Gas flows were controlled by Applied Materials model AFC 550 automatic N_2 mass flow controllers, which were, corrected for NH3 flow. The pressure in the reactor was measured with a barratry gauge from MKS. The N_2 calibration of the AFC was checked by delivering a fixed volume of gas (product of the metered flow rate and time) into the

known reaction chamber volume. The pressure increase was measured and used to calculate the volume of the gas corrected to the standard condition. (0°C, 1 atm). According to the gas law, the flow rate corrected to STP (sccm) is given by the formula :

$$\text{Flow Rate} = 60(\Delta P/\Delta t)(T_0 V/P_o T) \tag{3.3}$$

Where ΔP = pressure increase in Torr,

T_0 = 273 K

P_0 = 760 Torr

V = volume of the chamber, cm^3

Δt = time of delivering gas, sec.

Routine flow rate calibrations were conducted before every run.

3.3.3 Calibration of the Vapor Phase Flow Controller

$$PV = nRT \tag{3.4}$$

$$\Delta n/\Delta t = V/RT(\Delta P/\Delta t) \tag{3.5}$$

Where:

P = Pressure of the reactor chamber

R = Universal gas constant

T = Temperature of the chamber

n = number of moles of the gas

The reactor is maintained at room temperature. The volume of the reactor is calculated from the dimensions of the tube. By measuring the rate of pressure increase inside the reactor, the molar flowrate can be calculated from the equations above. Once the molar flowrate of the vapor has been calculated, the volumetric flow rate of the gas at standard conditions i.e., in sccm can be calculated using the equations given above.

3.4 Deposition Procedure

The boron nitride and titanium nitride films were deposited on 4 different types of substrates. (100) oriented single crystal p-type, boron-doped single-side polished Si wafers (Silicon Sense Inc.), (100) oriented single crystal p-type, heavily doped with boron single-side polished Si wafers (Silicon Sense Inc.), (111) oriented single crystal p-type , boron doped single-side polished Si wafers (Silicon Sense Inc.) and lastly fused quartz wafers (obtained from Hoya, Japan). The details of the Si wafers are given in Table 3.1. Apart from these substrates, the boron nitride films were also deposited on Platinum and Hafnium carbide films, which in turn were deposited on (100) p-type Si by Sputtering. The Titanium nitride films were also deposited on aluminum holders as well as on stainless steel watchstraps and dental drills

The wafers were labeled and accurately weighed (up to 4 decimal places) using an electronic balance. These wafers are then placed on a quartz boat. The wafers used to measure the stress on the film are placed back-to-back at a distance of 12.5 cm from one end of quartz boat and the quartz wafer at a distance of 4 cm from the stress monitors in

all the experiments. The boat was placed in the reaction chamber at a distance of 54 cm from the loading end.

Table 3.1 Specifications of the Si wafer

Property	Type - 1	Type – 2	Type - 3
Source	Silicon Sense Inc.	Silicon Sense Inc.	Silicon Sense Inc.
Diameter	100 mm	100 mm	100 mm
Orientation	<100>	<100>	<111>
Thickness	525 ± 25 μm	525 ± 25 μm	525 ± 25 μm
Type/Dopant	P/Boron	P/Boron	P/Boron
Resistivity	1 - 15	0.01 - 0.02	1 – 10
Grade	Test	Test	Test

Once the wafers are loaded, the door of the reactor is shut and all the inlet valves are closed. Now the bypass valve is opened and the chamber pressure is reduced from atmospheric pressure to 5 Torr. Then the outlet (main) valve is opened and pressure is dropped down to as low as 10 mTorr. This two-step procedure of reducing the chamber pressure ensures that the process wafers are not subjected to a sudden force and as a result they don't break. A low pressure is maintained inside the chamber using the vacuum pumps. The furnace is turned on and the required temperature is set. The reactor is then subjected to a baking period till the out gassing rate is very low. The average bake out time was found to be approximately 3 hours. precursor is injected into the reaction chamber through the vapor phase flow controller and Ammonia is added into the reaction chamber by means of the mass flow controller. Time of deposition was varied according to the required film thickness. Among the deposition parameters recorded were the background pressure, reaction temperature, flow rates of the reactants and the deposition

time. Experiments were performed to change the stoichiometry of deposited films by adding ammonia to the amine complex in the reactor.

Samples are allowed to cool to room temperature and the wafers are removed from the reactor by introducing nitrogen to fill the vacuum chamber and rise the pressure to atmospheric pressure. The samples are then weighed and the deposition rate can be calculated by knowing the mass gain (mg/hr) due to deposition. Samples were observed in an optical microscope for the presence of microcracks and for gas phase nucleation.

3.5 Characterization of Boron Nitride and Titanium Nitride Films

3.5.1 Thickness

The measurement of film thickness can be a fairly simple measurement or it can be a quite complex, depending on the nature of the film. The most direct technique is the measurement of the step height when a portion of the deposited film is etched away. This is done by electronically tracking the portion of a mechanical stylus as it is traversed across the step. In the case of a transparent film on a reflective substrate, the thickness of films can be measured by a polarizing spectrometer or “ellipsometer”. This is an instrument whose operation is based on the fact that elliptically polarized light changes its polarization upon reflection from a thin transparent film on a reflecting substrate. The ellipsometer creates an elliptically polarized monochromatic light beam on reflection from a thin film. The B-N-C-H film thickness was measured by Nanospec interferometer that bases its estimation on the monochromatic light interface fringes formed within a zone

limited by sample surface and a semi-transparent mirror. The device consists of Nanometrics Nanospec/AFT microarea gauge and SDP-2000T film thickness computer. The thickness of the film deposited on the wafer was measured at five different points. The refractive index provided was first estimated, as for silicon dioxide, 1.46 is the typical value. Thickness was measured at five different points on the wafer. Deposition rate was determined as the film thickness over the deposition time, and averaged over all the wafers in the run. The TiN film thickness was measured by a Sloan Dektak-II surface profilometer.

3.5.2 Growth Rate

Growth rate was determined in terms of Å/min, by dividing thickness by the time of deposition. Growth rate was used as measure of the rate of reaction and was studied with respect to the temperature of deposition as well as the partial pressures of the reactant gases in order to establish the rate equation.

3.5.3 Density

The films were deposited on just one side of the wafers by placing them back to back. The film was thus deposited on a known surface area of 78.5 sqcm and the thickness of the film was determined as described in section 3.5.1. Thus the volume of the film could be determined, and knowing the film weight, density could be determined as the ratio of mass (weight) to volume.

3.5.4 Refractive Index

The refractive index was determined by a Rudolph Research Auto EL ellipsometer, which consists of a polarizer and a compensator. Plane (45°) polarized light the polarizer is elliptically polarized when it passes through the compensator. It is then reflected by the sample surface, collected by a detector, analyzed for its intensity, and finally quantified by a set of delta psi values. The values were then fed to a computer that numerically solves the equation to give the refractive index of the film. The refractive index of the film deposited on the wafer was measured at five different points and then averaged out to the refractive index of the wafer.

3.5.5 Fourier Transform Infrared Spectroscopy

The vibrational motions of the chemically bound constituents of matter have frequencies in the infrared regime. The oscillations induced by certain vibrational modes provide a means for matter to couple with an impinging beam of infrared electromagnetic radiation and to exchange energy with it when the frequencies are in resonance. In this experiment, the intensity of a beam of infrared radiation is measured before (Io) and after (I) with the sample as a function of light frequency. A plot of I/Io versus the frequency is the "infrared spectrum". Fourier transform infrared (FTIR) spectra of the films obtained from Perkin - Elmer 580 were observed for B-N, B-N-B vibration modes and the presence of N-H, C-H bonding. The levels of interstitial oxygen and phosphorus were determined by using infrared absorption spectroscopy. The analysis was done on a Perkin-Elmer 1600 series FTIR spectrophotometer to determine the characteristics of the deposits. A spectrum of percent transmittance or absorption was obtained for samples of known thickness.

3.5.6 Film Stress

Stress develops in the film due to difference in the thermal coefficient of expansion of the film and the substrate, lattice mismatch between a crystalline film and the substrate, and also due to defects developed in the bulk during the growth process, which is termed as intrinsic stress. The stress in the film will cause the substrate to slightly bend after the deposition resulting in some radius of curvature.

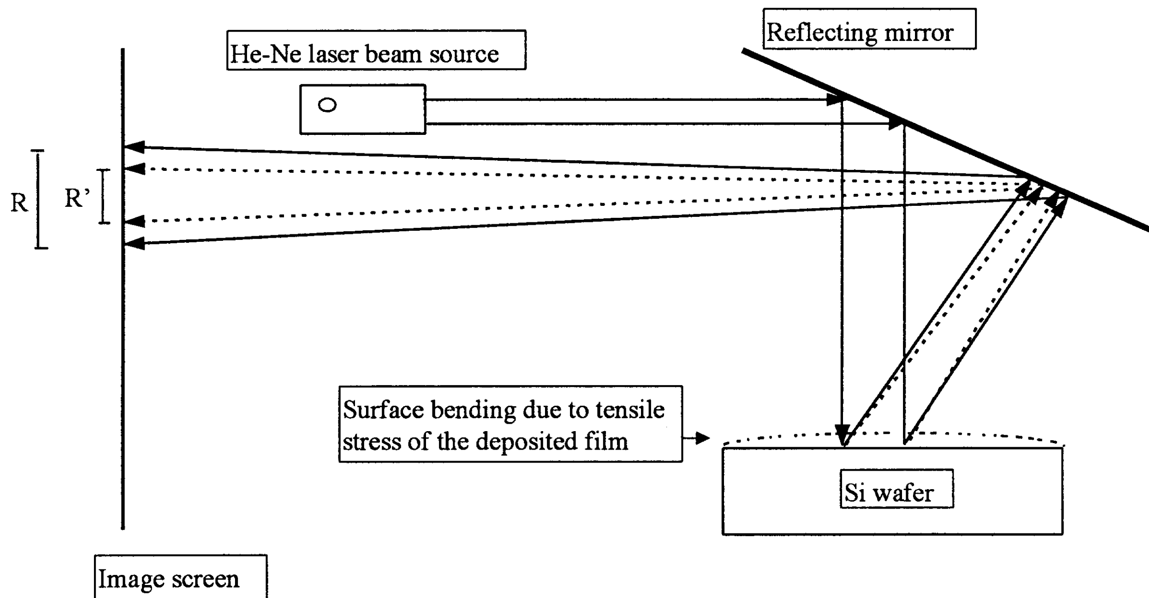

R - R' is the radius of curvature of bending

Figure 3.3 Schematic representation showing the experimental setup to measure the radius of curvature of the bending of silicon substrate due to stress in the film.

Stress of the film can be calculated using Stony's formula

$$\sigma_s = ED^2/6(1-\nu)Rt \qquad (3.6)$$

where E and ν are Young's modulus and Poisson ratio of the substrate. D, t are the substrate and film thickness' respectively, R is the radius of curvature of the composite. By convention R is negative for a convex wafer surface (compressive film stress) and positive for a concave wafer surface (tensile film stress).

Film stress was determined with a home-built system that measured changes in the radius of curvature of a wafer resulting from deposition on a single side. Such depositions were achieved by placing two wafers back to back. The experimental setup to measure the radius of curvature of the substrate bending is shown in Figure 3.3. The distance between two points generated by light from two fixed and parallel He-Ne lasers was determined after reflection from the surface of a wafer before and after deposition. An angled mirror was used to project the reflection of the two points onto a wall where their separation could be more accurately measured.

In the present set of experiments, for the wafers used, Young's modulus of the substrate was taken as 1.85 X 10^{11} Pa with a Poisson ratio of 0.3. Substrate average thickness was 525 μm. Considering the geometry of the instrument used, the equation (3.6) reduces to

$$\sigma_s(\mathrm{MPa}) = 12.3R'/t\ (\mu\mathrm{m}) \quad (3.7)$$

where R' is the difference of the deflection of the projected laser spots after and before deposition.

3.5.7 X-Ray Diffraction (XRD)

A collimated beam of X rays, with wavelength $\lambda \sim 0.5 - 2$ Å, was incident on the specimen and was diffracted by the crystalline phases in the specimen according to Bragg's law.

$$n\lambda = 2d\sin\theta \tag{3.8}$$

Where:

λ = X-ray wavelength,

d = Interplanar spacing,

θ = Bragg diffraction angle, and

n = Integer giving the order of the diffraction.

The intensity of the diffracted X rays is measured as a function of the diffraction angle 2θ and the specimen's orientation. This diffraction pattern was used to identify the specimen's orientation. This diffraction pattern was used to identify the specimen's crystalline phases and to measure its structural properties. This is a nondestructive technique with a probing depth of typically a few microns. The films deposited were analyzed using X-ray diffraction (XRD), so as to determine the orientation of the lattice planes. The equipment used was a Phillips X-ray Diffractometer, which was operated using APD software. A 40 kV voltage was used at a current of 45 mA to do the XRD. The angle (2θ) range scanned was 5° to 110° in a duration of 6 hours.

3.5.8 UV/Visible Spectrophotometer

The optical transmission of the films was measured using a Varian DMS 300 UV/visible spectrophotometer over a range of wavelength from 190nm to 900nm. This also gives an approximate estimation of the optical band gap of the semiconducting BN thin film. The optical transmission of the films were measured using a Varian DMS 300 UV/visible spectrophotometer over a range of wavelength from 200nm to 900nm. This was carried out with samples deposited on quartz substrate. The optical transmission of BN films were of particular interest at a wavelength of 6320 Å, since x-ray mask alignment equipiments rely on light rays around this wavelength. From the optical transmission spectrum, it is possible to estimate the optical band gap. The optical band gap is determined from the calculated values of absorption coefficient, α. The intensity of the transmitted wave, I, through a film of thickness t, is related to the intensity of incident wave I_o by Beer-Lambert law

$$I = I_o e^{-\alpha t} \tag{3.9}$$

If the average thickness of the film is known, then absorption coefficient for each wavelength can be calculated. The absorption coefficient of semiconducting films in the high-absorption region ($\alpha > 10^4$ cm^{-1}), assuming parabolic band edges and energy-independent matrix elements for interband transitions, is given according to Tauc by the following equation:

$$\alpha h\nu = K_1 \frac{(h\nu - E_{g(opt)})^2}{h\nu} \tag{3.10}$$

where hγ, $E_{g(opt)}$ and K_1 denote the photon energy, optical energy gap, and an energy-independent constant, respectively. Formally, the optical band gap $E_{g(opt)}$ is obtained as the intercept of the plot of $(\alpha * h\gamma)^{1/2}$ against hγ.

3.5.9 Hardness and Young's Modulus Measurements

The hardness and Young's modulus of the BN and TiN films were determined using a Nano Instruments indenter. The system consisted of a diamond tip, with the same area-to-depth ratio as the traditional. At the top of the loading column was a coil and magnet assembly that provided a controlled loading force with a resolution of about 0.5 μN. The position of the indenter was determined by a capacitance displacement gauge which allows one to detect displacement changes of 0.2-0.3 nm. In all cases a minimum of 16 curve represents the observed displacement due to an increased loading at a constant rate of 200 μN/s to a maximum of 4.5 mN. The second segment of the curve represents the unloading at the same constant rate down to 20% of maximum load. From that latter segment, the deformation contact depth h_p and elastic recovery depth h_e can be measured. A linear least squares fit of the upper segment extrapolated down to 0 yields the value of h_p. The difference between the maximum displacement and h_p yields the value of h_e. The hardness is obtained at the maximum displacement using the formula

$$H = P / A \tag{3.11}$$

where P is the applied load and A is the contact area calculated from the known geometry of the indenter

$$A = 24.56\, h_p^2 + 225.94\, h_p^{3/2} + 519.61\, h_p \tag{3.12}$$

Assuming that the area in contact remains constant during initial unloading and adopting Sneddon's solution for the elastic deformation of an isotropic elastic material, the elastic modulus is obtained from the contact stiffness S, the slope of the unloading curve, given by

$$S = dP / dh = 2 E_r \sqrt{A / \pi} \tag{3.13}$$

where h is the displacement of the indenter, and E_r is the composite moduus for the indenter/sample combination

$$E_r = \frac{1}{[(1-\nu_f^2)/E_f]+[(1-\nu_i^2)/E_i]} \tag{3.14}$$

where E_f and E_i are Young's moduli for film and indenter, respectively, and ν_f and ν_i are Poisson's ratios for the film and the indenter, respectively. Since ν appears as a quadratic term and therefore represents only a small correction, ν_f was taken as 0.3, while the values for the diamond indenter E_i and ν_i were taken to be 1010 GPa and 0.213, respectively.

3.5.10 X-ray Photoelectron Spectroscopy (XPS)

X-ray photoelectron spectroscopy was used for the compositional analysis of the boron nitride films. Low energy x-rays of K-alpha aluminum (which has energy of 1.487 keV) were used to cause the photoelectron emission. The principle used here is that just as the electron bombardment of materials can produce emitted electrons and x-rays, striking the material with x-rays can do the same. In this technique, only electrons from the top 1-10 monolayers are emitted without significant loss from collision. Thus even though the x-ray beam penetrates deep into the sample material, XPS is basically a surface analysis

technique. However the films were sputtered by ion milling to a depth of 500Å and then again the analysis was carried out. Hence both the surface as well as the composition in the film were determined by this technique.

3.5.11 Auger Electron Spectroscopy (AES)

Auger electron spectroscopy (AES) uses a focused electron beam to create secondary electrons near the surface of a solid sample. Some of these (the Auger electrons) have energies characteristic of the elements, and in many cases, of the chemical bonding of the atoms from which they are released. Because of their characteristic energies and shallow depth from which they escape without energy loss, Auger electrons are able to characterize the elemental composition and at times the chemistry of the surfaces of samples. AES has the attributes of high lateral resolution, relatively high sensitivity, standardless semiquantitative analysis, and chemical bonding information in some cases.

3.5.12 Scanning Electron Microscopy (SEM)

The scanning electron microscope (SEM) is often the first analytical instrument used when a quick look at a material is required and light microscopy no longer provides adequate resolution. In the SEM an electron beam is focused into a fine probe and subsequently raster scanned over a small rectangular area. As the beam interacts with the sample it creates various signals, all of which can be appropriately detected. These signals are highly localized to the area directly under the beam. By using these signals to modulate the brightness of a cathode ray tube, which is raster scanned in synchronism with the electron

beam, an image is formed on the screen. This image is highly magnified and usually has the look of a traditional microscopic image but with a much greater depth of field.

3.5.13 Rutherford Backscattering Spectrometry (RBS)

Rutherford backscattering spectrometry (RBS) analysis is performed by bombarding a sample target with a monoenergetic beam of high energy particles, typically helium, with an energy of a 2 MeV. A fraction of the incident atoms scatter backwards from heavier atoms in the near surface region of the target material, and usually are detected with a solid state detector that measures their energy. The energy of a backscatterred particle is related to the depth and mass of the target atom, while the number of backscattered particles detected from any given element is proportional to concentration. This relationship is used to generate a quantitative depth profile of the upper 1 – 2 micron of the sample. Alignment of the ion beam with the crystallographic axes of a sample permits crystal damage and lattice locations of impurities to be quantitatively measured and depth profiled.

3.5.14 Resistivity

A number of techniques are employed to measure electrical properties of thin films. For insulating films, where current flows through the film thickness, electrodes are situated on opposite film surfaces. Small evaporated or sputtered circular electrodes frequently serve as a set of equivalent contacts; the substrate is usually the other contact. For more conductive metal and semiconductor films, it is common to place all electrodes on the

same film surface. Such measurements employ four terminals - two to pass current and two to sense voltage. The following figure shows the contact configuration.

A very common way to report values of thin-film resistivity is in terms of sheet resistance with units "ohms per square." To understand this property and the units involved, consider the film of length l, width w, and thickness d. If the film resistivity is ρ, the film resistance is $R = \rho l/wd$. Furthermore, in the special case of a square film, ($l=w$),

$$R = Rs = \rho/d \text{ ohms}/\Box, \tag{3.15}$$

A very convenient way to measure the sheet resistance of a film is to lightly press a four-point metal tip probe assembly into the surface as shown in Fig. xyz. The outer probes are connected to the current source, and the inner probes detect the voltage drop. Electrostatic analysis of the electric potential and field distributions within the film yields

$$Rs = KV/I, \tag{3.16}$$

where K is a constant dependent on the configuration and spacing of the contacts. determine the resistivity of the film, first the sheet resistance was determined using a standard four-point probe. The sheet resistance when multiplied by thickness of the film gave the resistivity of the film.

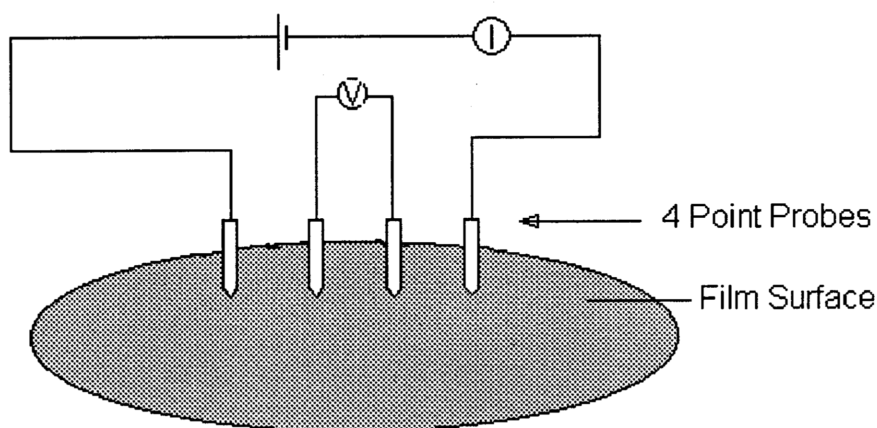

Figure 3.4 Schematic representation of a four point probe

3.5.15 Emissivity

Temperature dependent emissivity of TiN was acquired using a spectral emissometer. This emissometer consists of a Fourier transform infrared spectrometer designed specifically to facilitate simultaneous measurements of surface emittance and temperature by using optical techniques over the near- and mid-IR spectral range and temperatures ranging from 300 to 700 K. These measurements gave the spectral data for reflectance, transmittance and emittance of the films as a function of wavelength.

3.6 Electrical Characterization of BN Thin Films

3.6.1 Metallization of BN Films

The electrical properties of the synthesized films were determined by studying the characteristics of the devices made by the films. To study the electrical characteristics of

the device, an electrical contact is needed which was provided by Al metallization. The boron nitride thin films were coated with pure Al. This was done in an evaporator, and the important parameters of deposition are given in Table 3.2. A mask is used to obtain Al dots of diameter 300μm and 600μm on the boron nitride film, while a uniform coating of Al is deposited on the back surface (Si surface of the stress monitor).

Table 3.2 Parameters for metallization of BN thin films

Base pressure	10^{-6} Torr
Heating source	Tungsten filament (resistance heating)
Evaporating source	Al wire
Purity of evaporating source	99.9999% (Al)
Rate of deposition	50 Å/min.
Ultimate thickness of deposit	900 Å
Substrate temperature	room temperature
Distance between the filament and the substrate	200 mm
Size of the dots	300 μm and 600μm diameter

Thin Al films were deposited by applying heat to the source of the film material, thereby causing evaporation. The heated source was resided in a high-vacuum environment, hence the vaporized atoms/molecules are likely to strike the substrate without suffering any intervening collisions with other gas molecules. The rate of mass lost from the source per unit area per unit time, R, as a result of such evaporation, can be estimated from the Langmuir-Knudsen relation:

$$R = 4.43 \times 10^{-4} (M/T)^{1/2} P_e \quad (3.17)$$

$$R = 5.83 \times 10^{-2} (M/T)^{1/2} P_e \quad (3.18)$$

Where: M is the gram-molecular mass; T is the temperature in °K, and P_e is the vapor pressure in Pa.

Al films were deposited with resistance-heated source. That is, a wire of low vapor pressure metal Tungsten was used to support small strips of the metal to be evaporated. The substrate was placed above the source. The chamber is now evacuated and a pressure as low as 10^{-6} torr is achieved. Now the power supply to the resistance is slowly increased i.e., the W-wire is then resistively heated till Al on the resistance wire melts and evaporates. Once evaporated, the vacuum is broken and the chamber is opened. The substrate coated with the Al film is then removed.

3.6.2 Device Fabrication

Two kinds of devices were built using boron nitride thin films, the MOS (Metal Oxide Semiconductor) and the MIM (Metal Insulator Metal). Further, the MIM structures were built by 2 ways, in the first method a metal film was deposited on the Si substrate and in the second, a very highly conducting Si substrate was used i.e., type - 2 substrate as shown in the table. The process flow diagram for the fabrication of the devices is shown in detail as follows:

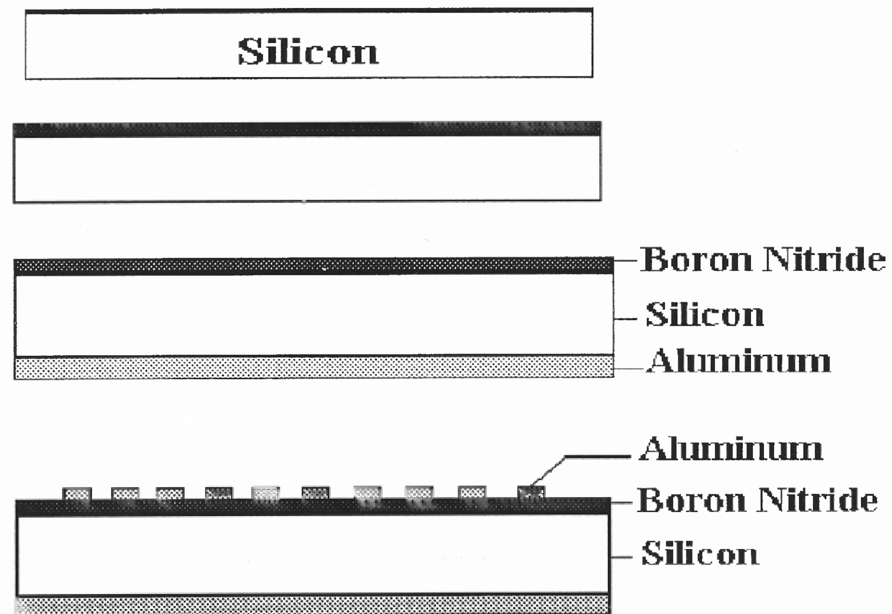

Figure 3.5 Process flow diagram for the fabrication of the MOS device.

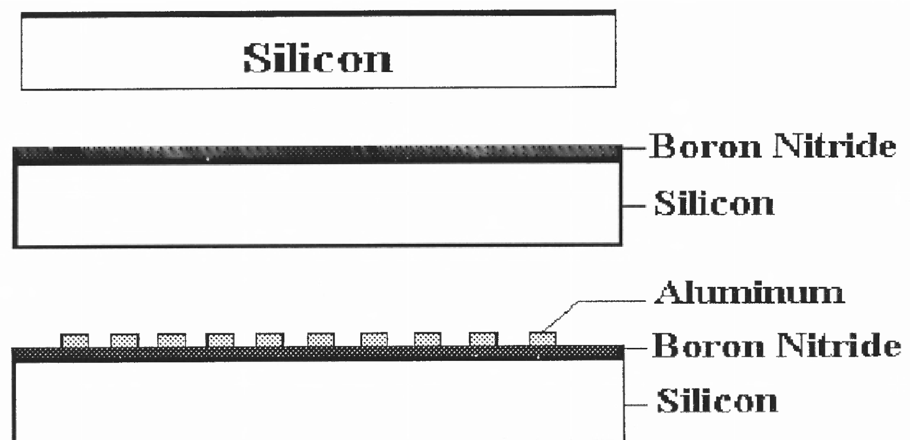

Figure 3.6 Process flow diagram for the fabrication of the MIM device (Si Type-2)

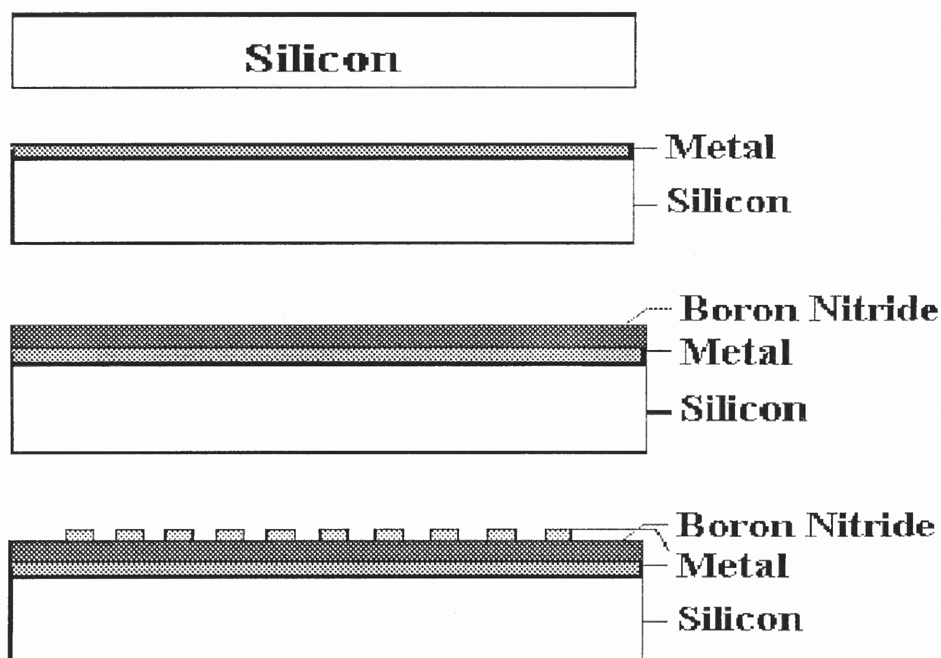

Figure 3.7 Process flow diagram for the fabrication of the MIM device with metal film

3.6.3 Capacitance - Voltage (C-V) and Current - Voltage (I-V) Measurements

Capacitance - voltage (C-V) and current - voltage (I-V) measurements was done for the films on both the low resistivity as well as the high resistivity p - type Si substrates. On the front side of BN, Al dots were evaporated through a shadow mask. The back side BN was removed by plasma etching (if necessary) and Al was deposited for back contact as explained in the previous section. The dielectric constant of the BN films were measured at five places and the breakdown voltage was determined. Subsequently, a bias stress study was made by applying a ± 1MV/cm for 2 - 5 minutes at room temperature and C-V measurements were done after each polarity of stress. Temperature-bias stress measurements were also made to find out if there are trapped charges in the insulator. This was done by applying a positive and negative polarity of 0.5 MV/cm for 10 minutes at 120 °C. To find out the nature of the charges, bias-temperature aging studies were done on the

samples. The recombination-generation kinetics of the electrons in the inversion region of the device was studied by taking the C-V measurements with a-c signals at different frequencies. Frequencies ranging from 10 Hz to 1Mhz were used in this study. Also, the mobility of charges and the presence of charge traps were studied by shining of light with different intensities on the devices.

3.7 Free Standing B-N-C-H membrane

3.71 Fabrication of Free Standing B-N-C-H Membranes

The process flow diagram for fabricating the freestanding X-ray windows and resulting cross sectional view are shown in Figures 3.8 and 3.9. P type (100) Si wafers were deposited with LPCVD B-N-C-H films on both sides and then processed in NJIT's class-10 clean room. The wafers were cleaned in the wet chemical stations with M-pyrol primary and secondary baths maintained at 90 °C for 10 minutes each and this was followed by a DI-water rinse for 10 minutes. This process was carried out to cleanse the wafer from any organic impurities. The wafers were then spin/rinse/dried in a Semitool systems dryer. Positive photoresist was then applied on the back side of the wafer and was soft baked at 110 °C for one minute. The wafer was then placed in the Karl Suss exposure tool with the mask and exposed for 30 seconds. This was followed by the pattern development for 6 minutes following which the wafers were hard baked at 115 °C. The patterned wafers were placed in the Phantom RIE reactive ion etcher with a CF_4 flow of 40 sccm, pressure of 250 mTorr and a power of 150 W. The wafers were etched for 6

minutes to form the pattern and after inspection were placed in a KOH bath at 90 °C for 10 hours to form the freestanding B-N-C-H membranes.

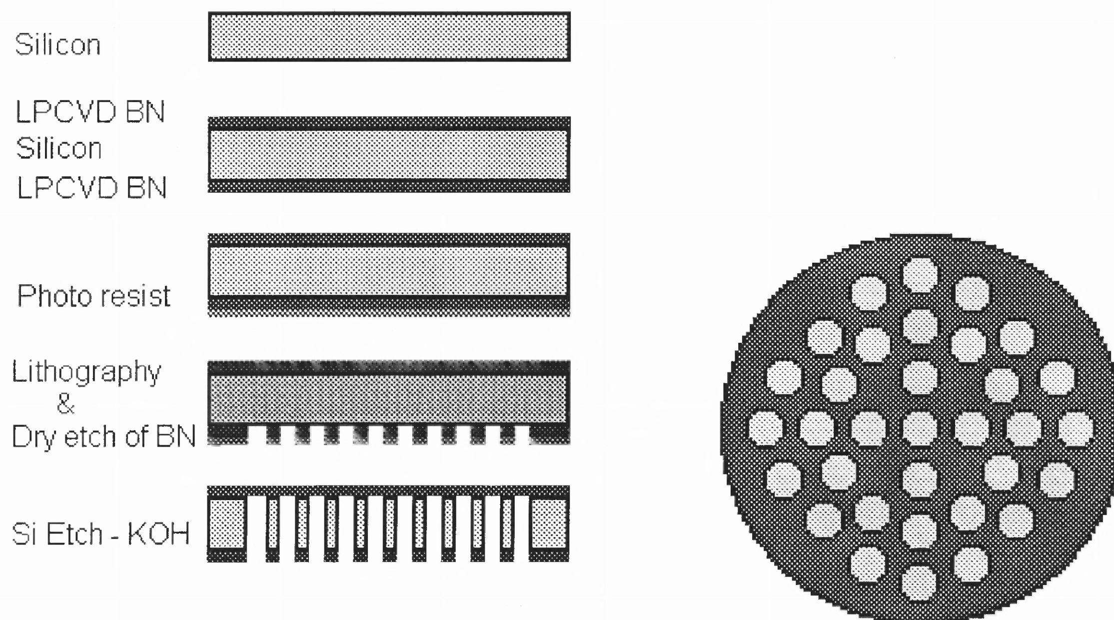

Figure 3.8 Process flow diagram for the fabrication of the free standing B-N-C-H membranes

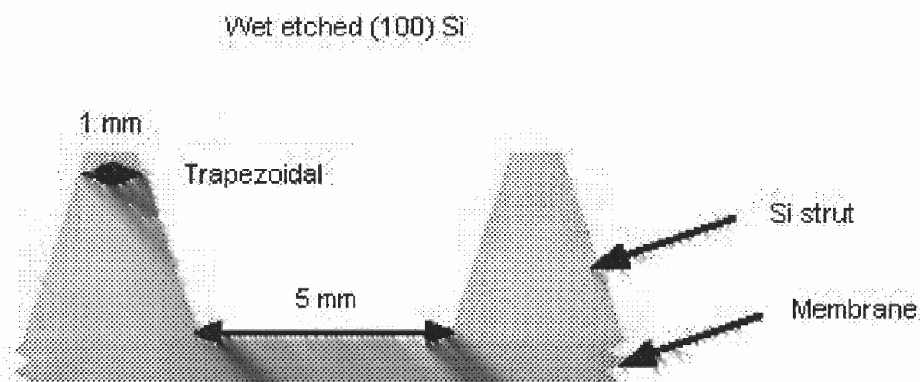

Figure 3.9 Cross sectional view of the X-ray window

3.7.2 Characterization of B-N-C-H Free Standing Membranes

The Freestanding membranes, which were fabricated as explained in the previous section were then reactive ion etched with CF_4 plasma to obtain membranes with different thickness. Freestanding membranes from 2000 Å to 10,000 Å were produced by this way. These membranes were then tested for X-ray transmission through them as a function of X-ray energy and were compared to the transmission obtained from the commercially used X-ray window.

CHAPTER 4

RESULTS AND DISCUSSION

4.1 Introduction

The growth kinetics, film properties, and applications of LPCVD boron nitride (B-N-C-H) and titanium nitride (Ti-N-Cl) films synthesized on Si and quartz substrates are discussed in this chapter. The numerous current and potential applications of these films are based on their properties, which are in turn dependent upon the stoichiometry and further on the deposition technique and the processing conditions. Hence, in this chapter an effort has been made to correlate the properties of the deposits with the stoichiometry and the film processing conditions. Changes in the mechanical, electrical, optical, and structural properties due to variations in the process parameters are also explained. Reaction mechanism explaining the experimental growth kinetics data for LPCVD TiN has also been discussed.

This chapter also discusses the fabrication, characterization and testing of the LPCVD B-N-C-H freestanding X-ray windows. The performance characteristics of these X-ray windows are discussed and compared with the commercially available ones. In addition to this, results from the investigation of LPCVD BN as an inorganic low dielectric constant material, LPCVD TiN as a highly reflective stoichiometric film at temperatures below 600 °C, and LPCVD TiN as a wear resistant coating for tooling applications are also discussed.

In all the experiments, films deposited were uniform and no peeling was observed indicating that the adhesion properties of both the B-N-C-H and Ti-N-Cl films on silicon and quartz substrates are excellent. There were no cracks on the film surface and the film thickness was found to be uniform across the wafer with a deviation of up to ±5%. Observation of the film under the optical microscope revealed no presence of particulate matter or voids, suggesting that gas phase nucleation was avoided. In this chapter, we shall first study the growth kinetics, film composition, and properties of the B-N-C-H films, which will be followed by the same for Ti-N-Cl films.

4.2 Kinetic Study of Boron Nitride Deposition by LPCVD

4.2.1 Influence of Temperature on the Deposition Rate and Film Composition

At a fixed TEAB complex flow rate of 17 sccm, total pressure of 500 mTorr, and a NH_3/TEAB flow ratio of 10/1, the deposition rate is shown in Figure 4.1 for the deposition temperature range of 300 to 850 °C. From 300 to 400 °C, the rate follows an Arrhenius behavior yielding an apparent activation energy of 22 kcal/mol. Above 400 °C, the growth rate is observed to decrease monotonically with increasing temperature due to a combination of effects, including the transition into the mass transfer limited regime, the adsorption of decomposition products which act as retardants to the growth process, a decrease in the equilibrium conversion for exothermic reactions, and due to the depletion of reactants caused by the reactions on the hot wall of the furnace. The decrease in deposition rate was seen to continue till 650 °C above which the triethylamine complex decomposes into nitrogen and low molecular weight hydrocarbons, which adsorb over the

surface resulting in the incorporation of carbon and hydrogen into the films and increasing the deposition rate. From this point the deposition rate is controlled by the breakup of the complex and it is seen to increase gradually as temperature is increased from 700 to 900 °C. It should be noted that at this point the film is composed primarily of carbon as observed by the AES compositional analysis. Increasing the temperature further increases this process and increases the carbon content.

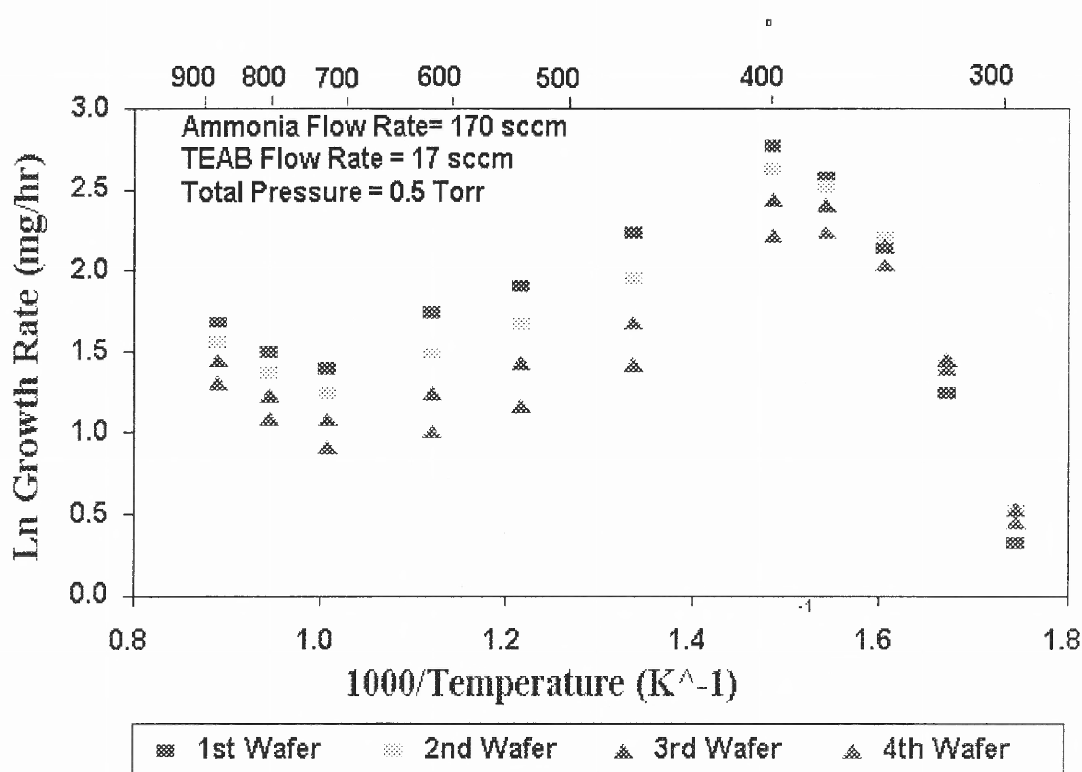

Figure 4.1 Variation of average growth rate as a function of temperature

It can be seen from Figure 4.2 that at any constant NH3/TEAB flow ratio, as the deposition temperature is increased from 400 to 600 °C, the B/N composition ratio decreases approaching stoichiometry. Since the TEAB complex is the limiting reactant,

operating in the mass transfer controlled regime results in the depletion of TEAB, which results in an increase in the adsorption of NH3 on the reaction sites and a subsequent increase in the nitrogen content resulting in the production of films trending towards stoichiometry. This trend continues only up to 600 °C, above that temperature, the reaction kinetics and the resulting film composition is controlled by the TEAB complex breakdown. For all the investigated NH3/TEAB flow ratios the carbon content in the films was seen to increase with an increase in deposition temperature from 400 to 600 °C as shown in Figure 4.3. This is due to the initiation of the breakup of the complex which occurs at ~ 650 °C. Films which were deposited at or above 700 °C were found to have up to 80 % carbon and 10 % each of boron and nitrogen.

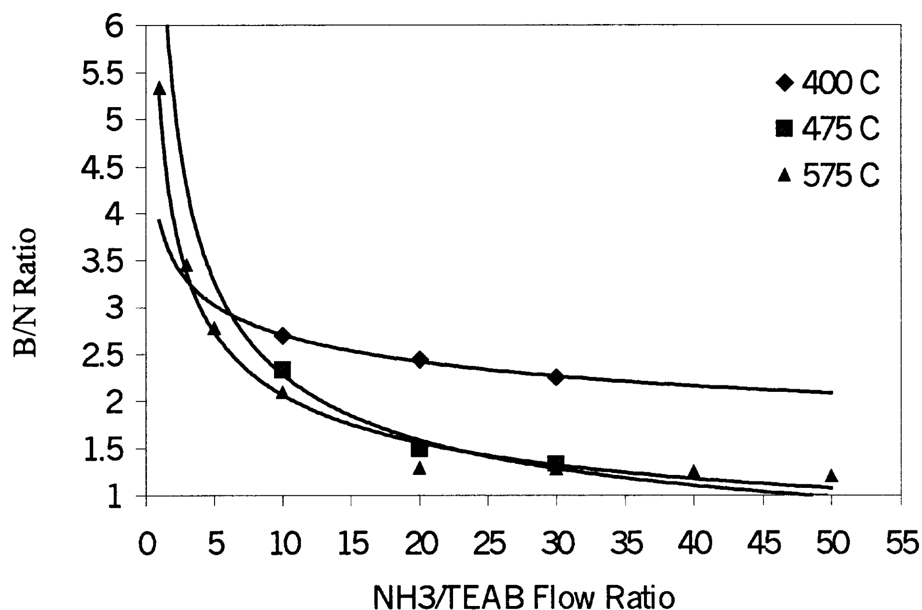

Figure 4.2 Film composition as a function of deposition temperature.

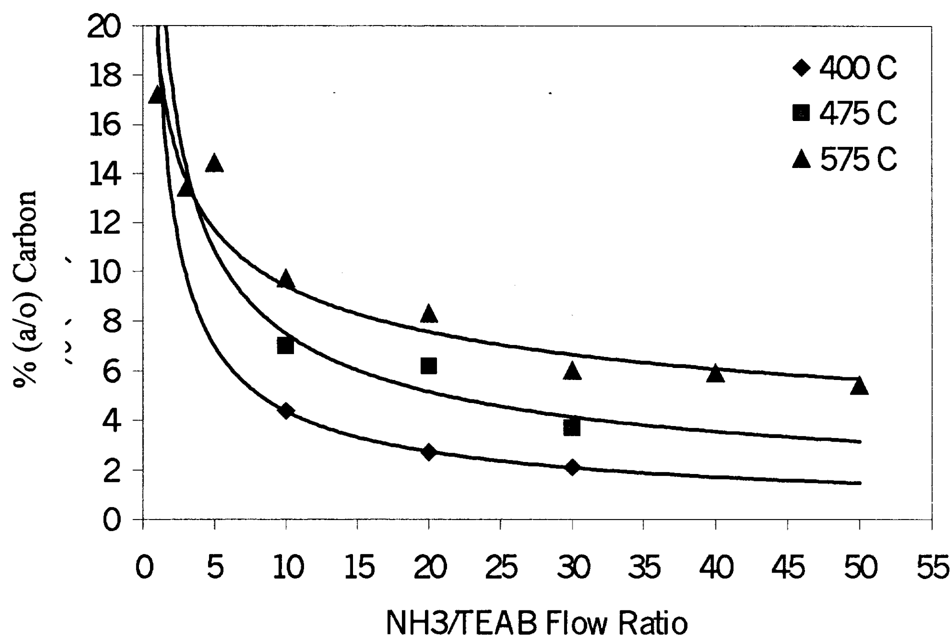

Figure 4.3 Carbon concentration in the films as a function of deposition temperature.

4.4.2 Influence of Reactant Flow ratio on the Deposition Rate and Film Composition

A plot of growth rate as a function of the flow ratio is shown in Figure 4.4. At a constant total pressure of 100 mTorr and deposition of 575 °C, it is seen that as the NH3/TEAB flow ratio is increased from 1 to 2000, the deposition rate decreases sharply from around 70 A/min to 5 A/min approaching a plateau at around 200 sccm. It is also important to note that the depletion along the reaction chamber decreases reaching a minimal spread at around 200 sccm. Both these observations are consistent with an incremental filling of surface sites by the higher presence of NH3 which not only dilutes the amount of TEAB, thus accounting for the reduced growth rate, but also makes more TEAB available to react downstream, thus, accounting for the reduced depletion effects. Figures 4.2, 4.3, and 4.5 show the variation in the film composition at different deposition temperatures with a

variation in the NH3/TEAB flow ratio. It is seen that at any constant deposition temperature, an increase in the NH3/TEAB flow ratio results in the decrease in the B/N ratio of the films. In other words, the films trend towards stoichiometry as the flow ratio is increased. At a deposition temperature of 575 °C, it can be seen that the B/N ratio decreased from ~5.5 to ~1 as the NH3/TEAB flow ratio was increased from 1 to 1000. At the same time, an increase in the NH3/TEAB flow ratio causes a decrease in the carbon content in the deposits. Both these figures confirm the previously suggested mechanism of NH3 dilution resulting at higher NH3/TEAB flow ratios.

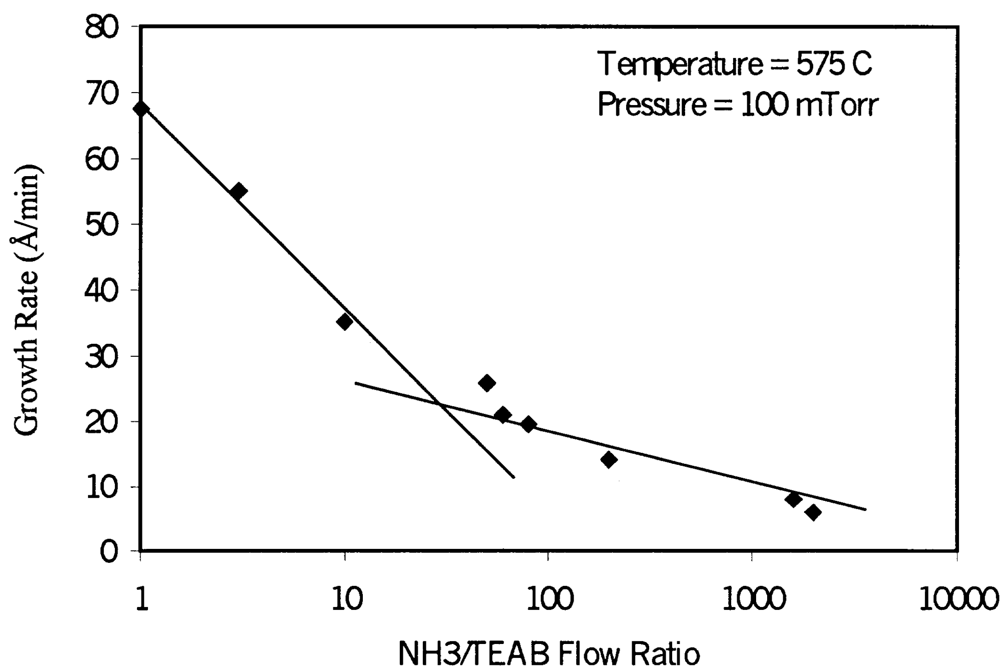

Figure 4.4 Variation of growth rate with the flow ratio of the reactants.

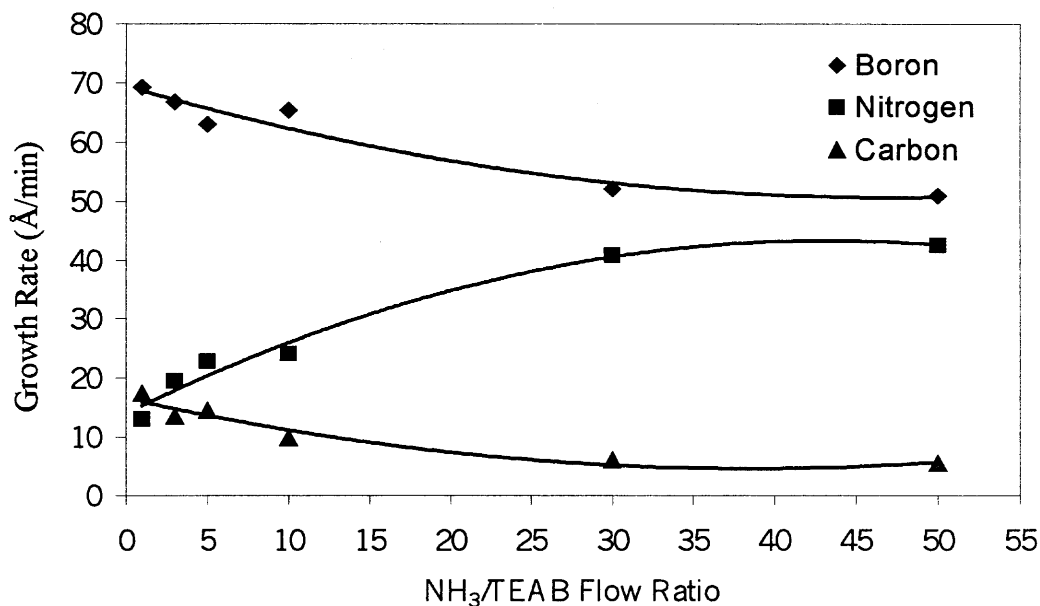

Figure 4.5 Variation of Film composition as a function of NH3/TEAB flow ratio

4.3 FTIR Spectroscopy and Auger Analysis of BN Thin Films

Infrared absorption spectroscopy showed large differences in the chemical bonding of hydrogen to both boron and nitrogen as B-H, NH_2 and possibly N-H. The broadness and frequency shifting of the B-N band also depends on experimental conditions. Peaks were seen at 3400 cm^{-1}; 3220 cm^{-1} and 1540 cm^{-1}; 2500 cm^{-1}; strong and asymmetric at 1400 cm^{-1}; and weaker and sharper at 800 cm^{-1}. These absorption bands were respectively attributed to the characteristic vibrations of N-H, NH_2, B-H bond stretching, B-N bond stretching and to B-N-B bond bending. The spectrum was sensitive to the deposition temperature. The typical FTIR absorption spectra of boron nitride thin films (Figure 4.3(a)) at 400°C, 0.5 Torr pressure and a flow ratio of NH3/TEAB = 10/1 showed absorption peaks at wavenumber of about 1350 cm^{-1} corresponding to the B-N vibration

mode, and a small peak close to 800 cm^{-1} corresponding to the B-N-B vibration. Apart from these major peaks, B-H peak at wavenumbers 2500 cm^{-1}, and N-H peaks at wavenumbers 3200 cm^{-1} and 3400 cm^{-1} C-H peak at 2900 cm^{-1} could be seen. Also a contamination O-H peak can be seen at about 3600 cm^{-1}.

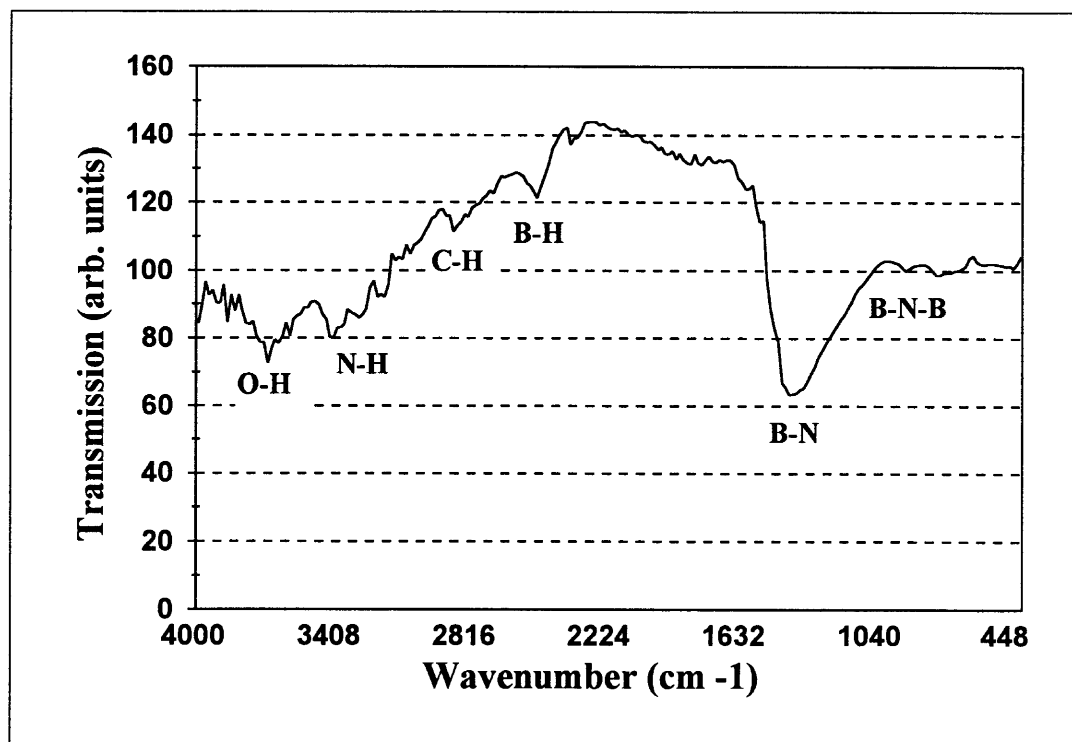

Figure 4.6(a) Typical FTIR spectrum of BN films at 400°C

It can be seen that the B-N and B-N-B absorption peaks increase with increasing flow rate of ammonia at all the temperatures under consideration. In addition, with increase in temperature, at 550°C (Figure 4.3(b)), the peaks at wavenumbers 3400 cm^{-1}, 3200 cm^{-1}, and 2900 cm^{-1} and 2500 cm^{-1} corresponding to N-H, C-H and B-H vibration modes respectively disappear.

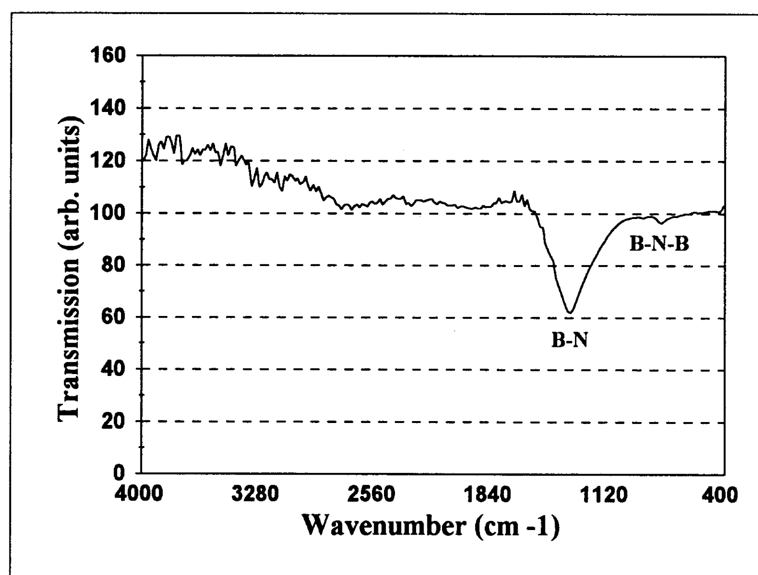

Figure 4.6(b) Typical FTIR spectrum of BN films at 575°C

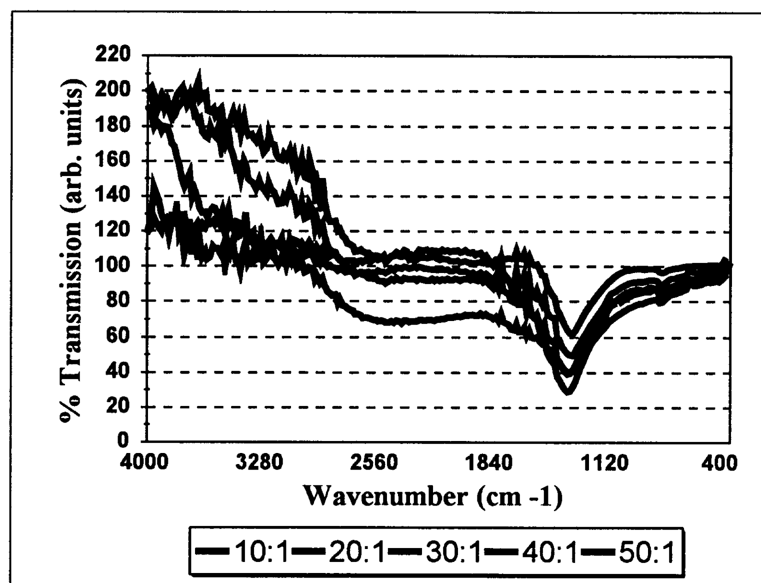

Figure 4.7 Variation in the spectra with the flow ratio at 550 C.

Figure 4.6(b) shows the shift in the peak position with increasing temperature at a constant flow ratio of NH_3/TEAB = 50/1. This indicates that the stoichiometry of the film is changing with increasing flow ratio. As the thickness increases, the intensity of the peak also increases. Auger analysis indicated a carbon percentage of about 8, but from the

infrared absorption spectra, no C-C or C-H peaks at high temperatures and at high flow rate could be identified. This reveals that it is not bonded in any carbide form, rather in an elemental form. Thus, FTIR is insensitive to the presence of carbon in the film. Thus the film is essentially amorphous carbon containing boron nitride.

4.4 Properties of LPCVD BN Thin Films

4.4.1 Film Density

The density of the films was determined by dividing weight gain by film volume as calculated from the product of film thickness and known area of the wafer. The thicknesses used were based on the values obtained by the Nano spectrophotometer. Figure 4.8 shows the variation of the film density as a function of deposition temperature for the NH3/TEAB flow ratios of 10/1, 20/1, and 30/1. At a constant deposition temperature, it is seen that the density increases with increase in flow ratio of NH_3/TEAB. This could be explained by the composition changes that take place with increasing flow ratio. Increasing the NH3/TEAB flow ratio causes the film stoichiometry to shift from B5N to B3N to BN, which means that the N content in the film increases as the flow ratio is increased, resulting in the increase in the film density. Examination of the films under the optical microscope did not show evidence of any gas phase nucleation or voids. For all the flow ratios, increase in the deposition temperature resulted in a slight increase of film density up to 550 C and decrease at higher deposition temperatures. Higher deposition temperature is believed to eliminate voids and decrease the incorporated hydrogen content from the deposits. This is consistent with the findings from FTIR spectroscopy where the N-H and B-H and C-H peaks were found to disappear at higher deposition temperatures.

Film density values as high as 2.22 g/cc were calculated which is near the 2.25 g/cc reported in the CRC handbook for hexagonal BN. However, as the deposition temperature approaches 600 C, at which the TEAB complex breaks down, the carbon concentration in the film begins to increase significantly. At a deposition temperature of 575 C and NH_3/TEAB flow ratio of 10/1, the film comprises of 65% B 25% N and 10% C. The C basically replacing the N sites and hence the density begins to decrease. At temperatures higher than 600 C, the film is composed primarily of carbon and it could be considered as a polymer for all practical purposes. The B and N content drop to around 10% each and hence the film density drops significantly.

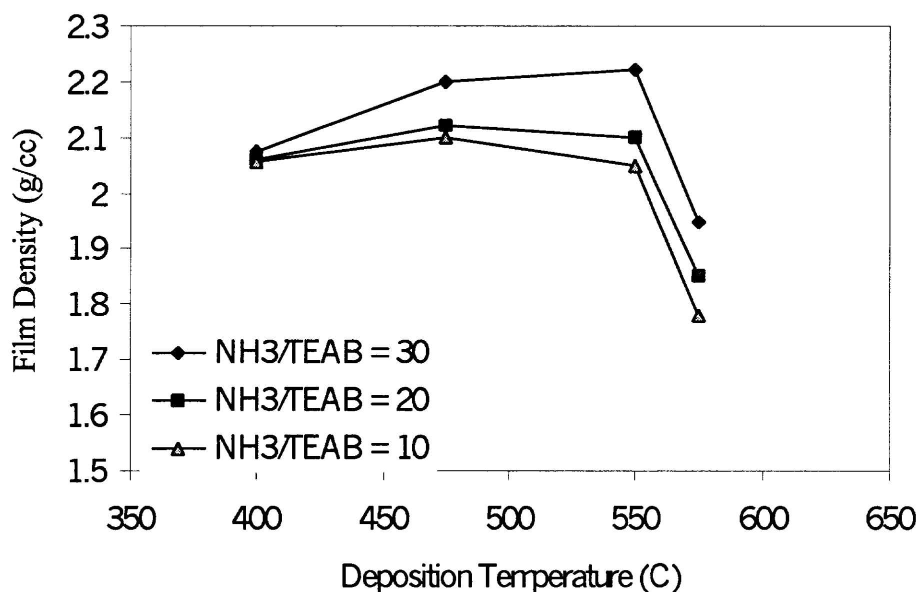

Figure 4.8 Variation of film density with increasing flow ratio of NH_3/TEAB

4.4.2 Refractive Index

Figure 4.9 shows the variation of the refractive indices of the film with the NH_3/TEAB flow ratio for the deposition temperatures of 400, 475, 500, and 575 C. In all cases,

increasing the NH3/TEAB flow ratio resulted in a decrease in the film refractive index. From the composition analysis we have seen that increasing the NH_3/TEAB flow ratio causes a reduction in the incorporated carbon in the films and the B/N ratio approaches stoichiometry. This could explain the decrease in the refractive index values. For a deposition temperature of 575 C, increasing the NH_3/TEAB flow ratio from 1/1 to 1000/1 caused the refractive index to decrease from 2.4 to 1.76. The decrease is sharp for the flow ratio change from 1/1 to 30/1, after which the refractive index stabilizes at around 1.8 up to an investigated flow ratio of 2000/1.

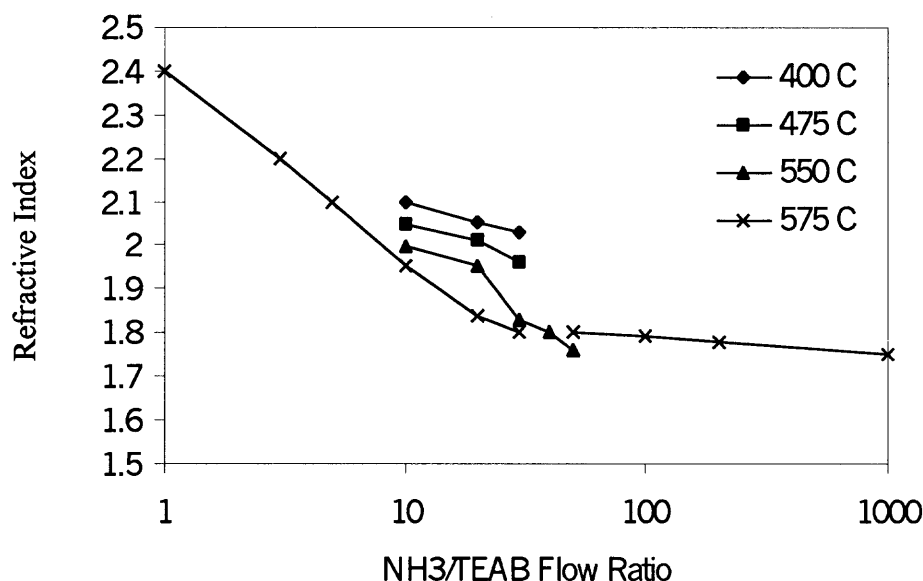

Figure 4.9 Variation of refractive index with increasing flow ratio of NH_3/TEAB

The changes in the refractive index track the compositional changes that take place due to the variation in the flow ratio. The carbon content is seen to exhibit a similar dependence on the NH3/TEAB flow ratio. An increase in the deposition temperature was seen to decrease the film refractive index consistently for the 4 deposition temperatures studied.

This is attributed to the formation of stoichiometric boron nitride films as the temperature is increased. It should be noted that this behavior holds only till 575 C, above which the breaking of the TEAB complex results in the incorporation of high amounts of carbon in the films and an increase in the refractive index.

4.4.3 Film Stress

The addition of an atom having different bonding radii to a matrix film is an effective method for changing the stress of the film. In a low pressure chemically vapor deposited BN film, it is difficult to obtain tensile stress except for extremely boron-rich films. The controllability of tensile stress in BN film was improved by the introduction of a small amount of carbon into the BN matrix, using LPCVD between 400 and 800 C. Also the radiation resistance of BNC deposited films was improved five times better than that of LPCVD BN. At lower flow ratios of 10:1 of NH_3:TEAB (Figure 4.10), the films were mildly tensile and the values are comparable (about 50MPa). With increase in the ammonia flow rate, the stresses in the film changed from mildly tensile to mildly compressive and the trend continued at higher flow ratios of 50:1 at 550°C. Within the temperature ranges studied the highest compressive stress attained was about 150 MPa. The effect is mainly due to the influence of ammonia which increases the nitrogen percentage in the films since the carbon percentage is almost constant over this range of temperature. At lower temperatures and low ammonia flow rate the films were mildly tensile and the films became more tensile with increase in temperature. while at higher flow ratios and lower temperature, the films were mildly compressive and the compressive stress increased with increase in temperature. Interestingly, a transition from mildly compressive to mildly

tensile behavior with increase in temperature was seen in the films at a constant NH_3/TEAB ratio of 20:1.

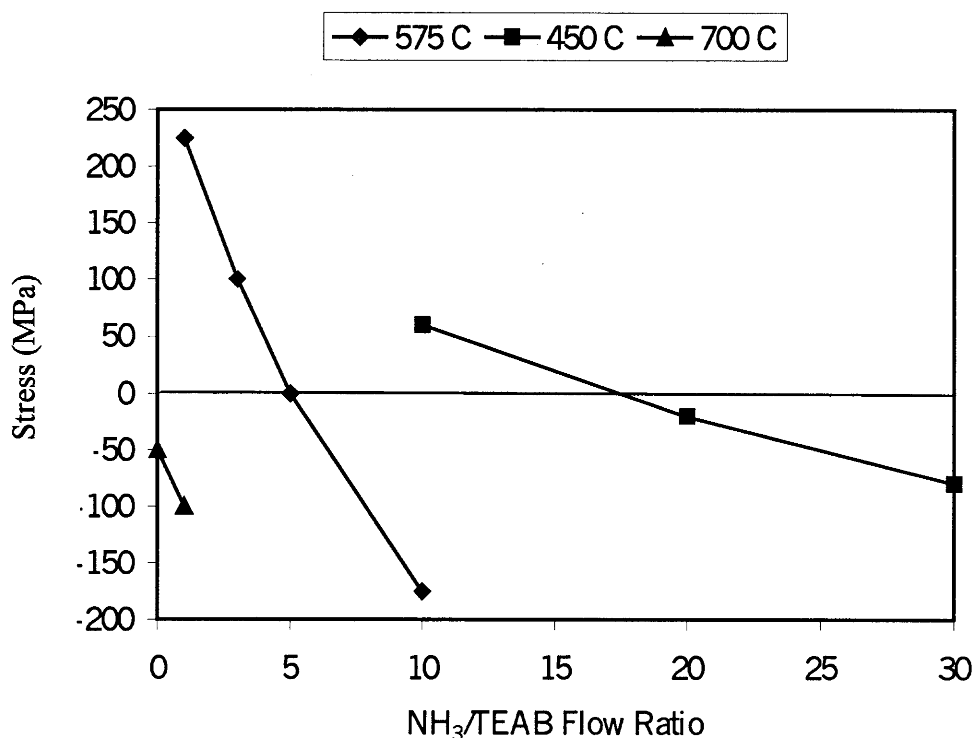

Figure 4.10 Variation of stress with increasing flow ratio of NH_3/TEAB

4.4.4 Optical Properties

The dispersion in the data presented in the literature confirms the critical role that particular film deposition technique exerts on the optical properties. Amorphous boron nitride with a B/N ratio of 1 has a refractive index of 1.8-1.9 at a wavelength of 633 nm and 1.7-1.8 at 541 nm, while polycrystalline films have a slightly higher index of 1.9-2.0, and cubic boron nitride has an index of 2.12. The refractive index is expected to vary with the content of both boron and carbon. Boron rich films have relatively higher refractive index values. The absorption edge Eg reported was approximately 5 eV for amorphous

BN, 5.90 eV for stoichiometric boron nitride BN, and 5.83 eV and 3.84 eV. The transmission was studied at a wavelength corresponding to red light (λ = 6330Å). The absorption coefficient α was calculated using Beer-Lambert law:

$$I/I_o = \exp(-\alpha x)$$

Where I/I_o is the fraction of the transmitted light and x, the thickness of the film. The optical transmission of the films synthesized varied from 92% to 72% at 633nm (corresponding to red light) depending on the thickness of the film and the stoichiometry of boron, nitrogen and carbon ratios in the films. As the wavelength is reduced from the visible region to the ultra violet region (approx. < 300nm) the transmission goes down and at about 210nm the light is completely absorbed. This is typical of a semiconducting

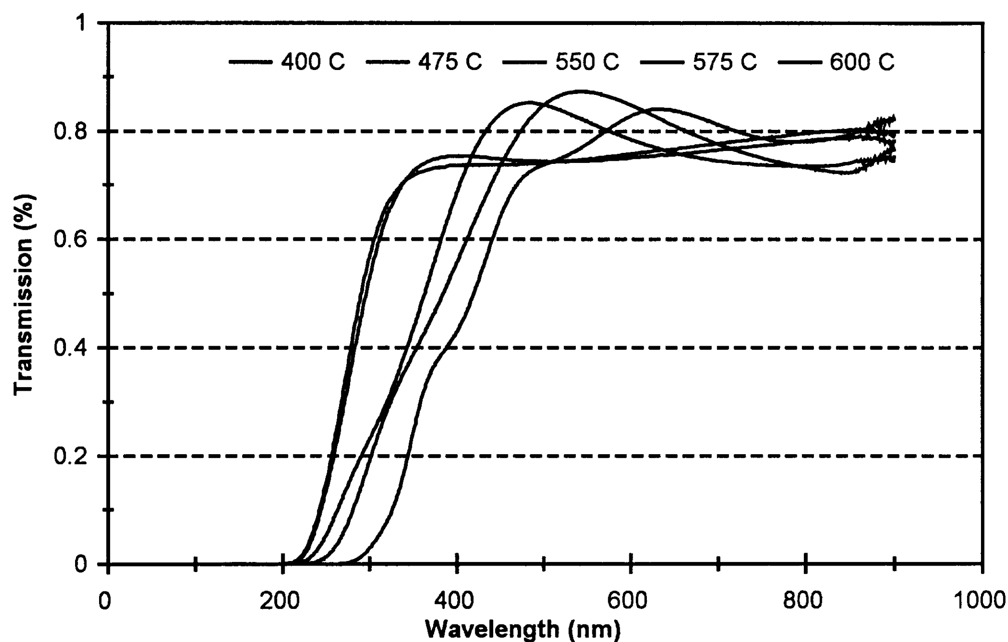

Figure 4.11 Optical transmission of BN thin films

material with the electrons jumping from the valence band to the conduction band as a result of the excitation of the electrons due to this supplied quanta of energy (by a photon). All thicknesses were normalized to 1 cm and the absorption coefficient was calculated. It was seen that near stoichiometric BN films are reasonably optically transparent. Typical optical transmission curve is shown in Figure 4.11.

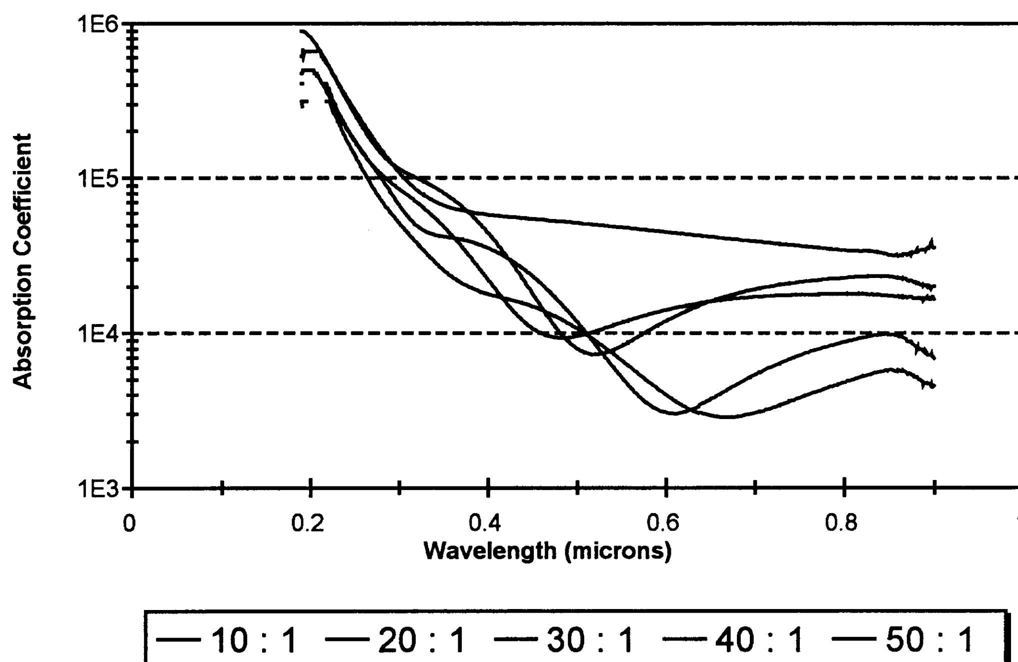

Figure 4.12 Optical absorption coefficient α as a function of the incident photon wavelength for varying NH3/TEAB flow ratios.

In general, the optical absorption edge of this amorphous wide band gap semiconductor consists of a low energy region 1 in which α varies as exp hν, and a high energy region 2 in which α varies as $(h\nu)^m$, m=1/2 for direct band gap materials and m=2 for indirect band gap materials. Historically region 2 has received the most attention because it

predominates in amorphous Si and tetrahedral-bonded narrow band gap semiconductors. However, there are significant differences between the spectra of amorphous narrow band gap semiconductors of which BN is representative. In the latter case, it is equally important for these two regions.

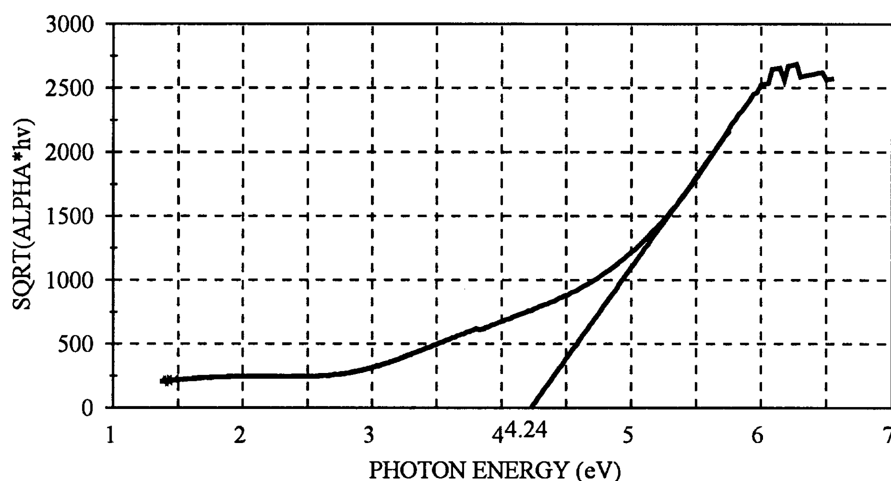

Figure 4.13 Determination of the optical band gap from the plot of $(\alpha h\nu)^{1/2}$ vs $h\nu$.

For the LPCVD B-N-C-H films composed of the single amorphous BN phase, the absorption coefficient α has the form $\alpha h\nu = K1(h\nu - Eg)^2$ in region 2 where K1 is a materials constant, and Eg is the optical band gap. The plot of $(\alpha h\nu)1/2$ versus $h\nu$ is shown in Figure 4.13 The optical band gap of 4.24 is calculated from the X axis intercept of the linear part of the plot $(\alpha h\nu)1/2$ versus $h\nu$. As the deposition temperature was increased from 400 to 600 C, the optical band gap was found to increase from 3.0 to 4.5,

while at a constant temperature, increase in the NH3/TEAB flow ratio from 1/1 to 50/1 did not result in any significant change in the optical band gap.

4.4.5 Structure Study

In the case of synthesis of BN thin films, a heterogeneous reaction must occur in order to obtain good films. However, some portions of the overall reaction may occur in the gas phase. BN molecules adsorbed on the Si wafer surface diffuse randomly and have a greater opportunity to re-evaporate (desorb) because they are less firmly bound to the surface. As the adsorbed molecules diffuse on the surface, they may encounter other diffusing molecules and form a pair. This molecule pair would be more stable than an isolated molecule and would less likely to desorb. As the pairs diffuse on the surface, they may join other molecules, forming a larger and more stable cluster, until the cluster had a low probability of desorbing and a critical cluster or stable nucleus was formed. The probability of diffusing molecules encountering each other depends strongly on the number of adsorbed molecules on the surface. Thus, it is a strong function of their arrival rate (through the pressures of the precursors) and their desorption rate (through the temperature of substrate and the binding energy of the diffusing molecules to exposed surface). After stable deposited nuclei formed, additional adsorbed molecules diffusing on the surface can either initiate additional nuclei or join existing nuclei. When the existing nuclei were close enough together, additional molecules were more likely to join an existing nucleus, and the number of nuclei saturated and remained constant as the size of each nuclei grows. The saturation number of nuclei depended on the substrate, the arrival rate of molecules, and the temperature. Thus, a continuous film formed as the nuclei

impinged on each other. Ever after a continuous film formed, the structure was strongly influenced by the thermal energy available for surface migration. At very low temperatures, the adsorbed BN molecules had little thermal energy and cannot diffuse significantly on the substrate surface before they were covered by subsequently arriving molecules. Once they were covered, their random arrangement was locked into place, and an amorphous structure with no long-range order formed. At higher temperatures, adequate surface diffusion was possible to allow a crystalline structure to form[41]. The X-ray diffraction pattern of BN films deposited on silicon at the highest deposition temperature of 575 °C (shown in Figure 4.14) only exhibits the peak of Si (100) at about 69 °, the peaks of BN are not present. Therefore, the films are amorphous at all temperatures that were studied.

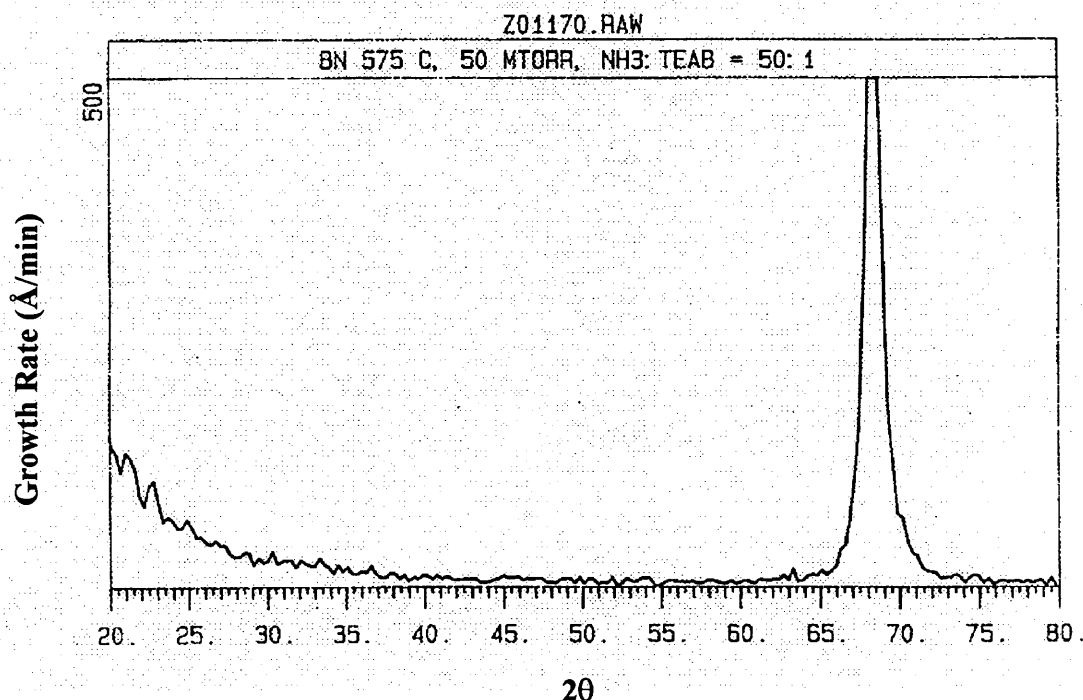

Figure 4.14 X-ray diffraction pattern for a boron nitride film on silicon deposited at a temperature of 575 °C, pressure of 0.05 Torr, TEAB flow rate of 1 sccm, and NH_3 flow rate of 50 sccm.

4.4.6 Electrical Characterization of BN Films

A detailed electrical characterization was done to determine the potential of these films as low ε IMD. CV and IV measurements were done for the films on both the type-1 and type-2 substrates. MIS and MIM structures were fabricated to study the CV and IV behavior exhibited by the films. The following table gives the summary of the electrical measurements carried out on the boron nitride films.

Table 4.1 Electrical data measured for BN films

Substrate	Thickness (Å)	Dielectric constant
type 1-Si	1500	3.1 – 5.5
type 2-Si	1500	3.1 – 5.5

4.4.6.1 Dielectric Constant Measurements: The dielectric constant of BN films measured at five locations on every sample was in the range of 3.1 to 5.5. The breakdown voltage was more than 4 MV/cm which is the equipment limit. The dielectric constant was found to be frequency dependent and was measured at different frequencies ranging from 1KHz to 1MHz by a HP4194A CV/IV measuring instrument. The dielectric constant ε was measured using the formula

$$\varepsilon = Cd/A$$

where d is the thickness of the film, A the area of the capacitor (area of the Al contacts - 300μm and 600μm) and C is the effective series capacitance of the dielectric as well as the intrinsic capacitance generated due the applied potential on the minority carriers of the dopant of the Si wafers. The latter varies with changes in applied voltage across the Al contacts. CV plot obtained for BN films on the HP4149A is shown in Figure 4.15.

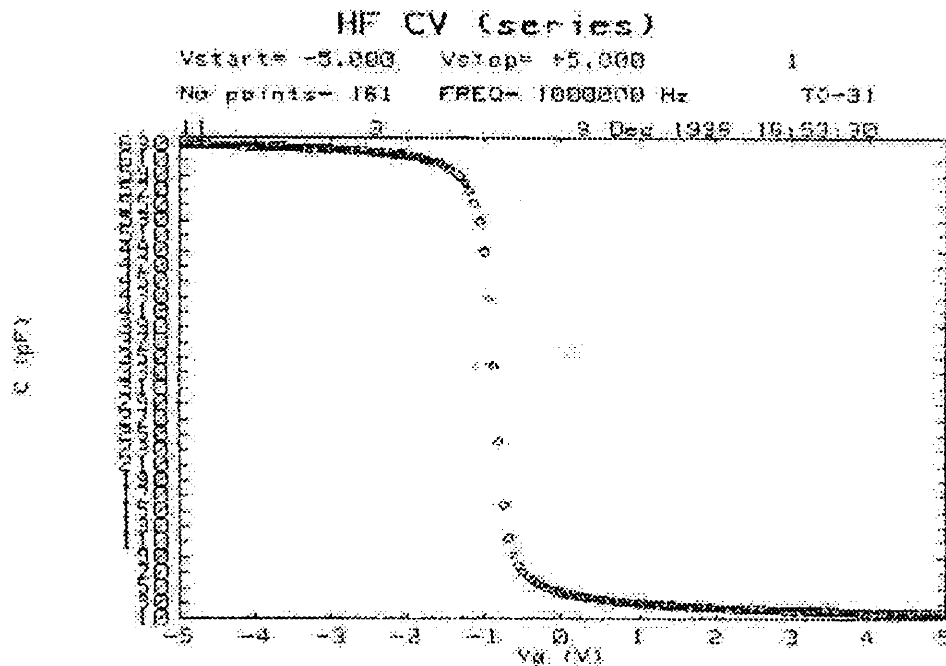

Figure 4.15 Typical MIS capacitance-voltage curves for LPCVD boron nitride

In describing this curve we begin at the left side (negative voltage), where we have an accumulation of holes and therefore a high differential capacitance of the semiconductor. As a result the total capacitance is close to the insulator capacitance. As the negative voltage is reduced sufficiently, a depletion region that acts as a dielectric in series with the insulator is formed near the semiconductor surface and the total capacitance decreases. The capacitance decreases until finally inversion is reached. With inversion there is no further change in the capacitance, since the depletion width has reached its maximum.

4.4.6.2 Investigation of LPCVD BN-Si Surfaces Using MIS Structures: The exact nature of the BN-Si interface is not yet fully understood. The MIS characteristics is greatly influenced by the interface traps and the oxide charges that exist. Hence the properties of the BN film can be studied by an investigation of the MIS structure having BN as the insulator. The basic classifications of the traps and charges are as follows:

1. Interface trapped charges,
2. Fixed oxide charges,
3. Nitride trapped charges and
4. Mobile ionic charges

An interface trap is considered as a donor if it can become neutral or positive by donating an electron. An acceptor interface trap can become neutral or negative by accepting an electron. When a voltage is applied, the interface-trap levels move up or down with the valence and the conduction bands while the fermi level remains fixed. This change of charge contributes to the MIS capacitance and alters the ideal MIS curve. In other words, the interface trap exhibits a frequency dependent behavior. Hence the presence of interface traps may be detected by the frequency dependent study of the MIS structures. The result of such a study is shown in the fig. 4.16.

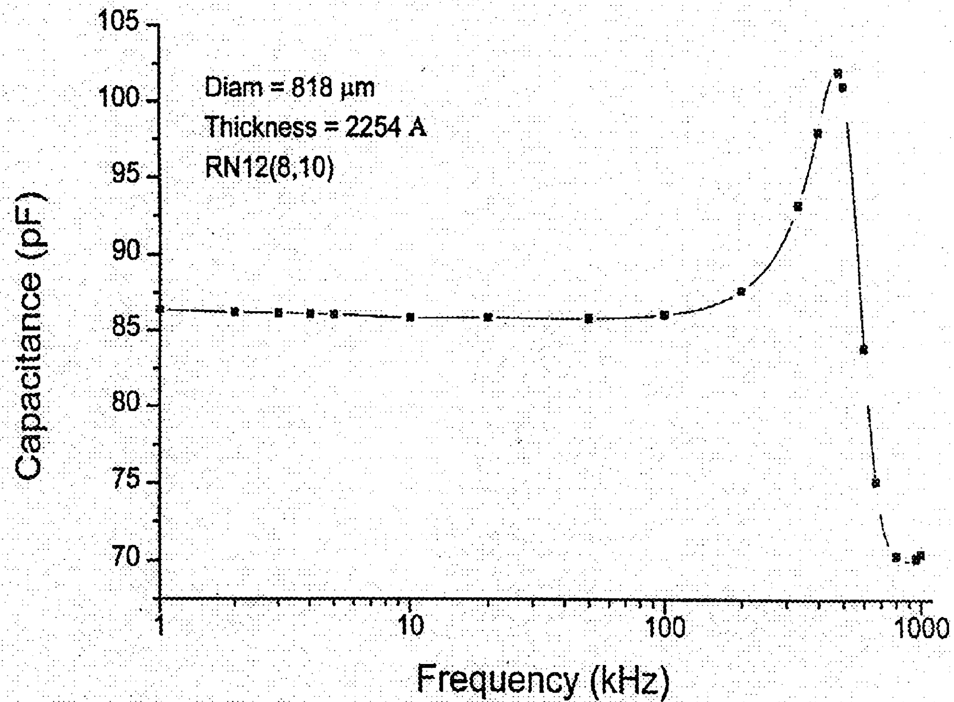

Figure 4.16 Capacitance-frequency plot for BN MIS structures

From the Figure 4.11 we can see that as the frequency is increased, the accumulation capacitance decreases. The reason being, at high frequencies the interface traps cannot follow the ac voltage swing, which yields a capacitance free of the interface traps. Hence we can conclude that the MIS structures which were fabricated contained significant density of the interface traps. This could be one of the reasons for not achieving lower dielectric constants.

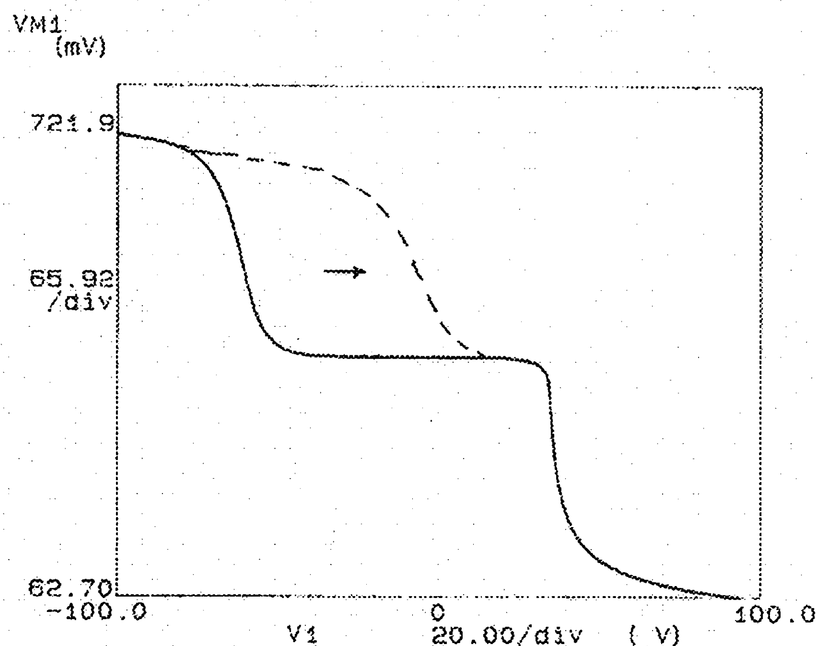

Figure 4.17 C-V curve shift along the voltage axis due to (+) or (-) fixed oxide charge

The fixed oxide charge has the following properties: It is fixed and cannot be discharged or charged over a wide variation of the surface potential; it is located within the order of 30 Å of the Si-SiO2 interface; its density is not greatly affected by the oxide thickness or by the type or concentration of the impurities in silicon; it is generally positive and depends on oxidation and annealing conditions, and on the silicon orientation. The presence of fixed charge would cause a shift in the C-V curve, in accordance with the principle of charge neutrality. The presence of ionic charges like sodium also causes the shift of the C-V curve because these ions are free and can move back and forth through the film, depending on the biasing situation. Also the presence of the nitride trapped charge causes the C-V curve shift. These traps are associated with the defects in the film.

They are usually neutral, and are charged by introducing electrons and holes in the film. Once charged, for the same surface potential, the applied voltage would be reduced indicating a shift in the C-V curve. Figure 4.17 shows significant shift in the C-V curve suggesting the presence of a good number of a combination of fixed oxide charges, ionic charges and nitride trapped charges.

Bias temperature cycle not only indicated the presence of mobile ions, it also shows the presence of trapped positive charges in the bulk of the insulator. Although some of the trapped negative charges can be discharged in the gate or in the semiconductor, the trapped positive charges are essentially immobile on this field and temperature range. These trapped charges could be due to the dangling bonds caused by the following 2 reasons:

1. the boron rich nature of this non-stoichiometry of the films
2. the elemental carbon in the films.

These two facts is already shown in the XPS analysis. Low precursor ratio yielded boron rich films whereas high substrate temperatures caused the unbonded excessive carbon. CV shift in response to the polarities indicates a presence of mobile ions in the insulator. Third, there is considerable trapped immobile charges in the bulk of the insulator for which the flat-band does not go back to the original value prior to the aging. Fourth, the possibility of trapped negative charges being attracted to the gate electrode or to the semiconductor and consequently being discharged cannot be excluded.

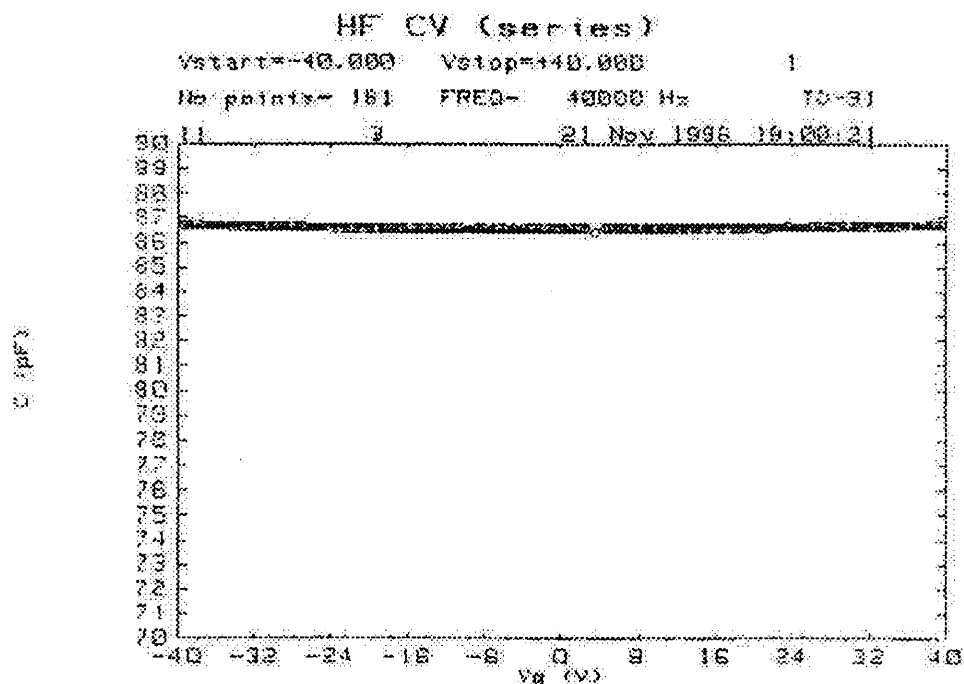

Figure 4.18 Capacitance-Voltage measurements on MIM structures

It is seen that in all the cases the dielectric constant of the films increased with increase in flow ratio. This could be due to the varying stoichiometry in the films, or the variation of thickness of the film or could be due to the effect of carbon impurity in the boron nitride film. The least value obtained was 3.12 at a deposition of 575°C, pressure of 0.05 Torr and a flow ratio of NH_3/TEAB = 50/1. From the XPS analysis also it is seen that the films tend to attain stoichiometry and more transparent films at these deposition conditions.

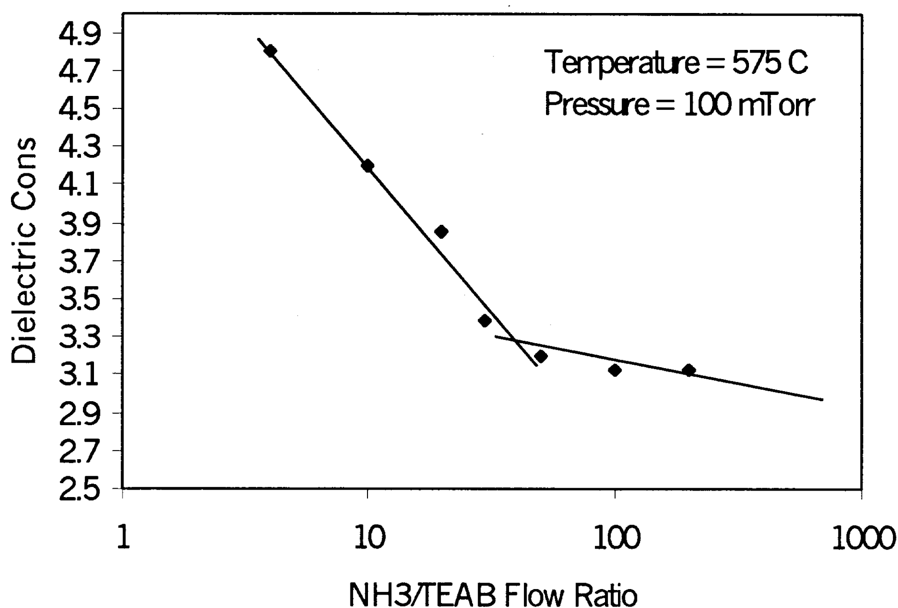

Figure 4.19 Variation of dielectric constant with flow ratio of NH_3/TEAB

A dielectric constant reacts to electromagnetic radiation differently from free space because it contains electrical charges that can be displaced. For a sinusoidal electromagnetic wave, there is a change in the wave velocity and intensity described by the complex coefficient of refraction

$$n^* = n - ik$$

where n is the index of refraction and k is the index of absorption. The coefficient of refraction is related to the complex dielectric constant $(n^*)^2 = \varepsilon^* = \varepsilon' - i\varepsilon''$, where ε' is the relative dielectric constant and ε'' is the relative dielectric loss factor. Neglecting the imaginary terms, the dielectric constant is equal to the square of the index of refraction.

$$\varepsilon = n^2$$

Thus by knowing the refractive index of the film, a fairly good idea of the dielectric constant of the material can be estimated.

4.4.6.3 Current-Voltage (I-V) Characteristics of the Films: Figure 4.20 (a)/(b) shows the I-V characteristics of BN films deposited on type-1 and type-2 Si wafers respectively. The resistivity of the films was always greater 4.5 x 10^{14} Ω-cm.

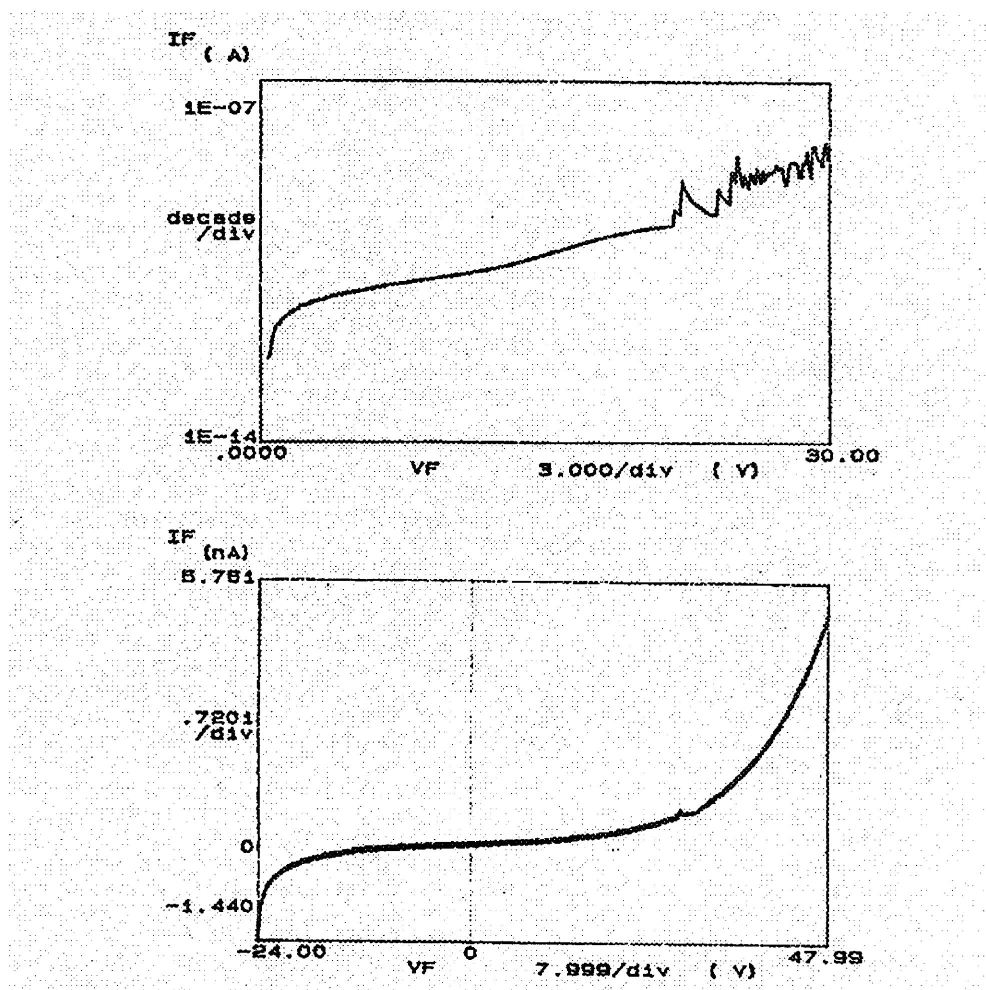

Figure 4.20 I- V characteristics of BN films on (a) type-1 Si and (b) type-2 Si

4.4.7 Boron Nitride X-ray Mask & Windows

It is well known that it is easy to change the atomic structure of materials having low coordination number, such as a material with many bondings terminated by hydrogen atoms having one fold coordination. Therefore the stress relaxes easily due to changes in the atomic structure. Since the atomic structure of BNC is mainly dominated by B-N bonding networks with a large binding energy, the radiation resistance of BNC must exceed that of BN films. A transparent ternary boron compound film B-C-N was first reported by Montasser et al. at room temperature[32]. According to the optical data however, the films are considered as organic soft films. Addition of small amounts of carbon introduced tension successfully and improved the film stoichiometry and decreased the hydrogen content. The increase in the stoichiometric structures of boron to nitrogen increased optical transparency. The low hydrogen content also led to increase in Young's modulus of the film. The mechanical stress and optical transparency of the films exhibit a correlation with the dc electrical resisitivity. This is mainly attributed to the important role of hydrogen. Hydrogen is present in multiple configurations in the as-deposited films, and is essentially randomly distributed as monohydrides and with a homogeneous concentration. The tensile stress decreases monotonically with the hydrogen content, whereas the optical transparency is found to increase.

4.4.7.1 B-N-C-H X-Ray Window Fabrication: The etch rate of B-N-C-H films as a function of power and CF_4 flow rate are shown in Figures 4.21 and 4.22. We can see that at a constant pressure of 200 mTorr and a constant CF_4 flow rate of 40 sccm, the etch rate increases sharply up to a power of 350 W and then stabilizes. However, at a constant flow

rate of 40 sccm, as the Power was increased from 20 to 80 sccm, the etch rate increases linearly from 250 to 2500 Å/min. From these etch kinetics plots we can conclude that the etch rate was transport limited. This is advantageous since we need to etch these films at a very controlled rate so as to avoid damaging the freestanding membranes. In order to fabricate membranes of the order of 2000 to 3000 Å, the membranes were thinned initially at etch rates as high as 2000 Å/min, following which conditions were changed so as to operate at etch rates of 100 Å /min to maintain better control over the thickness.

Wet etching of the B-N-C-H films was also tried in Sodium Hypochlorite solution (CLOROX), but the freestanding membranes were too delicate and popped due to the movement in the solution.

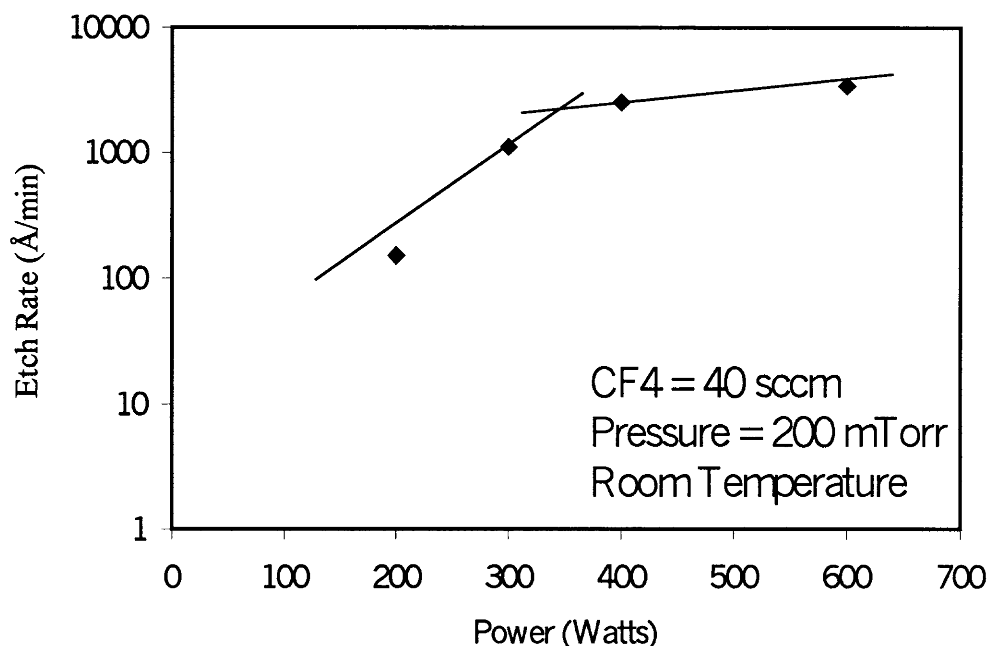

Figure 4.21 Variation of etch rate of the B-N-C-H films with power.

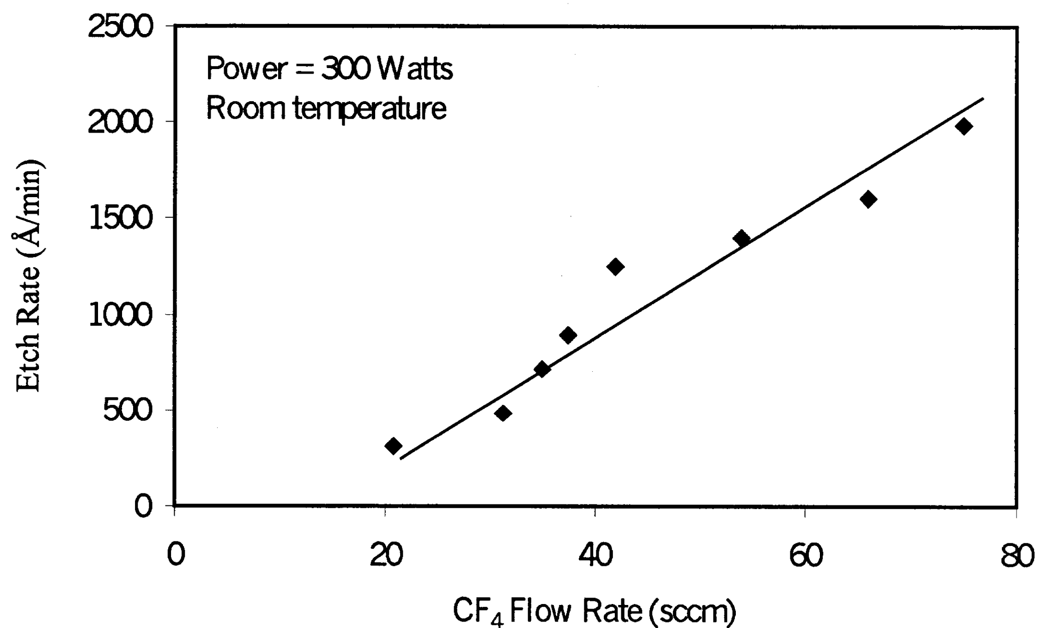

Figure 4.22 Variation of etch rate of the B-N-C-H films with CF_4 flow.

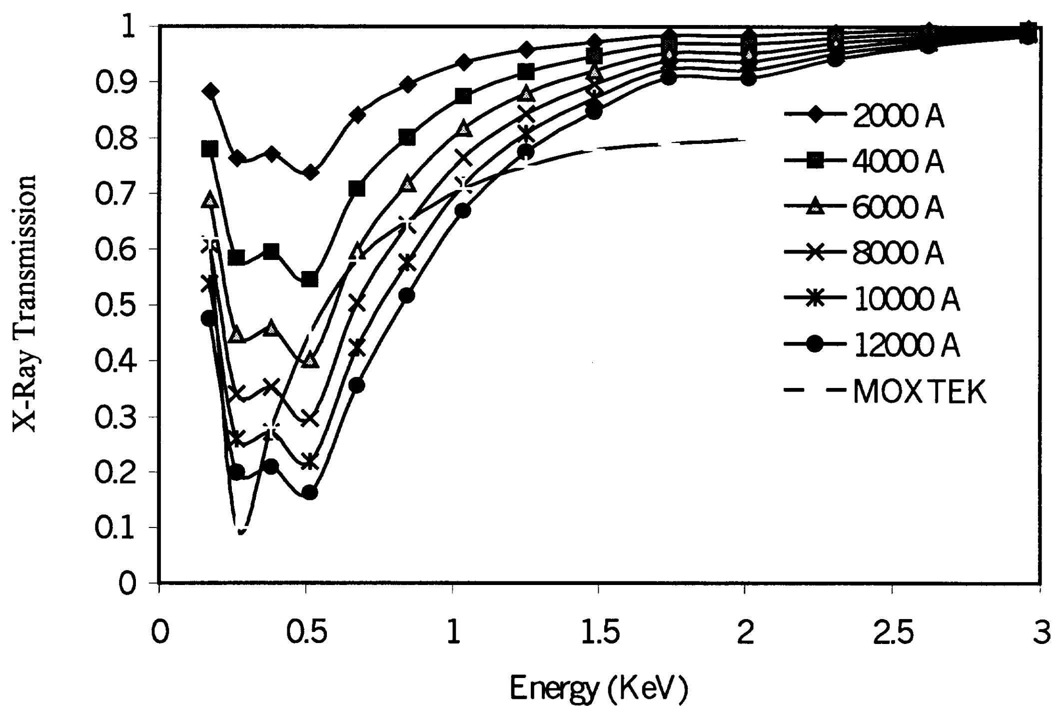

Figure 4.23 X-ray transmission through the B-N-C-H films of varying thickness.

4.4.7.2 Characterization of B-N-C-H X-Ray Windows: Figure 4.23 gives a comparison of the X-ray transmission for the B-N-C-H freestanding membranes of thickness ranging from 2000 to 12,000 Å and the commercially available MOXTEK at energies as low as 0.1 keV. From this figure we can see that all the B-N-C-H membranes showed X-ray transmissions much higher than the MOXTEK! Even membranes thicker than a micron exhibited much better performance. The MOXTEK was seen to exhibit a X-ray transmission of ~10% at an energy of 0.25 keV, while the fabricated freestanding B-N-C-H membrane allowed more than 80% transmission. Also, the membranes were loaded into the detector column and tested for vacuum tightness and it was found that the membranes held vacuum with negligible leakage.

4.5 Kinetic Study of LPCVD Titanium Nitride

4.5.1 Influence of Temperature on Deposition Rate

TiN films were deposited at different temperatures while keeping all other parameters such as total pressure, reactant partial pressures, and reactant flow rates constant. Two sets of data were obtained: (a) For a $NH_3/TiCl_4$ flow ratio of 10, experiments were carried out at 450, 475, 500, 530, 550, 600 and 700 °C and (b) For a NH_3 /$TiCl_4$ flow ratio of 5, experiments were carried out at 600, 700, 800 and 850 °C. Film deposition rate is a measure of the rate of the chemical reaction and can be expressed as follows:

$$\text{Rate} = k(P_{NH3})^x(P_{TiCl4})^y \quad (4.1)$$

$$k = A_0 * \exp(-1000E_a/RT) \quad (4.2)$$

Where:

P_A = partial pressure of species A

x,y = reaction rate orders

k = rate constant of the reaction

E_a = activation energy for the reaction, kcal mol^{-1}

R = gas constant, 1.987 cal K^{-1} mol^{-1}

T = temperature, K

A_0 = constant

Since the flow rates of the reactants and the total pressure were maintained constant, the growth rate for each of these experiments was dependent only on the exponential terms of

the reactant species in eq. 4.2. Thus the apparent activation energy was calculated from the slope of the line obtained by plotting growth rate as a function of 1000/T on a semi log scale.

At a fixed total pressure of 70 mTorr and NH_3 flow rate of 50 sccm, the growth rate dependence on deposition temperature is shown in Figure 4.24 for $NH_3/TiCl_4$ flow rate ratios of 5:1 and 10:1. For both these flow rate ratios, an Arrhenius behavior was observed yielding an apparent activation energy of 42 KJ/mol. The apparent activation energy depends on the adsorption heat of the reactant which itself depends on the surface coverage. As a consequence, the apparent activation energy is strongly dependent on gas injection configuration which explains why this value is lower than those reported by Buiting et al (61 KJ/mol) and Imhoff et al (78.9 KJ/mol). For the $NH_3/TiCl_4$ flow rate ratio of 10:1, the growth rate is seen to saturate above 550 °C reflecting the onset of the mass transfer limited regime. No such saturation was noted for the flow rate ratio of 5:1 up to the investigated deposition temperature of 850 °C.

It is worth noting that the reaction between NH_3 and $TiCl_4$ is thermodynamically feasible at room temperature, the product being a yellow soft powder complex ($TiCl_4.nNH_3$) [8-9]. Formation of that powder was indeed evident in the front and exhaust ends of the reactor tube, which was situated outside the heating zone of the furnace. In order to minimize this undesirable byproduct formation, the $TiCl_4$ gas was introduced through a stainless steel tube into the hot reaction zone and allowed to mix with the NH_3 only close to the wafers. Fig. 4.25 illustrates the dependence of elemental film composition on deposition

temperature in the two regimes where the $NH_3/TiCl_4$ flow rate ratio was 5:1 and 10:1. For both these flow rate ratios, it appears that the films are Ti rich and become progressively richer as the deposition temperature is increased. At the lowest investigated deposition temperature of 450 °C and flow rate ratio of 10:1, the Ti/N ratio was closest to the stoichiometric value. The increase in Ti concentration with higher deposition temperatures was compensated by a decrease in the Cl content of the films. Over the temperature range of 450 to 850 °C, the Cl content in the films decreased from ~8 % (a/o) down to ~0.2% (a/o).

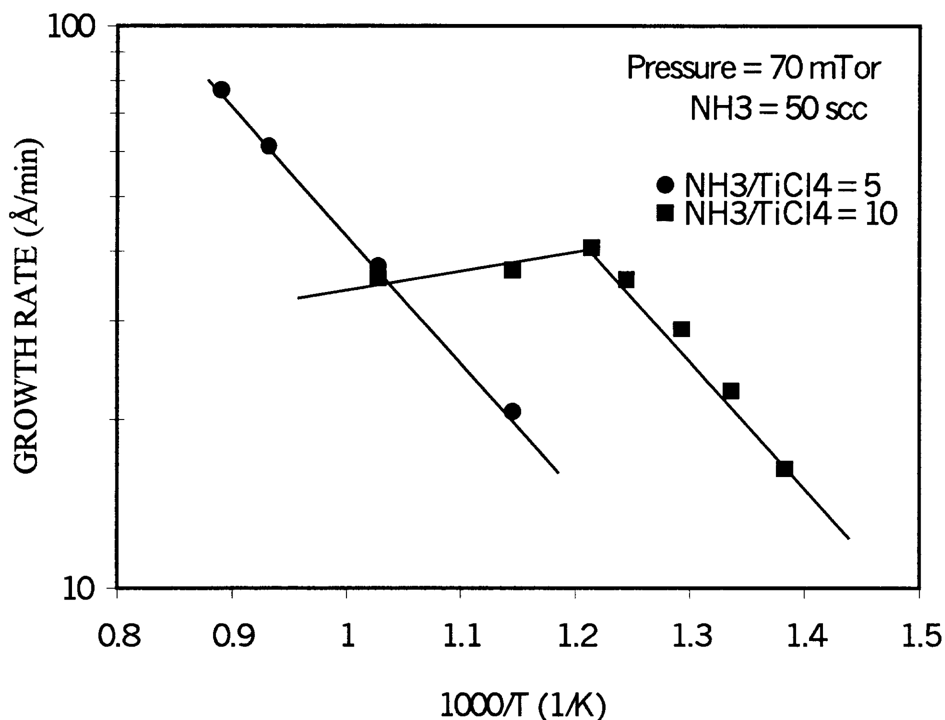

Figure 4.24 Plot of growth rate vs. 1000/T for TiN films.

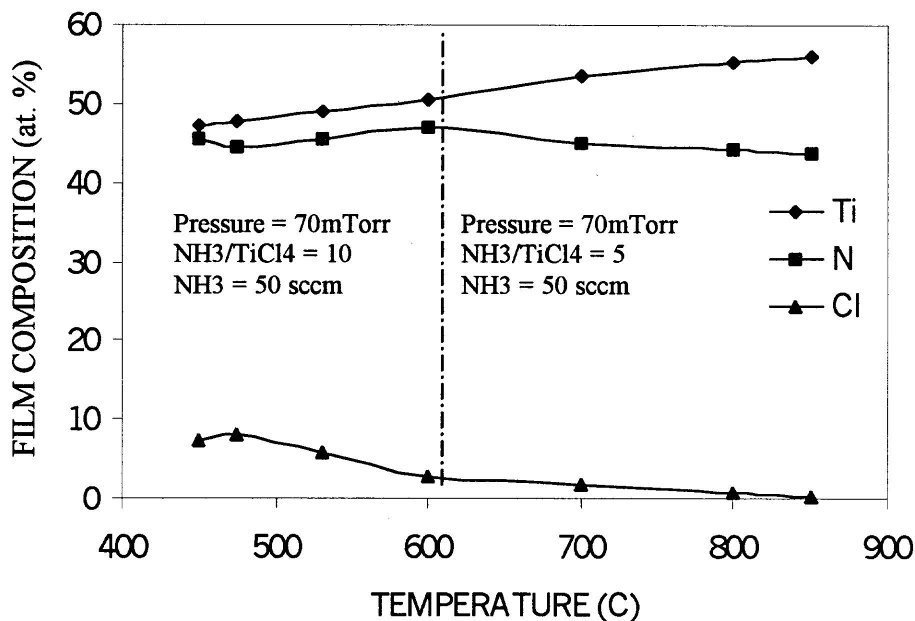

Figure 4.25 Variation of Film Composition with Deposition Temperature

4.5.2 Influence of Reactant Partial Pressures on Deposition Rate

The reaction orders for the $TiCl_4$ and NH_3 reaction were determined for a deposition temperature of 600°C and a total pressure of 110 mTorr. These conditions were selected to allow a sufficient partial pressure span, while maintaining a reasonable deposition rate and a Cl content deemed acceptable. Keeping the NH_3 partial pressure constant at 50 mTorr, the partial pressure of $TiCl_4$ was varied from 1 to 12 mTorr while also varying the argon carrier gas partial pressure in order to maintain a constant total pressure within the reaction chamber. Similarly, while keeping the TiCl4 partial pressure constant at 8 mTorr, the partial pressure of NH_3 was varied from 50 to 100 mTorr with corresponding variations in argon partial pressure to maintain the aforementioned total pressure. The

growth rate plotted on a double logarithmic scale as a function of the partial pressures of $TiCl_4$ and NH_3 are shown in Figures 4.26 and 4.27 respectively. These plots indicate an increase in growth rate with the decrease in $TiCl_4$ partial pressure and the increase in NH_3 partial pressure in agreement with the results of Buiting et. al [8]. From the slopes of these plots the reaction orders with respect to $TiCl_4$ and NH_3 were calculated as -0.42 and 1.37 respectively. Since all other parameters being constant in equation 4.1, the growth rate is proportional to the partial pressure of the varying reactant. If x is the order of proportionality, then we have,

$$\text{Rate} = \text{Constant} * (P_{reactant})^{x} \tag{4.4}$$

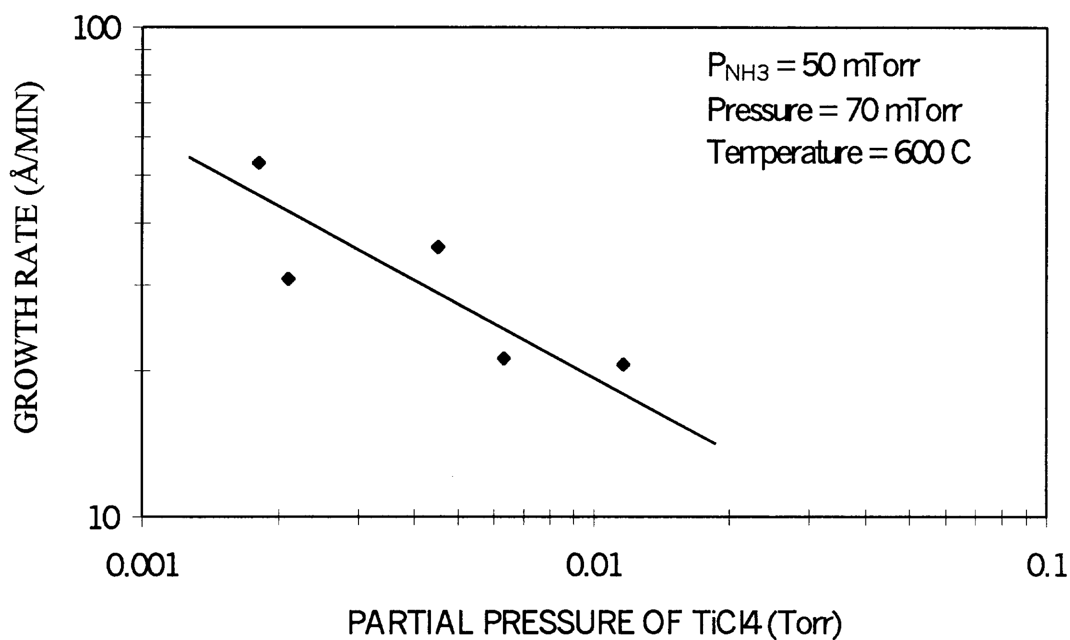

Figure 4.26 Plot of growth rate as a function of partial pressure of $TiCl_4$.

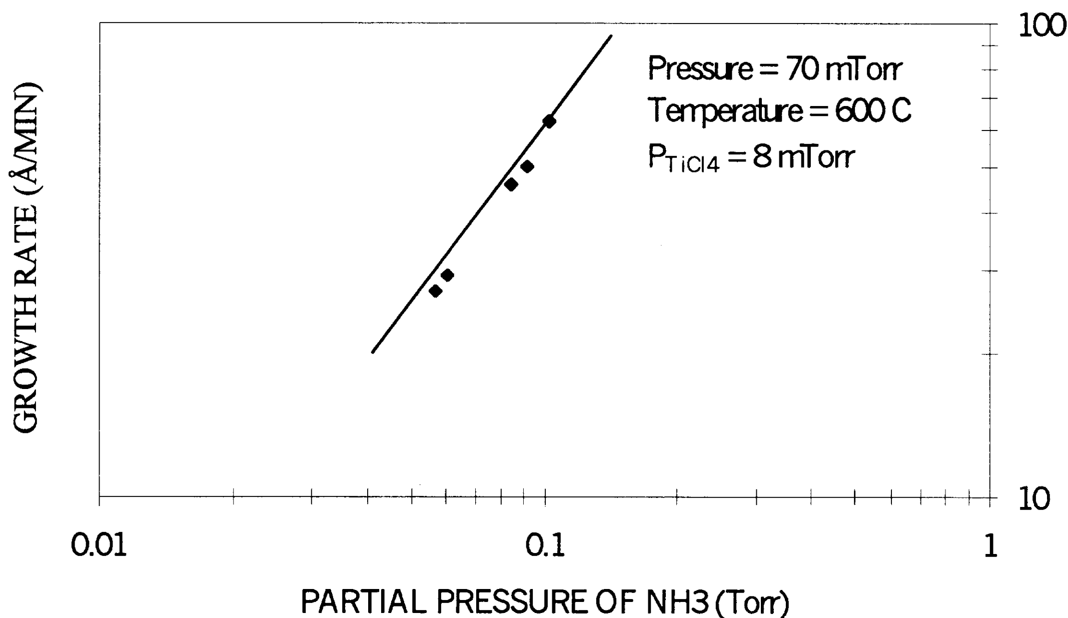

Figure 4.27 Plot of growth rate as a function of partial pressure of NH_3.

The dependence of film composition on partial pressure of the reactants is shown in Figures 4.28 and 4.29. The Ti/N ratio appears not to vary significantly with changes in the $TiCl_4$ partial pressure. This may be explained by the preferential adsorption of that specie as a result of the close proximity of the $TiCl_4$ delivery tube to the wafers. On the other hand, the increase in NH_3 partial pressure has the effect of reducing the Ti/N ratios to values that progressively approach stoichiometry. This results from the higher number of NH_3 molecules available to compete with $TiCl_4$ for available adsorption sites. Changes in the partial pressures of both reactants appear to have no effect on the incorporated Cl content of the films.

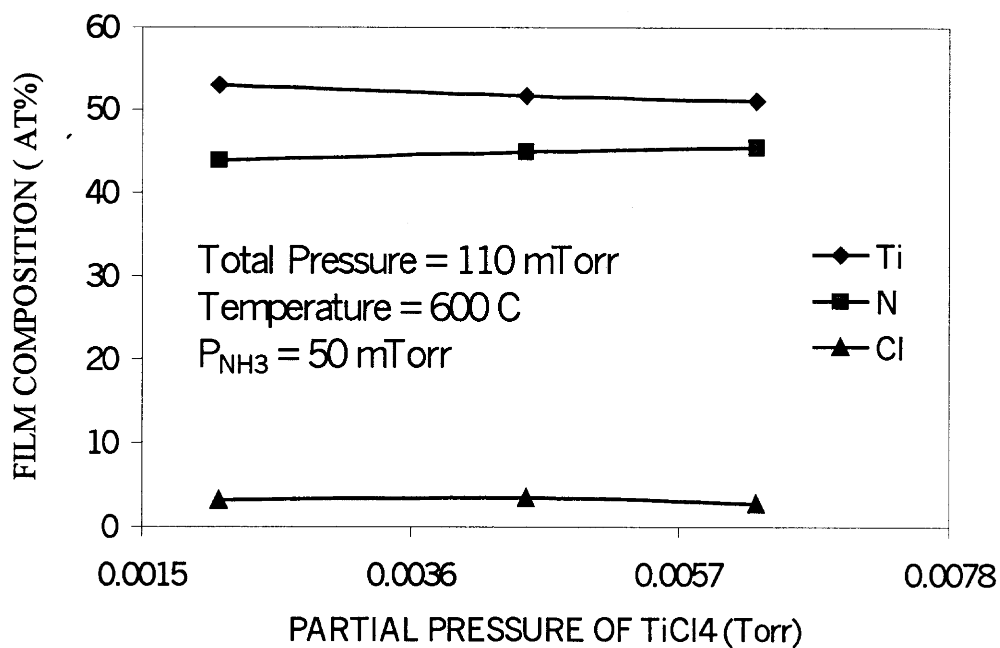

Figure 4.28 Variation of Film Composition as a Function of TiCl4 Partial Pressure

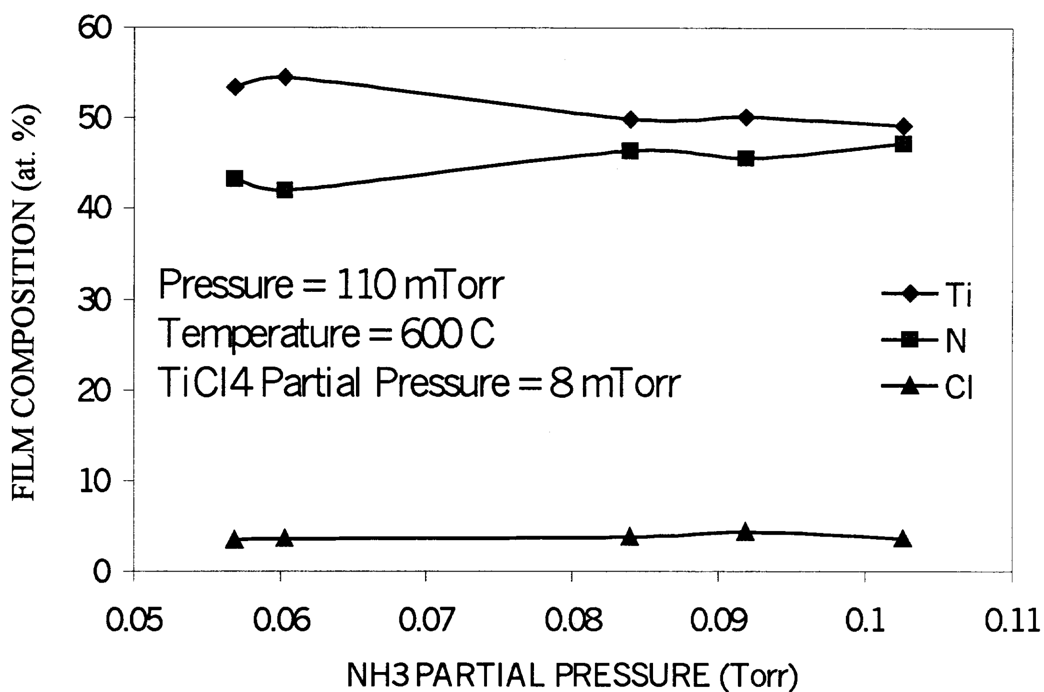

Figure 4.29 Variation of Film Composition as a function of NH3 Partial Pressure

4.5.3 Rate Equation

Knowing the values of the activation energy and the rate orders with respect to NH_3 and $TiCl_4$ from the experimental deposition rate results, the following rate equation is established.

$$r = 4.35 \times 10^{-5} \exp(-5150/T)(P_{NH3})^{1.37}(P_{TiCl4})^{-0.42}$$

where:

r = deposition rate, mol cm^{-2} min^{-1}

T = deposition temperature, K

P_a = partial pressure of reactant a, Pa

The occurrence of the negative order of the reaction with respect to $TiCl_4$ suggests that the reaction mechanism may involve: (1) competitive adsorption of two or more gases on the surface and a reaction rate which is dependent on the surface fractions covered by these two gases [Langmuir-Hinshelwood like mechanism] and (2) competitive reaction paths consisting of the intended deposition reaction and parallel reactions. In the later case, increasing partial pressure of $TiCl_4$ could drive the reaction towards the complex formation, which in turn results in the decrease in TiN formation, as less NH_3 is available. The rate equation obtained is consistent with the model put forth by Imhoff et. al. [9] using Langmuir-Hinshelwood kinetics for the case of competitive adsorption. For competing reactions, at low partial pressures of the reactant, the growth rate increases with the partial pressure of the reactant resulting in a positive reaction order. At high

partial pressures of the reactant, the growth rate decreases with increasing reactant partial pressure resulting in a negative reaction order. Pintchovski et al. report positive reaction orders with respect to both NH_3 and $TiCl_4$. This result does not confute the observed mechanism because experiments were performed by using both NH_3 and $TiCl_4$ injections far from the substrate. Neither NH_3 nor $TiCl_4$ can act as the poisonous species, so growth rate always increases with increasing NH_3 or $TiCl_4$ partial pressures. Imhoff et al. have injected NH_3 near the substrate and reported a reaction order of -0.63. In the present study, $TiCl_4$ having being introduced close to the wafers may also explain the observed negative rate order. Our results are consistent with those of Buiting et al who similarly introduced $TiCl_4$ close to the wafers and reported rate orders of –0.5 and 1.37 for $TiCl_4$ and NH_3, respectively.

The dependence of film composition on partial pressure of the reactants is shown in Figures 4.28 and 4.29. The Ti/N ratio appears not to vary significantly with changes in the $TiCl_4$ partial pressure. This may be explained by the preferential adsorption of that specie as a result of the close proximity of the $TiCl_4$ delivery tube to the wafers. On the other hand, the increase in NH_3 partial pressure has the effect of reducing the Ti/N ratios to values that progressively approach stoichiometry. This results from the higher number of NH_3 molecules available to compete with $TiCl_4$ for available adsorption sites. Changes in the partial pressures of both reactants appear to have no effect on the incorporated Cl content of the films.

4.5.4 Reaction Mechanism

In the gaseous phase at lower temperatures, NH_3 and $TiCl_4$ are known to form a $TiCl_4.nNH_3$ complex. In accordance with this, a yellow powder, presumably to be of $TiCl_4.2NH_3$, was observed at the cooler pumping-side exhaust in the experiments carried out. At higher temperatures, the complex is believed to finally decompose into TiN.

To study the reaction mechanism in detail, consider the following elementary reactions:

(1) $TiCl_4$ adsorption: Because of the sp^3 hybridization of the Ti atom in the $TiCl_4$ molecule, direct adsorption of $TiCl_4$ on one site is less probable. Instead it adsorbs dissociatively on 2 adjacent sites, according to

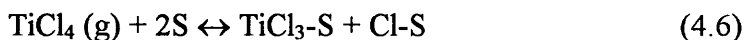

$$TiCl_4\,(g) + 2S \leftrightarrow TiCl_3\text{-}S + Cl\text{-}S \qquad (4.6)$$

(2) NH_3 adsorption: On hot surface, NH_3 adsorption is dissociative according to the following steps,

$$NH_3\,(g) + 2S \leftrightarrow NH_2\text{-}S + H\text{-}S \qquad (4.7)$$

$$NH_2\text{-}S + S \leftrightarrow NH\text{-}S + H\text{-}S \qquad (4.8)$$

$$NH_3\text{-}\ S + S \leftrightarrow N\text{-}S + H\text{-}S \qquad (4.9)$$

(3) Surface reaction: $TiCl_3$-S reacts with either of NH_2-S, NH-S and N-S to give TiN, according to the following reaction:

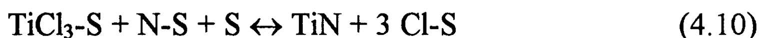

$$TiCl_3\text{-}S + N\text{-}S + S \leftrightarrow TiN + 3\ Cl\text{-}S \qquad (4.10)$$

$$TiCl_3\text{-}S + NH\text{-}S \leftrightarrow TiN + 2\ Cl\text{-}S + HCl\,(g) \qquad (4.11)$$

$$TiCl_3\text{-}S + NH_2\text{-}S \leftrightarrow TiN + Cl\text{-}S + S + HCl\,(g) \qquad (4.12)$$

Reaction 4.10 is improbable because it involves three species. Reaction 4.11 involves two steps with three sites, and reaction 4.12 involves only one step with two sites for NH3

dissociation. So, reaction 4.11 is less probable than reaction 4.12. According to the Langmuir-Hinshelwood theory, the numerator of the growth rate expression is related to the adsorption phenomena leading to TiN formation. The denominator is related to the adsorption which inhibits TiN deposition by poisoning surface sites. Thus at a fixed temperature the growth rate can be given as,

$$r = K\frac{P_{TiCl3}P^{1/2}{}_{NH3}}{(1+K_{TiCl3-S}\Theta_{TiCl3}+K_{N-S}\Theta_{N}+K_{Cl-S}\Theta_{Cl}+K_{NH-S}\Theta_{NH}+K_{NH2-S}\Theta_{NH2})^{2}} \quad (4.13)$$

Where Θi is the surface coverage rate, Ki is the equilibrium constant of the adsorption reaction of the species i, Pi is the thermodynamic equilibrium partial pressure of the species i, and K is a proportionality constant depending on the temperature. The growth rate, r, is proportional to the TiCl3 partial pressure because of direct adsorption, and to the square root of the NH3 partial pressure because of dissociative adsorption. As a consequence adsorption and desorption are generally not rate-determining steps of the overall process. Then, the denominator is close to one, and r is expressed by

$$r \approx K.P_{TiCl3}P^{1/2}{}_{NH3} \quad (4.14)$$

and the rate determining step is eq. 4.11 or 4.12. For the TiCl4-N2-H2 gaseous phase, Dekker et a. also claimed that the rate determining step is the reaction between TiCl3 and NH-s. In our case, TiCl4 is introduced quite near the substrate, so we can expect a very

high TiCl4 coverage. ΘTiCl3 can no longer be neglected. The rate equation has to include the surface poisoning by TiCl3 species as in the equation

$$r \approx K \frac{P_{TiCl3} P^{1/2}{}_{NH3}}{(K_{TiCl3-S} \Theta_{TiCl3})^2} \tag{4.15}$$

Hence,

$$r \propto P_{TiCl3}^{-1} P_{NH3}{}^{1/2} \tag{4.16}$$

The equilibrium constant can be written as

$$K12 = \frac{[TiCl3]^2[HCl]^2}{[TiCl4]^2[H2]} = \frac{[TiCl3]^4}{[TiCl4]^2[H2]} \tag{4.17}$$

then

$$[TiCl3] = K_{12}^{1/4}\ [TiCl4]^{1/2}\ [H2]^{1/4} \tag{4.18}$$

By keeping in mind that hydrogen is used in excess, we can assume that the TiCl3 partial pressure is proportional to the square root of the TiCl4 partial pressure. Finally, for our experimental conditions, the rate expression can be written as

$$r = K_r P_{TiCl4}^{-1/2} P_{NH3}^{1/2} \tag{4.19}$$

We find satisfying fit for the reaction order with respect to the preponderant species near the substrate surface (here it is the TiCl4). Ammonia is introduced far from the substrate

and then impinges a TiCl4 poisoning surface. So an attenuating exponent α must be introduced in order to lead to a reaction order of 1.37.

4.6 Characterization Study

4.6.1 X-ray Photoelectron Spectroscopy

Spectra were acquired on a Physical Electron Quantum 2000 ESCA system. The X-ray source on this instrument could be focused to a spot size of approximately 10 μm. The acceptance angle is ±23°. Depth profiles were obtained by alternating an acquisition cycle with a sputter cycle during which material was removed from the sample using a 4 keV Ar source raster over a 4 mm x 4 mm area. In order to eliminate crater wall effects, the data was acquired from a smaller region in the center of the sputter area. The equivalent sputter rate in SiO2 with this source using these conditions is ~ 76 Å/min.

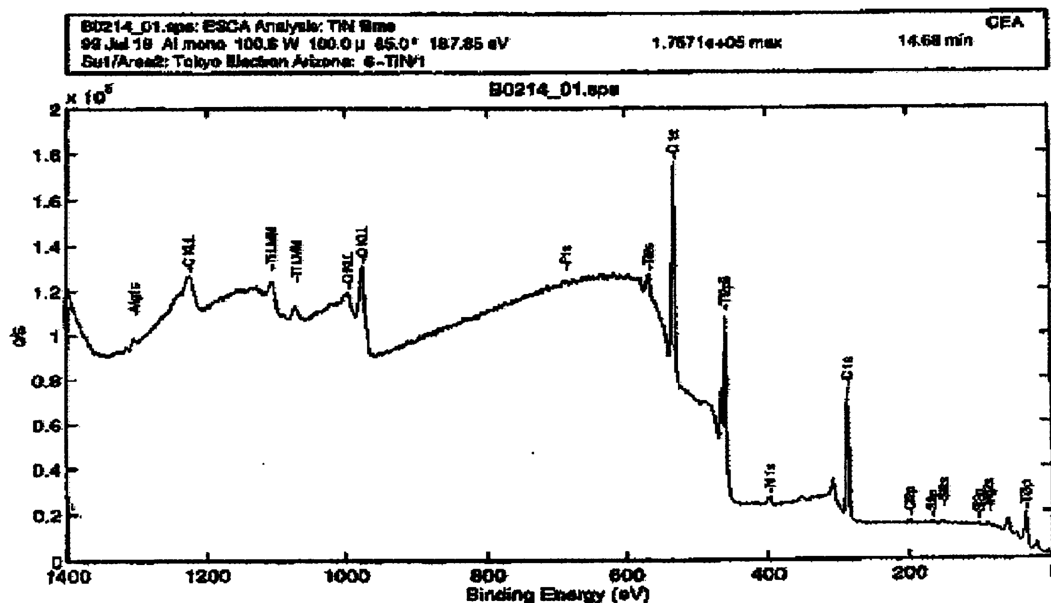

Figure 4.30 Elemental compositional analysis by X-ray photoelectron spectroscopy.

Figure 4.30 shows a typical XPS spectra obtained for the TiN deposits. Figures 4.31 and 4.32 show the elemental concentration as a function of sputter time giving information about the depth profile. From these figures we can see that the elements detected on the surfaces of the samples include C, N, O, F, Si, S, Cl, and Ti. However, carbon was observed only on the surface. Also, the oxygen concentration dropped sharply from the surface into the bulk of the film.

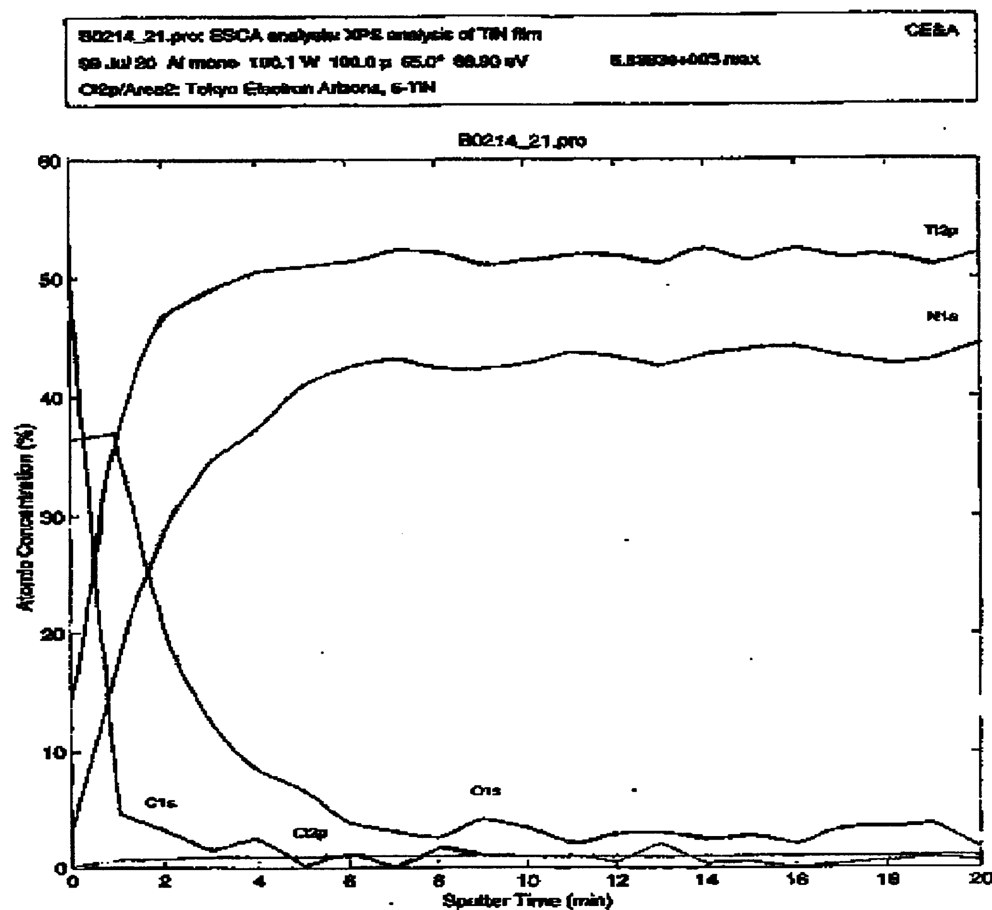

Figure 4.31 Depth analysis of the TiN films by RBS.

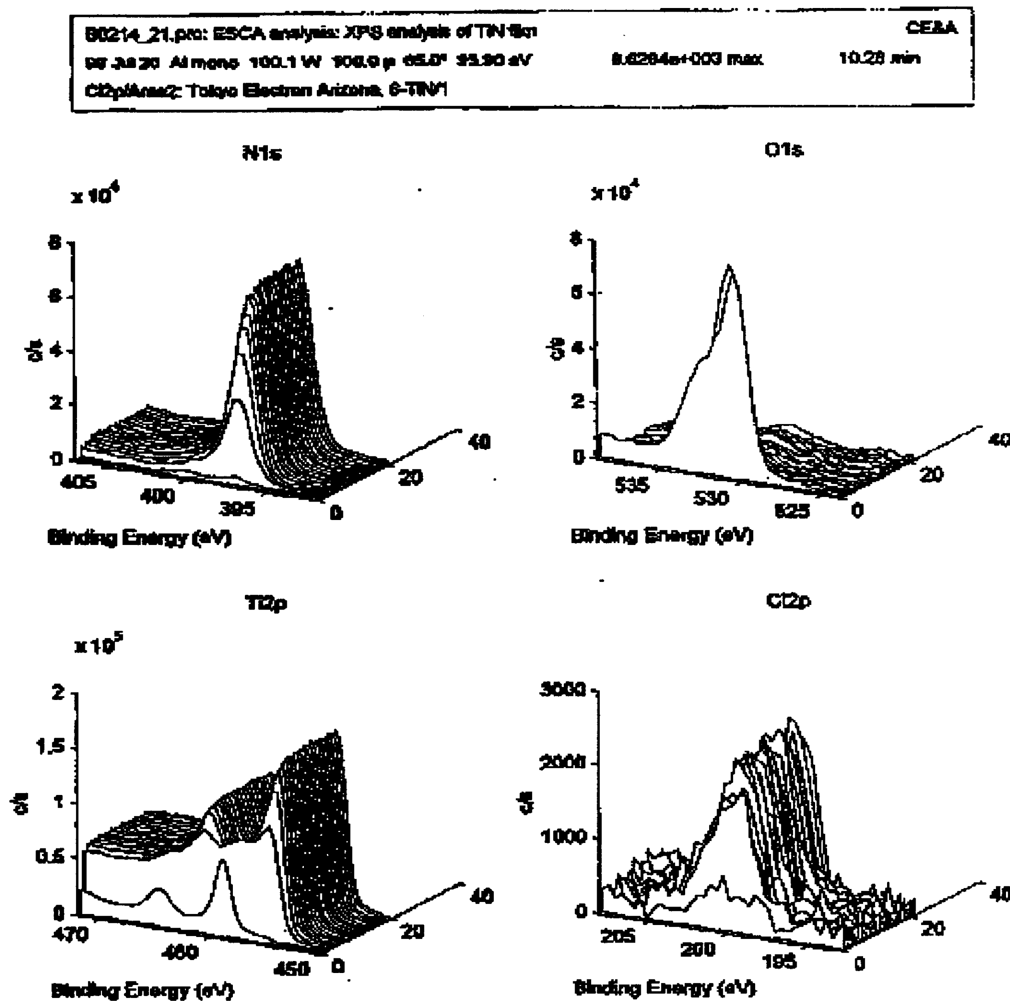

Figure 4.32 Depth analysis of the TiN deposits by XPS.

4.6.2 Rutherford Backscattering Spectrometry (RBS)

The Ti, N, Cl, and O concentrations were also measured by Rutherford Backscattering Spectrometry. A typical RBS spectra for the deposits is shown in Figure 4.33. RBS spectra were fitted with simulated spectra, from which the compositions were derived. The thickness of the sample plays an important role here since too thick samples do not allow separation of the component signals and hence the precision and signal accuracy is

degraded. Hence, films with thickness less than a micron were deposited. RBS measurements gave information about the areal density of Ti atoms, from which the thickness of the deposits were verified by using the values of the film density.

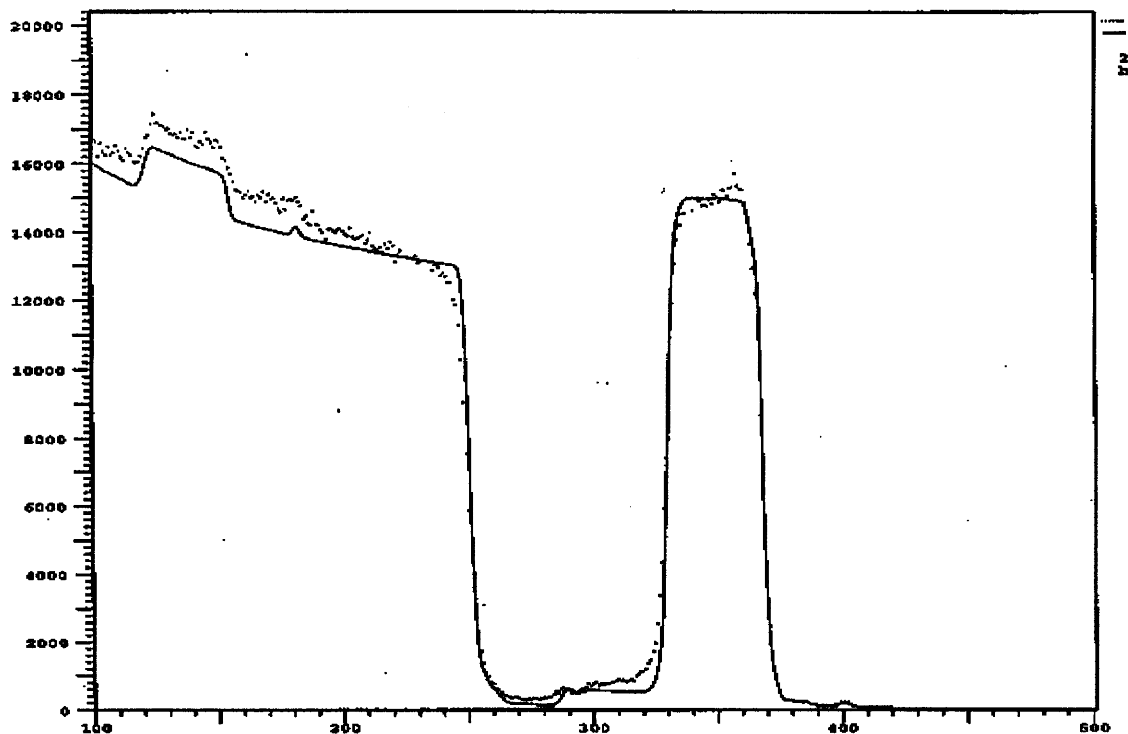

Figure 4.33 Rutherford backscattering spectrometry of the TiN films.

4.7 Properties of LPCVD TiN Films

4.7.1. Color

The color of pure TiN films has been reported to be golden. The color of the TiN deposits was found to be dependent on deposition temperature. In the temperature range of 450 to 600 °C, the films appear to be reddish while from 600 to 800 °C the color turned to brownish. At 800 °C and above, the deposits exhibited the golden color characteristic of

the TiN used for decoration. This color change is believed to be due to higher concentrations of Ti in the films as the temperature is increased which causes a shift in the absorbed spectra towards higher energies.

4.7.2 Density

A series of experiments was carried out at a constant $NH_3/TiCl_4$ flow ratio of 5 and pressure of 70 mTorr at 600, 700, 800 and 850 °C. The density of the films deposited was determined by dividing the film weight by film volume as calculated from the product of film thickness and known area of the wafer. The thickness in this case was obtained using Sloan Dektak as mentioned in section 3.4.2. There is a sight increase in the density with temperature. Higher density at higher deposition temperatures might be an indication that films were becoming purer and thus achieving a density closer to that of bulk TiN.

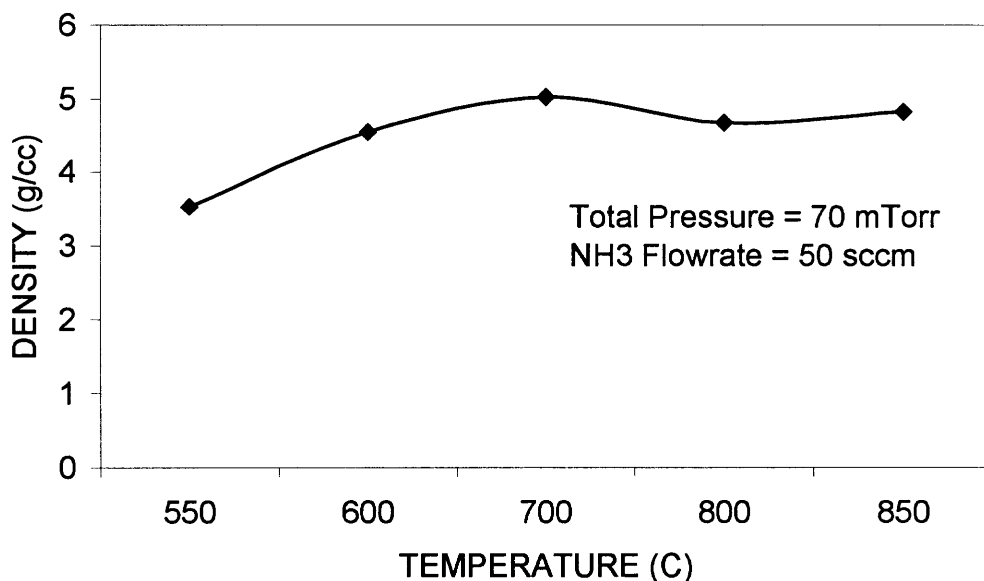

Figure 4.34 Variation in film density with deposition temperature.

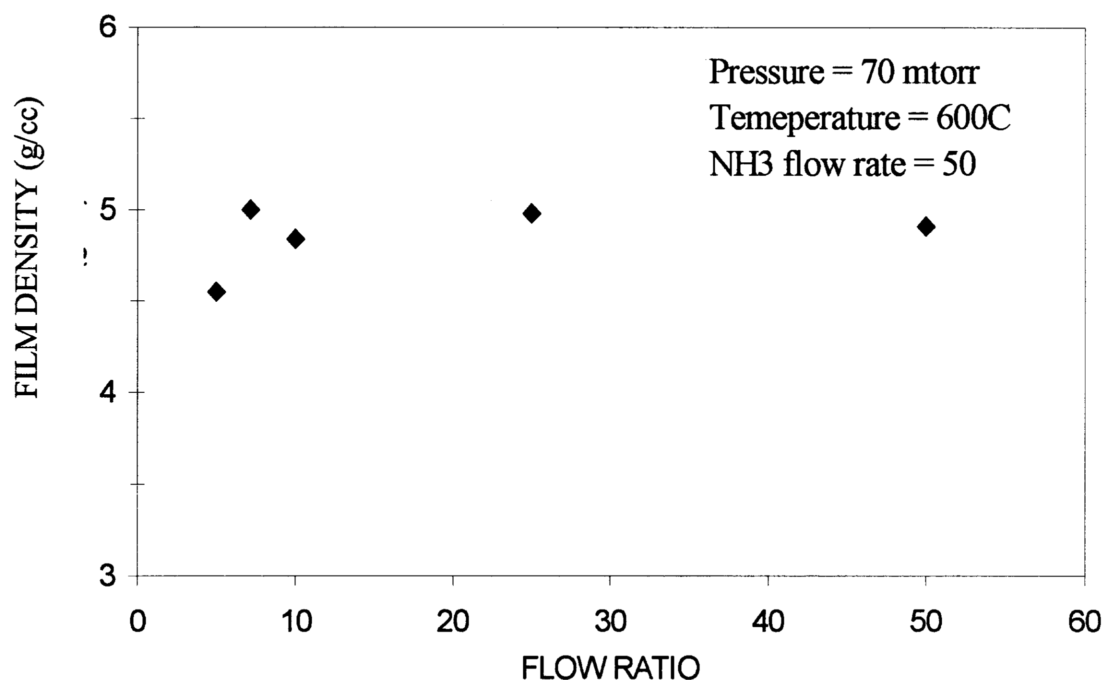

Figure 4.35 Variation in film density with $NH_3/TiCl_4$ flow ratio.

As the flow ratio was increased, the density increased at first but then became constant at a value of around 4.9 gm/cc (Figure 4.35). The films in this case were deposited at a temperature of 600 °C and pressure of 70 mTorr. This variation in the density might be due to the change in the composition of the film.

4.7.3 Film Stress

Stress was determined for the films deposited at a pressure of 70 mtorr at four different temperatures for each of the flow ratios of 5 and 10. It was found to be tensile. This means that the film causes the wafer to be concave on the side it is deposited. Figure 4.36 shows the results plotted for the two different flow ratios. The stress decreased with the increase in temperature. The lowest stress was observed to be 40 MPa at a deposition

temperature of 850°C, for a flow ratio of 5. Since it is not desirable of films to exert stress on the wafer, either tensile or compressive, low stress means better film quality

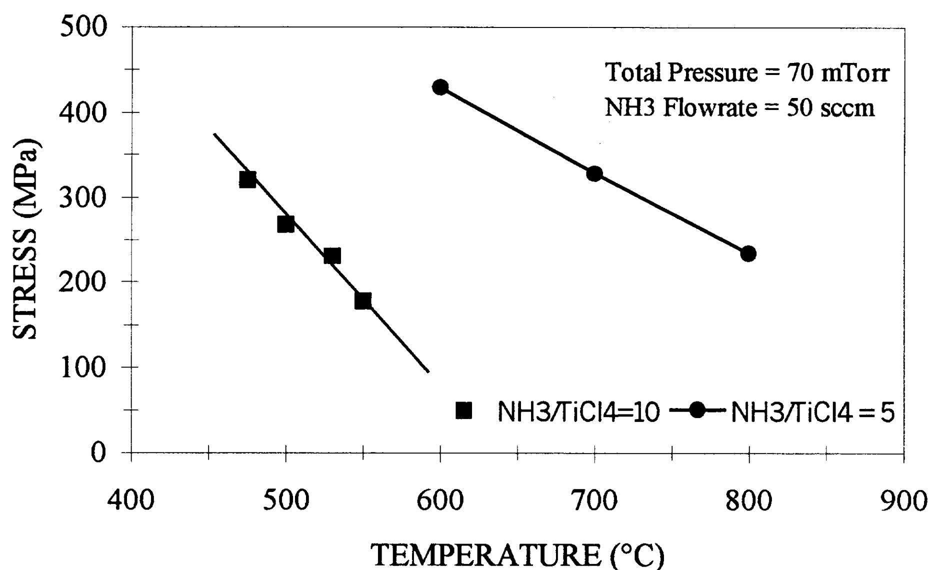

Figure 4.36 Variation in film stress with deposition temperature.

4.7.4 Resistivity

The variation in resistivity with temperature was also studied at 2 different flow ratios. Figure 4.37 shows the results. Resistivity was found to decrease with increasing temperature. All the experiments were carried out at a pressure of 70 mtorr. The lowest resistivity obtained was 86 μohm-cm at a temperature of 850°C and flow ratio of 10. Since TiN is used in the microelectronics industry as a diffusion barrier, low film resistivity is an important characteristic, and again, high temperature leads to this desirable film quality.

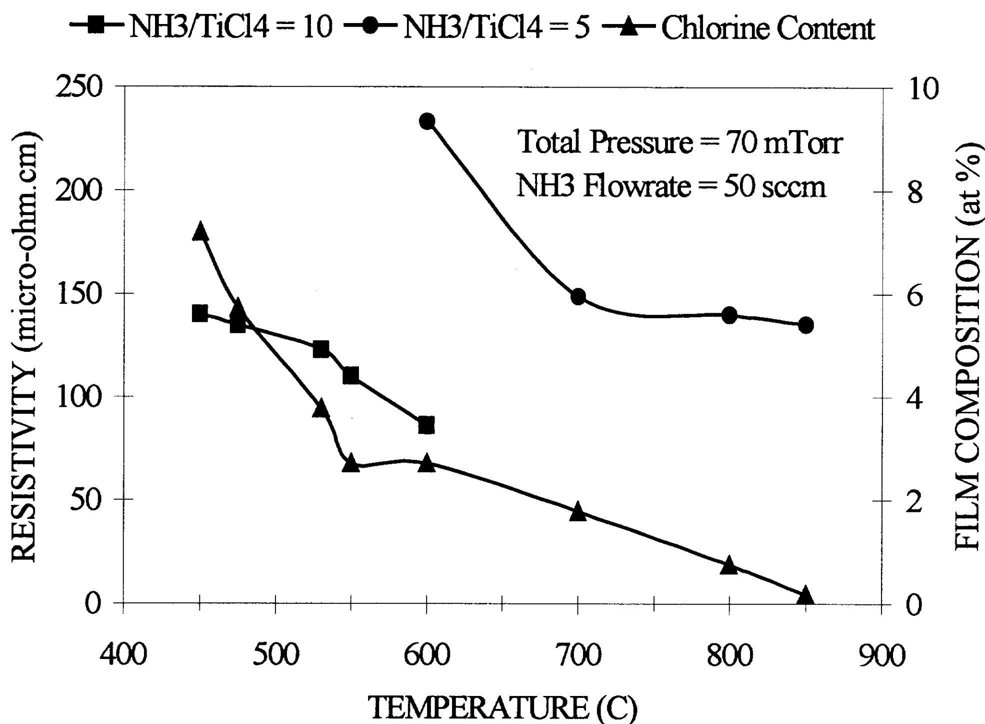

Figure 4.37 Variation in film resistivity with deposition temperature.

4.7.5 Hardness and Young's Modulus

On an average, the titanium nitride films were 50% harder than silicon. At an indentation of 200 nm, the value of the hardness ranged from 13 to 17 GPa depending on the film deposition process parameters while the hardness for silicon was found to be about 10 GPa. Study of the variation in the film hardness with the deposition temperature (Figure 4.38) showed that the film hardness decreased with increasing film deposition temperature, for a NH_3:$TiCl_4$ ratio of 5.

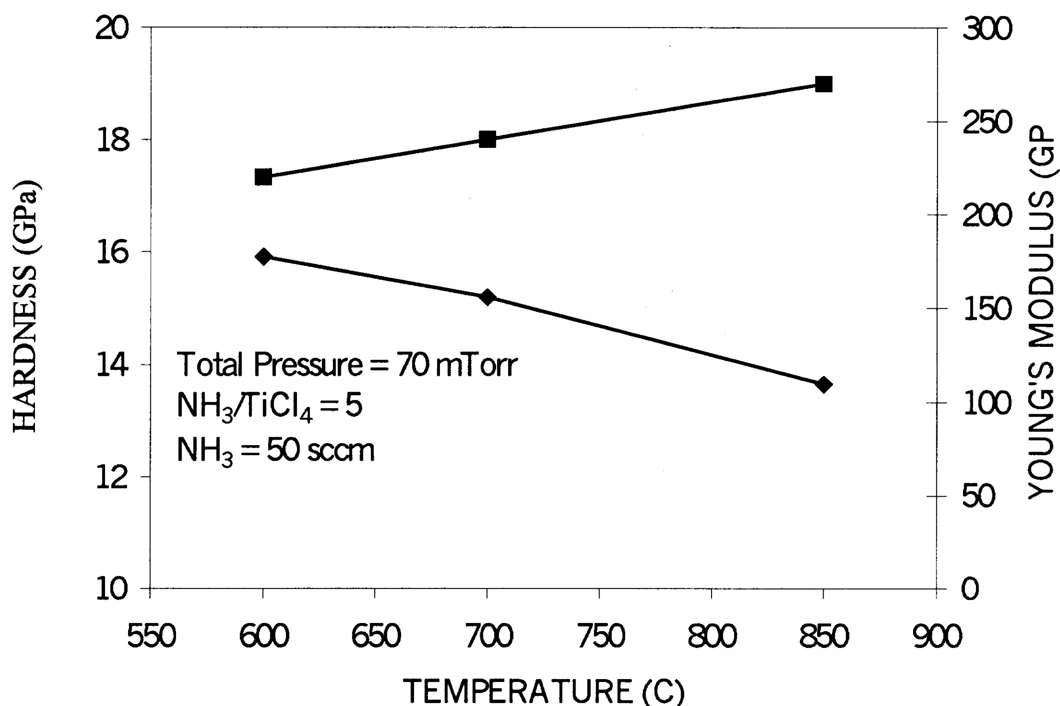

Figure 4.38 Variation in film hardness with deposition temperature.

4.7.6 Optical Properties

Figure 4.10 shows the optical characterization of a Tin film deposited at 600°C and 70 mtorr pressure, using a NH_3:$TiCl_4$ flow ratio of 5. From the reflectance, emittance and transmittance spectra in the IR region, it can be concluded that TiN films can act as a good reflector of IR radiation (i. e. heat), since they reflect more than 80% of the radiation. It is for this heat reflecting property of TiN films that they have been used as heat mirrors in architectural applications. Almost zero radiation is transmitted while a very small percent is emitted. However this behavior was found to change at a deposition temperature of around 750°C, where the reflectance went down considerably and the

emittance increased; the transmittance remained unchanged. The probable cause for this was formation of some kind of oxide that had different optical properties.

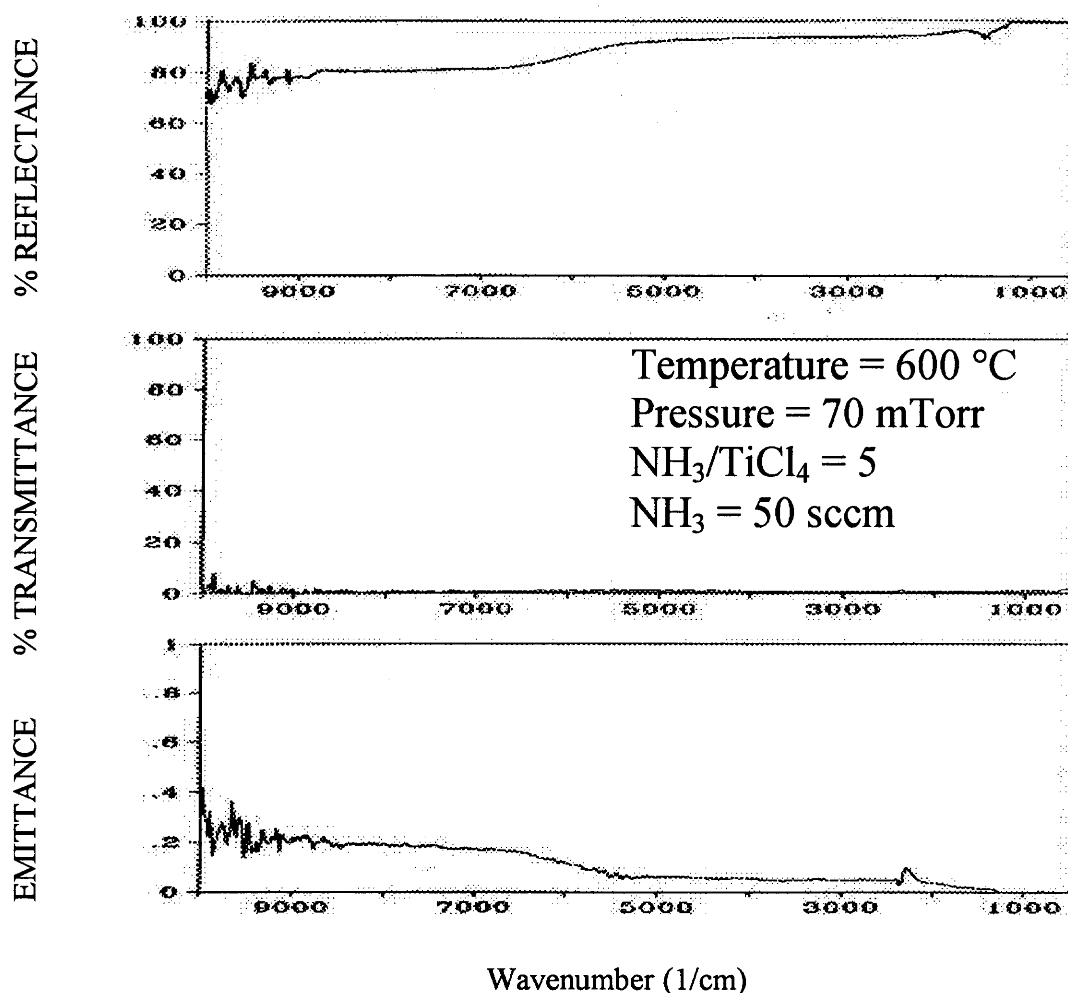

Figure 4.39 Optical Properties of TiN.

4.7.7 Step Coverage and Film Morphology

Figures 4.40-4.43 illustrate the step coverage of TiN films deposited at 475 for aspect ratios of ~2:1 and ~5:1 and at 600 °C for an aspect ratio of ~2:1. Its apparent that the step coverage is quite conformal at both deposition temperatures and for both aspect ratios. A

plug exhibiting no voids is readily observed for the aspect ratio of ~5:1. Columnar growth is evident in all three micrographs, which impacts the surface topography and is typical for metallic films deposited at this temperature regime.

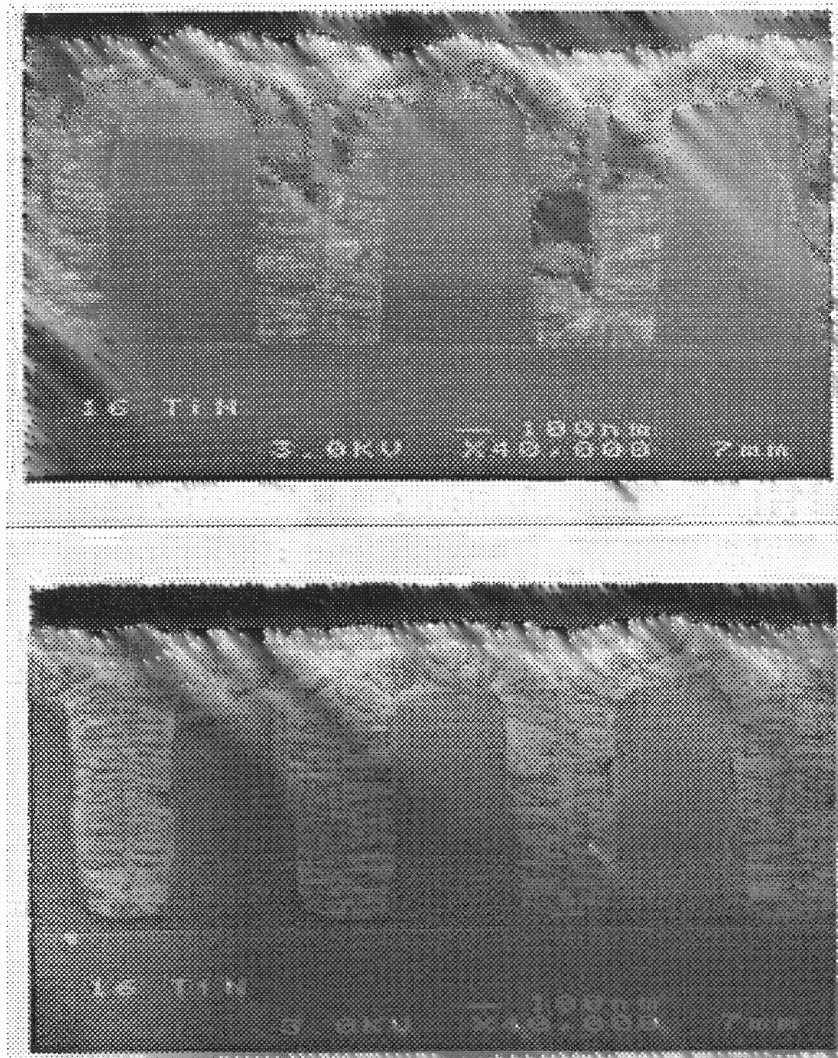

Figure 4.40 SEM micrograph of TiN deposited at 475°C and NH_3/TEAB of 10/1.

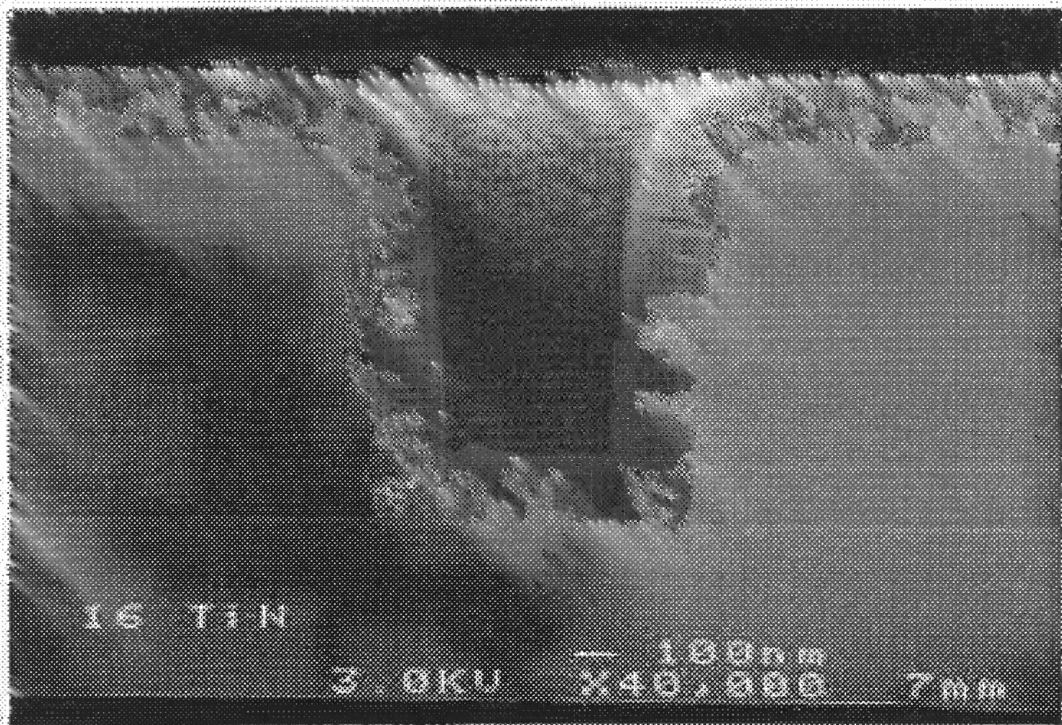

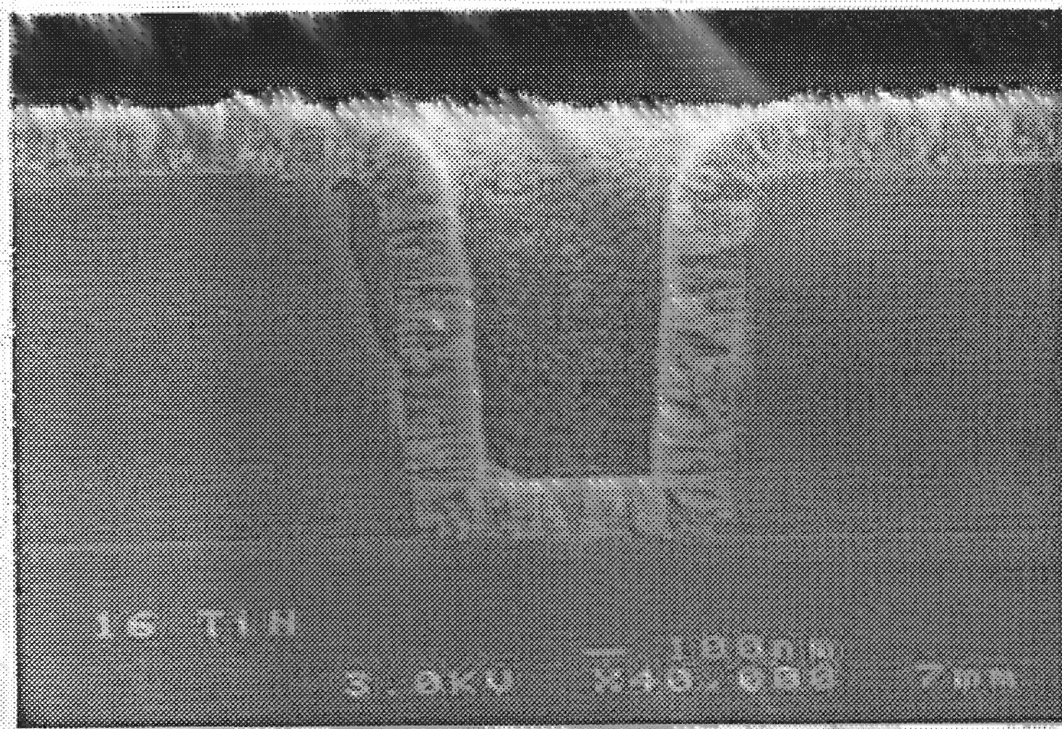

Figure 4.41 SEM micrograph of TiN deposited at 475°C and NH_3/TEAB of 10/1.

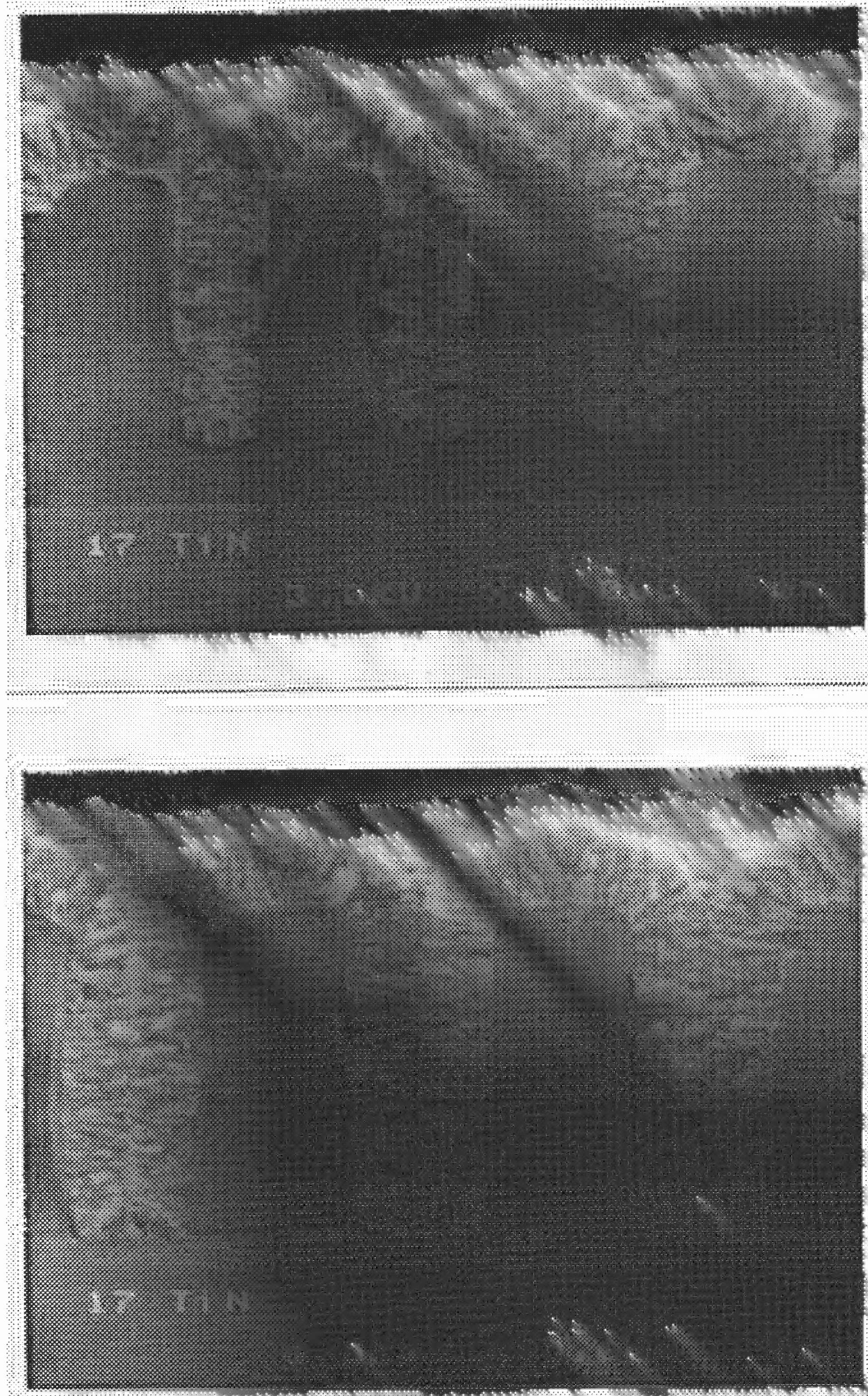

Figure 4.42 SEM micrograph of TiN deposited at 525°C and NH_3/TEAB of 10/1.

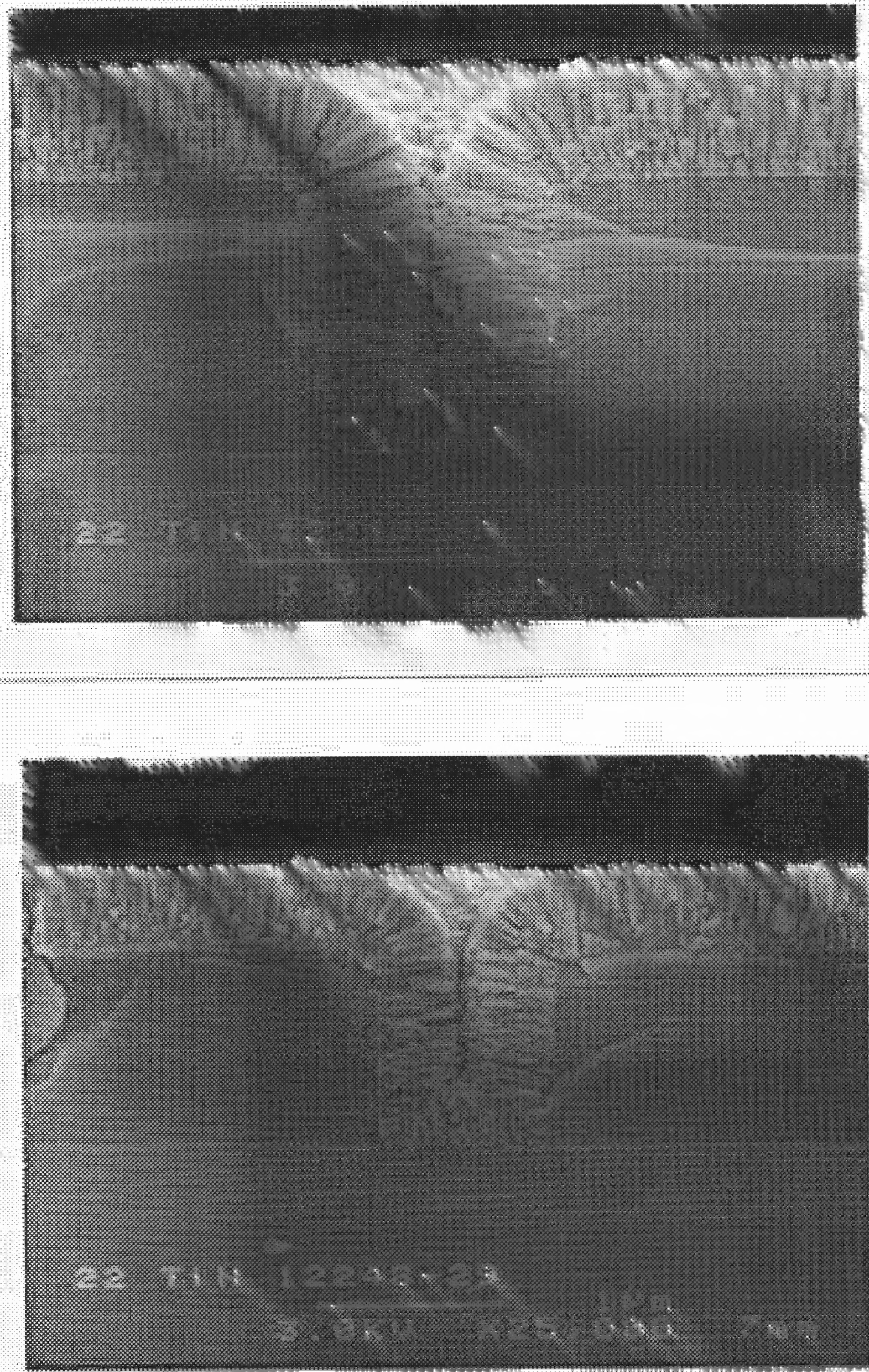

Figure 4.4 3 SEM micrograph of TiN deposited at 600°C and NH_3/TEAB of 10/1.

4.7.8 X-ray Diffraction (XRD)

X-ray diffraction analysis was carried out for a TiN film of thickness 2578 Å deposited at 600°C and 70 mtorr, using a NH_3:$TiCl_4$ flow ratio of 5. The corresponding X-ray diffraction plot is shown in Figure 4.44. From the d-value of 2.13 Å for the (200) plane, the lattice constant was calculated as 4.26 Å.

Table 4.1 compares the relative intensities of different orientations for the above film with those given in the diffraction data card for TiN. Looking at the minimal relative intensities of the peaks for orientations other than (200), we can safely say that the orientation of the film is (200). This is in agreement with the findings of Oh et. al., who have confirmed that for lower thickness (<5900Å), TiN films exhibit a preferred orientation of (200).

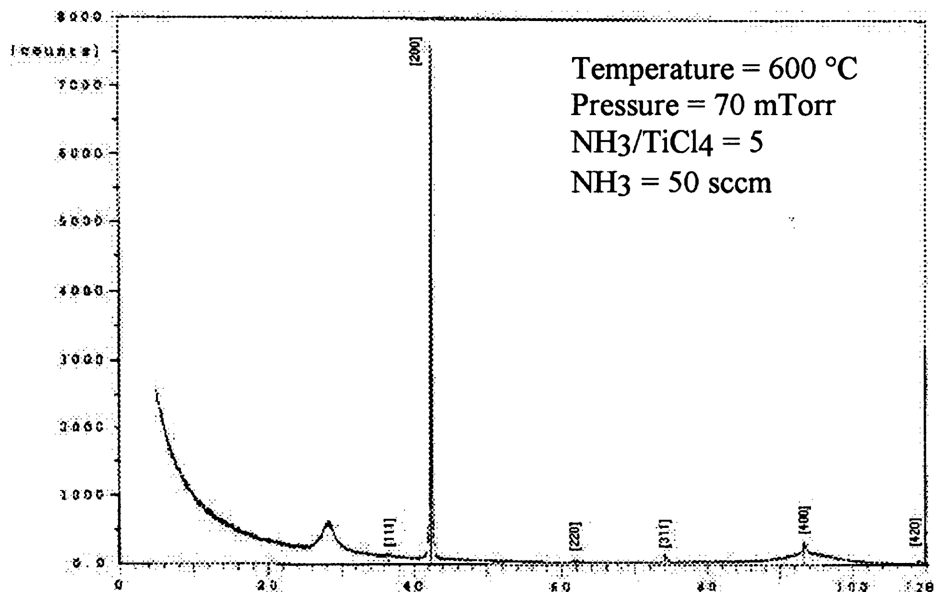

Figure 4.44 X-ray Diffraction plot for TiN.

Table 4.1 Comparison of experimental XRD data with standard data.

Orientation (hkl)	Standard Data for TiN		Experimental Data	
	d (Å)	Rel. int. (%)	d (Å)	Rel. int. (%)
111	2.44	77	2.46	0.5
200	2.12	100	2.13	100
220	1.496	56	1.498	0.4
311	1.277	26	1.278	0.1
222	1.223	16	No peak	
400	1.059	7	1.0598	2.2
331	0.972	11	0.9475	0.6
420	0.948	22	No peak	
422	0.865	21	No peak	

4.8 Etching Study

In many applications of thin film deposition, etching of the film is an important aspect. In wet etching, mostly hydrogen fluoride (HF) is used for etching of thin films. However, HF is a very dangerous chemical and is notorious for causing skin burns. Thus finding an alternative to HF for etching becomes essential. In the case of TiN thin films, Buiting et. al. have reported that the mixture of ammonium hydroxide, hydrogen peroxide and water is effective in etching the film.

Etching experiments were carried out using an etching solution containing NH_4OH, H_2O_2 and H_2O in different proportions. The wafers etched were all from the same experiment. NH_4OH used was concentrated while H_2O_2 was used as a 30% solution. The different 1:1:0. Figure 4.45 shows the results of the etching experiments. The rate of etching

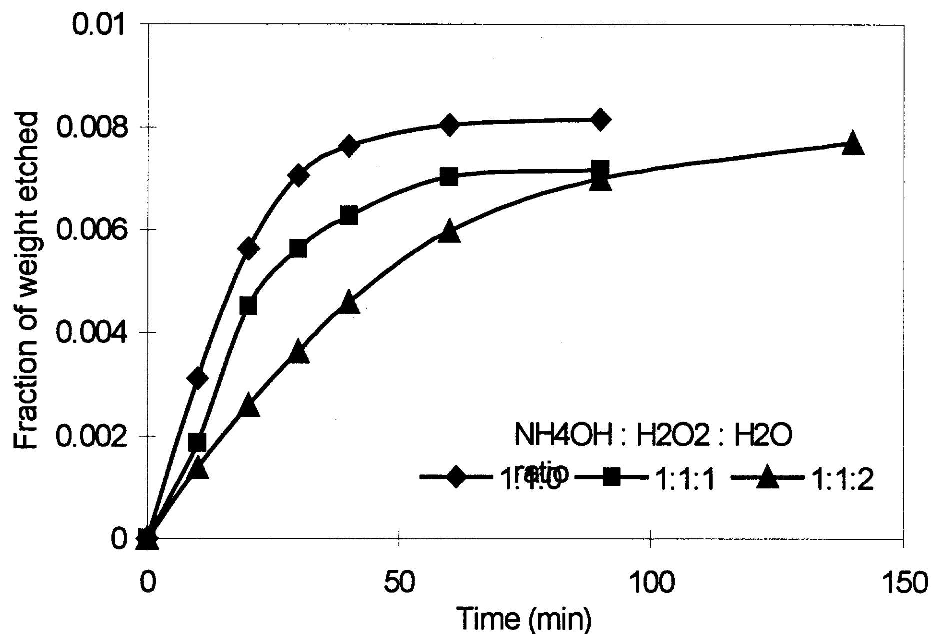

Figure 4.45 Etching characteristics in NH4OH/H2O2/H2O solution.

(given by the slope of the plot during the initial stages of etching) decreased as the proportion of water was increased, i.e. as the etching solution was diluted. In the case where no water was added, the film etched almost completely within just half an hour, while it took more than 2 hours in the case where dilution was maximum. In all the cases, the etching was complete and uniform, thus proving the ammonium hydroxide-hydrogen peroxide mixture as an efficient etching solution for etching of TiN thin films.

4.9 Effect of Aluminum on LPCVD of TiN

During one of the experiments, it was observed that the presence of aluminum in the reactor altered the color of the TiN film deposited. In the case of deposition carried out at 600°C, in the presence of aluminum, the color of the film deposited was found to be brilliant golden, which is characteristic of pure TiN films. However for the deposition

carried out under the same process conditions but in the absence of aluminum, the color of the film deposited was observed to be reddish brown. This implied that the presence of aluminum was affecting the composition of the deposited film.

However, the same golden color of the film is observed for deposition carried out at higher temperatures (~850°C). This implies that there is some similarity between the composition of the film deposited at 600°C in the presence of aluminum and the one deposited at 850°C in the absence of aluminum. This similarity was presumed to be low chlorine content in both the films. The chlorine content in the case of film deposited at 850°C is low since the chlorine content decreases with increase in the deposition temperature. So it was suggested that the low chlorine content of the film deposited in the presence of aluminum was a result of the fact that aluminum reacted with the chlorine to form $AlCl_3$. Thus lesser chlorine went into the film, thereby imparting a golden color to the film. This inference was further strengthened by the fact that the resistivity of this film was very low (21 μΩcm). This aspect of TiN deposition might be particularly useful in the applications where TiN coating is used for decorative purposes or as a low resistivity film and the substrate on which the film is deposited cannot tolerate the temperature at which a pure TiN film is deposited. By carrying out the deposition in the presence of aluminum, this might be achieved at considerably lower temperature, which the substrate can survive. Apart from making the process feasible, this also results in huge savings in energy and time. Essentially, an entire separate study can be carried on the LPCVD of TiN in the presence of aluminum.

CHAPTER 5

CONCLUSIONS

In this study, Boron Nitride (B-N-C-H) and Titanium Nitride (Ti-N-Cl) films have been deposited by low pressure chemical vapor deposition (LPCVD), using ammonia (NH_3)/triethylamine borane and NH_3/titanium tetrachloride ($TiCl_4$) as precursor materials, respectively. Growth kinetics, film stoichiometry and properties have been investigated as a function of the deposition parameters. Several analytical techniques such as FTIR, XPS, AES, RBS, and XRD have been used to study the composition and structure of the deposits.

The B-N-C-H films were synthesized over a temperature range of 300 to 850°C for the NH_3/TEAB flow ratios of up to 2000/1 and total pressure range of 50 to 150 mTorr. The deposits were found to be amorphous in all cases, with an index of refraction ranging between 1.76 and 2.47, dielectric constant ranging between 3.12 and 5.5, and stress varying from +240 to –200 MPa depending on the composition of the films. Hardness and Young's modulus were found to be between 5 to 12 and 50 to 120 GPa, respectively. Freestanding X-ray windows were fabricated, tested, and seen to be more sensitive for light element detection than the commercially available X-ray windows. The B-N-C-H films of 2000 Å thickness exhibited X-ray transmission of 80% at energies of 0.25 to 0.5 keV compared to 10% by the commercially available X-ray windows. The deposits were boron rich at lower temperatures, but with increasing temperature, the films attained compositions close to stoichiometric BN. There was about 8% carbon in the films that

was not in a compound form. It was found that the film stress was either mildly tensile or compressive (+100MPa - -150MPa) depending on the deposition conditions. The static dielectric constant varied from 3.12 to 5.5 depending on the deposition condition. The optical and the static dielectric constant behavior were similar. At higher flow rates the films tend to be stoichiometric and transparent.

In this study, we have also investigated the interrelationships governing the growth kinetics, resulting compositions, and properties of titanium nitride (TiN) films synthesized by low pressure chemical vapor deposition (LPCVD) using titanium tetrachloride ($TiCl_4$) and ammonia (NH_3) as reactants. The kinetics of the reaction between $TiCl_4$ and NH_3 was first established resulting to formulation of a rate equation showing the dependence of the reaction on the partial pressures of both reactants, which is shown as follows:

$$r = 4.35 \times 10^{-5} \exp(-5150/T)\,(P_{NH3})^{1.37}\,(P_{TiCl4})^{-0.42}$$

For the reactor geometry used, the reaction rate was found to be inversely proportional to $TiCl_4$ partial pressure and directly proportional to NH_3 partial pressure. Deposition rate as a function of temperature was found to follow an Arrhenius behavior in the temperature range of 450 to 550 °C, yielding an apparent activation energy of 41.82 kJ/mol. The RBS results show that the films produced were nearly stoichiometric with chlorine atomic concentration ranging from 0.15 to 7.19 % (a/o). The electrical, mechanical, and structural properties of the TiN films were also determined. The film density values were seen to increase from 3.53 to 5.02 g/cm^3 as the deposition temperature was increased from 550 to

850 °C. The resistivity of the films was found to be dependent on changes in deposition temperature and flow rate ratios. The lowest resistivity value of 86 μΩcm was measured for a deposition temperature of 600°C and an $NH_3/TiCl_4$ flow ratio of 10/1.The film stress was tensile for all deposits and was seen to decrease with higher deposition temperatures. Nano-indentation measurements yielded values for the hardness and Young's modulus of the films to be around 15 and 250 GPa, respectively. X-ray diffraction studies indicate that cubic TiN films were formed. It is known that Al is very sensitive to the presence of chlorine, which means that the chlorine content should be as low as possible. At a temperature of 600°C, by operating at high $NH_3/TiCl_4$ ratios, films with negligible chlorine content were produced.

REFERENCES

1. R. Turton. 1995. *The Quantom Dot*. New York: Oxford University Press.
2. M. Kaku. 1997. *Visions*. New York: Oxford University Press.
3. W. F. Smith. 1996. *Principles of Materials Science and Engineering*. New York: McGraw-Hill, Inc.
4. F. S. Galasso. 1991. *Chemical Vapor Deposited Materials*. New York. CRC Press.
5. C. A. Harper and R. N. Sampson. 1993. *Electronic Materials and Processes Handbook*. New York: McGraw-Hill, Inc.
6. M.J. Rand and J.F. Roberts, *J. Electrochem*. Soc., **15**, 423 (1968).
7. L.G. Carpenter and P.J. Kirby, *J. Phys*. D, **15**, 1143 (1982).
8. A. Simpson and A.D. Stuckes, *J. Phys*. C, **4**, 1710 (1971).
9. M. Hirayama and K. Shohno, *J. Electrochem. Soc*., **122**,1671 (1975).
10. T.M. Duncan, R. A. Levy, *J. Appl. Phys*. **64**(6), 15 September 1988.
11. W. Schintlmeister, O. Pacher, and K. Pfaffinger, *J. Electrochem. Soc.*, **123,** 924 (1976).
12. C. Y. Ting, J. Vac. Sci. Technol., **21**, 14 (1982).
13. M. Witter, Appl. Phys. Lett., **37**, 540 (1980).
14. M. Witter and H. Melchoir, *Thin Solid Films*, **93**, 397 (1982).
15. L. Roux, J. Hanus, J. C. Francois and M. Sigrist, *Sol. Energy Mater.*, 7, 299 (1982).
16. E. Valkonen, T. Karlsson, B. Karlsson, and B. O. Johansson, *Thin Film Technology*, Proc. Soc. Photo-Opt. Instrum. Eng., **41**, 375 (1983).
17. T. Usami, K. Shimokawa and M. Yoshimaru, *J. Appl. Phys.*, **33**, 408 (1994).
18. W.P. Kuo, "Synthesis and Characterization of LPCVD Boron Nitride Films for X-ray Lithography, *MS Thesis*, New Jersey Institute of Technology, Newark, NJ (1993).

19. Advanced Semiconductor Materials America, Inc., "Micro 3 Manual".

20. R.A. Levy, E. Mastromatteo, J.M. Grow, V. Paturi and W.P. Kuo, *J. Of Mater. Res.*, **10**, 320 (1995).

21. R.A. Levy, Microelectronic Materials and Processes, Kluwer Academic Publishers, 1989.

22. Neil H. Hendricks, *Solid State Technology*, July 1995.

23. Keiichiro Kata, Yuzo Shimada and Hideo Takamizawa, *IEEE Trans. on components, hybrids, and manufacturing technology*, **13**, 2, June 1990.

24. M. Hatanaka, Y. Mizushima, O. Hataishi and Y. Furumura, *Proc. VLSI Multilevel Interconnection Conf.*, 435 (1991).

25. B.L. Chin and E.P. Van de Ven, *Solid state Technol.*, **31**, 119 (1988).

26. Yu, D. Favreau, E. Martin and A. Manocha, *Proc. VLSI Multilevel Interconnect-ion Conf.*, 166 (1990).

27. S. Mizuno, A. Verma, P. Lee and B. Nguyen, *Int. Conf. On Metallurgical Coatings and Thin Films Abstract* (1995).

28. D.C. Rich, P. Cebe and A.K. St.Clair, *Mat. Res. Soc. Symp. Proc.* **323**, 301 (1994).

29. Y. Negi, Y. Suzuki, I. Kawamura, T. Hagiwara, Y. Takahashi, M. Ijima, Y. Imai and M. Kakimoto, *J. Polym. Sci.* **A30**, 2281 (1992).

30. M. Maeda, Japan. *J. Appl. Phys.*, **29** 1789 (1990).

31. M. Maeda, T. Makino, E. Yamamoto and S. Konaka, *IEEE Trans. Electron Devices*, **36**, 1610 (1989).

32. K. Montasser, S. Hatori and S. Morita Plasma Chem., Plasma Process., **4**, 251 (1984); J. Appl. Phys., **58**, 3185 (1985).

33. A. Sherman. 1987. *Chemical Vapor Deposition for Microelectronics*. New Jersey: Noyes Publication.

34. K. J. Laidler. 1950. *Chemical Kinetics*, New York: McGraw-Hill Publication.

35. R. A. Levy, *Chemical Vapor Deposition*, Microelectronics Material Processes Ch.5, Kluwer Academic Publishers, Boston, MA (1989).

36. W. Kern and V. S. Ban, "Chemical Vapor Deposition of Inorganic Thin Films," *Thin Film Processes*, Eds. J. L. Vossen and W. Kern, Academic Press, New York (1978).

37. Hugh O. Pierson, *Handbook of Chemical Vapor Deposition*, Noyes Publications, New Jersey, 1992.

38. J. G. Lee, Conf. Proc. ULSI XI 1996, Materials Research Society.

39. CRC Handbook of Chemistry and Physics, 60th edition, 1979-1980.

40. M. Ohring. 1991. The Materials Science of Thin Films. New York: Academic Press.

41. W. Baronian, *Mat. Res. Bull.*, 7,119 (1972).

42. M Sano, *Thin Solid Films*, **83**, 247 (1981).

43. S Motojima, Y. Tamura and A. Sugiyama, *Thin Solid Films*, **88**, 269 (1982).

44. T. Takahashi, H. Itoh and A. Takeuchi, *J. Crystal Growth*, **47**, 245 (1979).

45. T. Takahashi, H. Itoh and M. Kuroda, *J. Crystal Growth*, **53**,1981 (1981).

46. K. Nakamura, *J. Electrochem. Soc.*,**132**, 1757 (1985).

47. Robert T. Paine and Chaitanya k. Narula, *Chemical Reviews*, **90**, 1 (1990).

48. S.S. Dana and J.R. Maldonado, *J. Vac. Sci. Technol.*, **B4**, 235 (1986).

49. A.C. Adams, *J. Electrochem. Soc.*, **128**, 1378 (1981).

50. A.C. Adams and C.D. Capio, *J. Electrochem. Soc.*, **127**, 399 (1980).

51. S.B. Hyder and T.O. Yep, *J. Electrochem. Soc.*, **123**, 1721 (1976).

52. O. Gafri, A. Grill and D. Itzhak, *Thin Solid Films*, **72**,523 (1980).

53. W. Schomolla and H.L. Hartnagel, *J. Appl. Phys.*, **15**,L95 (1982).

54. W. Schomolla and H.L. Hartnagel, *Solid State Electronics*, **26**, 931 (1983).

55. A.J. Noreika, and M.H. Francombe, *Thin Solid Films*, **101**, 722 (1983).

56. M.D. Wiggins and C.R. Aita, *J. Vac. Sci. Technol.* **A2**, 322 (1984).

57. E.H. Lee and H. Poppa, *J. Vac. Sci. Technol.*, **14**, 223 (1977).

58. Weissmantel, K. Bewilogua, K. Breuer, D. Dietrich, U. Ebersbach, H.J. Erler, V. Rao and G. Reisse, *Thin Solid Films*, **96**, 31 (1982).

59. Weissmantel, *J. Vac. Sci. Technol.*, **18**, 2082 (1981).

60. S. Shanfield and R. Wolfson, *J. Vac. Sci. Technol.*, **A1**, 323 (1983).

61. M. Satou and F. Fujimoto, *J. Appl. Phys.*, **22**, L171 (1983).

62. L. Guzman, F. Marchetti, I. Scotoni and F. Ferrari, *Thin Solid Films*, **117**, L63 (1984).

63. M. Sokolowski, A. Sokolowska, A. Michlski, Z. Romanowski, A.R. Mazurek and M.Wronikowski, *Thin Solid Films*, **80**, 249 (1981).

64. T. S. Cale, G. B. Raupp, J. T. Hillman, and M. J. Rice, Conf. Proc. ULSI- VIII (1993) Materials Research Society.

65. J. T. Hillman, R. Arora, and R. Foster, Proc. of the Third Sony Research Forum (1993).

66. J. T. Hillman, D. Srinivas, R. F. Foster, R. J. Graham, F. Shaapur, and M. R. McCartney, Conf. Proc. ULSI- IX (1994) Materials Research Society.

67. I. J. M. M. Raaijmakers, B. E. Roberts, T. Itoh, T. J. Konno, and R. Sinclair, Advanced Metallization for Devices and Circuits - Science, Technology and Manufacturability, San Francisco, CA (1994).

68. J. T. Hillman, D. W. Studiner, M. J. Rice Jr., and C. Arena, *Microelectronic Engineering*, **19** (1992).

69. M. J. Buiting, A. F. Otterloo, and A. H. Montree, *J. Electrochem. Soc.*, 138, 2 (1991).

70. S. R. Kurtz and R. G Gordon, Thin Solid Films, 140, 277 (1986).

71. J. P. Dekker, P. J. Van Der Put, H. J. Veringa, and J. Schoonman, *J. Electrochem. Soc.*, **141**, 3 (1994).

72. F. Marchetti, M. Dapor, S. Girandi, F. Giazomozzi, and A. Cavalerri, "Physical Properties of TiN thin films," *Mat. Sci. and Eng.*, A115 (1989).

73. E. Roman, J. L. De Segovia, A. Alberdi, J. Calvo, and J. Laucirica, Vacuum, **43**, 5-7 (1992).

74. L. Imhoff, A. Bouteville, and J. C. Remy, *J. Electrochem. Soc.*, 145, 5 (1998).

75. C. -C. Jiang, T. Goto, and T. Hirai, *J. of Mat. Sci.*, 28 (1993).

76. A. Bouteville, L. Imhoff, and J. C. Remy, *J. Electrochem. Soc.*, **143**, 10 (1996).

77. S.P. Murarka, C.C. Chang, D.N.K. Wang and T.E. Smith, *J. Electrochem.Soc.*, **126**, 1951 (1979).

78. M. Maeda and T. Makino, Japan. *J. Appl. Phys.*, **26**, 660 (1987).

79. W.A. Johnson, R.A. Levy, D.J. Resnic, T.E. Saunders, A.W. Yanof, H. Oertel, and H. Huber, *J. Vac. Sci. Technol.* **B5**, 257 (1987).

80. A. Intemann, F. Koch, and H. Koerner, *J. Electrochem. Soc.*, **140**, 11 (1993).

81. Arena, J. Fagnet, R. F. Foster, J. T. Hillman, D. Srinivas, Conf. Proc. ULSI- IX (1994) Materials Research Society.

82. U. Z. Wu, T. C. Chou, A. Mishra, D. R. Anderson, J. K. Lampert, and S. C. Gujrathi, *Thin Solid Films*, 191 (1990).

83. U. C. Oh, Jung Ho Je, and Jeong Y. Lee, *J. Mater. Res.*, 13, 5 (1998).

84. N. Yokoyama, K. Hinode, and Y. Homma, *J. Electrochem. Soc.*, **138**, 1 (1991).

85. R.A. Levy, D.J. Resnic, R.C. Frye, A.W. Yanof, G.M. Wells and F. Cerina, *J. Vac. Sci. Technol.*, **B6**, 154 (1988).

86. Maydan, G.A. Coquin, H.J. Levinstein, A.K. Sinha, and D.N.K. Wang, *J. Vac. Sci. Technol.* **16**, 1959 (1979).

87. R.E. Acosta, J.R. Maldonado and R. Fair, *J. Vac. Sci. Technol.* **B4**, 240 (1986).

88. R.K.Laxman, *Semicond. Int.*, **5**, 71 (1995).

89. Tue Nguyen, Son Van Nyugen, and David M. Dubuzinsky, *Appl. Phys. Lett.* **63** (15), 11 October 1993.

90. S.P. Murarka, *Solid State Technology*, March 1996.

91. ASM handbook. 1996. Materials Characterization. **10**, ASM international.

92. N. Ramanuja and M. Kim, Tech. Observer, **2**, 1 (2000).